9950-283

(NASA-CR-162831) HIGH TEMPERATURE SOLAR THERMAL RECEIVER Final Report (Sanders Associates, Inc.) 109 p HC A06/MF A01 CSCL 10A

N80-19621

Unclas
G3/44 47472

HIGH TEMPERATURE SOLAR THERMAL RECEIVER

FINAL REPORT

DECEMBER 1979

JPL Contract No. 955454

Sanders Associates, Inc.
Energy Systems Center
95 Canal Street
Nashua, NH 03061

This work was performed for the Jet Propulsion Laboratory, California Institute of Technology sponsored by the US Department of Energy

ABSTRACT

Sanders Associates, Inc. has developed a design concept for a High Temperature Solar Thermal Receiver (HTSTR) to operate at 3 atmospheres pressure and 2500°F outlet. A parametric analysis wherein several receiver types were compared was performed during the first two months of the study. The performance and complexity of windowed matrix, tube-header and extended surface receivers were evaluated and the windowed matrix receiver proved to offer substantial cost and performance benefits. Subsequent effort was devoted to definitizing and pricing the receiver as a production unit. The unit has evolved as an efficient (80%) and economical ($25/KWt) receiver for operation at temperatures of 2500°F or less.

TABLE OF CONTENTS

TABLE OF CONTENTS (Continued)

LIST OF ILLUSTRATIONS

LIST OF ILLUSTRATIONS (Continued)

LIST OF TABLES

SECTION 1
SUMMARY

JPL has identified areas of Advanced Technology requirements wherein study level funding could lead to development of conceptual designs for solar receivers to augment or displace fossil (or other conventional) energy sources for application in the 2000 - 3000°F and 2 to 8 atmosphere pressure range.

Sanders Associates, Inc. has, under the aegis of one such program, performed parametric analyses of high temperature receivers in the 25 - 150 KWt range. Based on the findings of the parametric study, Sanders recommended further effort be applied to a windowed matrix receiver operating at 60 KWt output, 3 atmospheres absolute, and 2500°F outlet. During the second performance interval of this contract, Sanders developed and analytically evaluated a hardware design for a cost effective high temperature solar thermal receiver which can be readily interfaced to fuels and chemicals processes or to heat engines for power generation. The strict adherence to Design-to-Cost-Goal principles, and the parallel effort to employ only those materials currently within present production technology, has led to a design which offers an efficient and immediately cost effective alternate to other pressurized receivers in the above 540°C (1000°F) range. The design is fully within today's materials' state of the (manufacturing) art. This receiver could be built in production for less than $25.00 per KWt. The design performance analyses support an efficiency prediction of 79% to 86% including reflection and reradiation effects.

The Sanders HTSTR (Figure 1) is a pressurized cavity receiver which utilizes a fused quartz window at the aperture for pressure containment and silicon carbide honeycomb panels as the active solar conversion element. Internal receiver structure and integral thermal impedance is provided by the use of preformed semirigid insulation.

The receiver housing functions both as an ecto-skeleton and pressure vessel, per the ASME* boiler code using 0.25-inch thick cold-rolled steel. In view of the small internal volume of the receiver and dissimilitude of air and steam as working fluids, an obvious area of potential cost reduction is present in the housing structure.

*Section VIII ASME Boiler and Pressure Vessel Code, Unfired Pressure Vessels

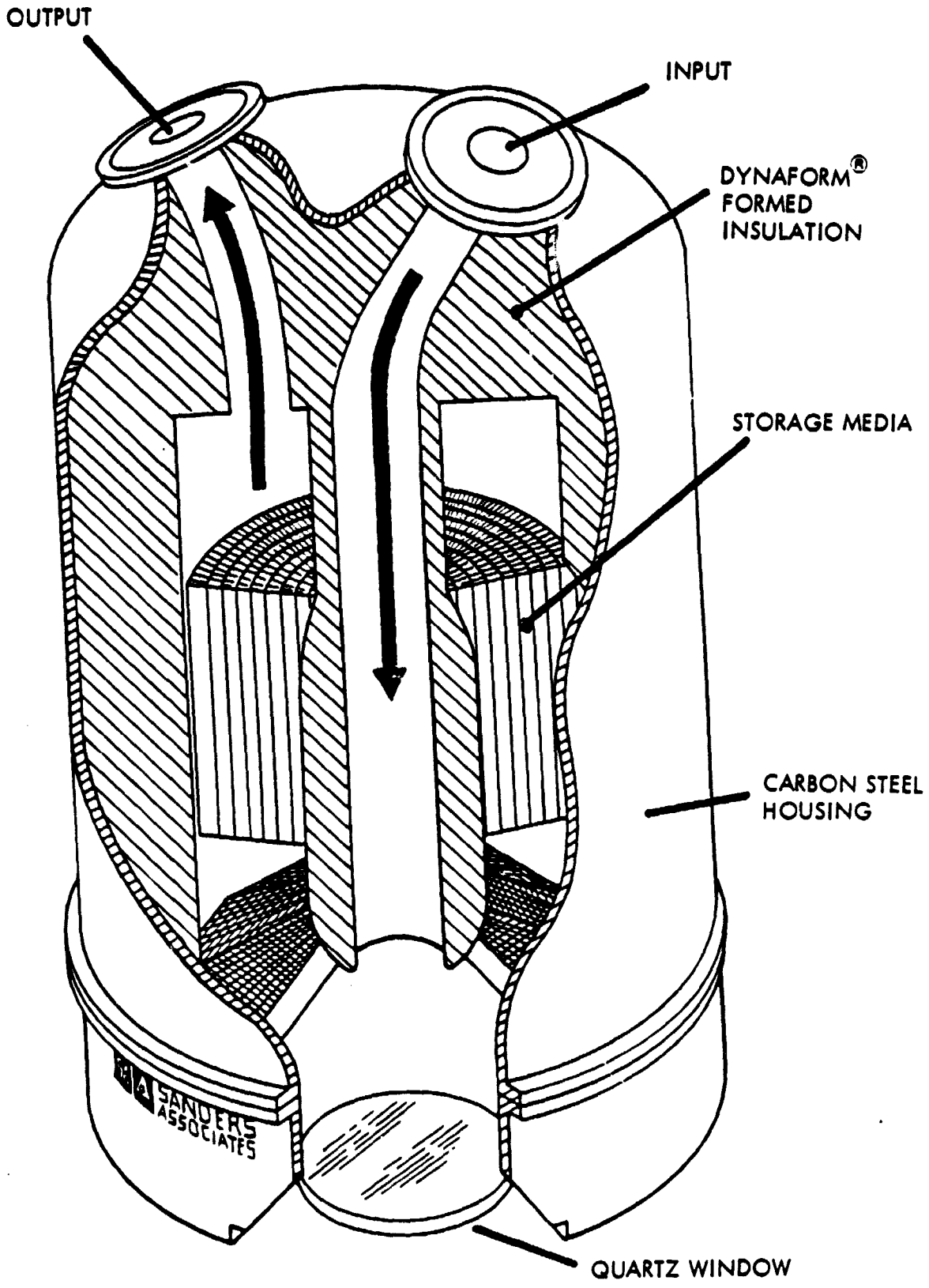

Figure 1. Pressurized Matrix HTSTR

Cost savings of up to $3.50 per kilowatt could be realized by use of a functionally designed housing in lieu of a boiler code constrained pressure vessel. This is a problem which appropriately should be addressed before mass production is initiated.

Silicon carbide (SiC) was selected for the active receiver panels because of its demonstrated suitability to the application. The panels are well within the present firing capacity size limits. Reliable and extended service is predicted for SiC in air at temperatures in the 2700° - 3000°F range. The material's high thermal conductivity, visible absorptivity, and thermal shock resistance support its selection as an unstressed matrix material.

The mullite storage material was chosen for its high temperature stability, sensible heat storage capacity, and low cost. As employed in the Sanders receiver, the mullite is not subject to sudden or severe thermal transients.

The key consideration in establishing the functional viability of the design is the development of an in-depth understanding of the flux distribution and its effects on the receiver. To this end, extensive flux modeling, window analysis, and receiver thermal simulation were conducted according to the flow chart of Figure 2.

The flow chart portrays the methodology employed in the iterative design and analysis process used to evolve the receiver from concept to preliminary prototype status. CPCFLX is an in-house code developed to predict flux distribution and power captured at the receiver.

Typical flux distributions are shown in Figure 3 for a receiver operating both with and without a CPC. Based on these projected flux levels at the receiver aperture, a window thermal analysis was performed using the optical and physical material properties of the selected fused quartz window. The window heat loading results from the spatial integration of the convoluted solar, cavity IR, and window transmittance spectra. Thermal analysis shows maximum window temperatures of 950°C or less.

The window analysis predictions, combined with Sanders' own real experience at White Sands in 1977, allows the prediction of long-term reliability for the windowed matrix HTSTR.

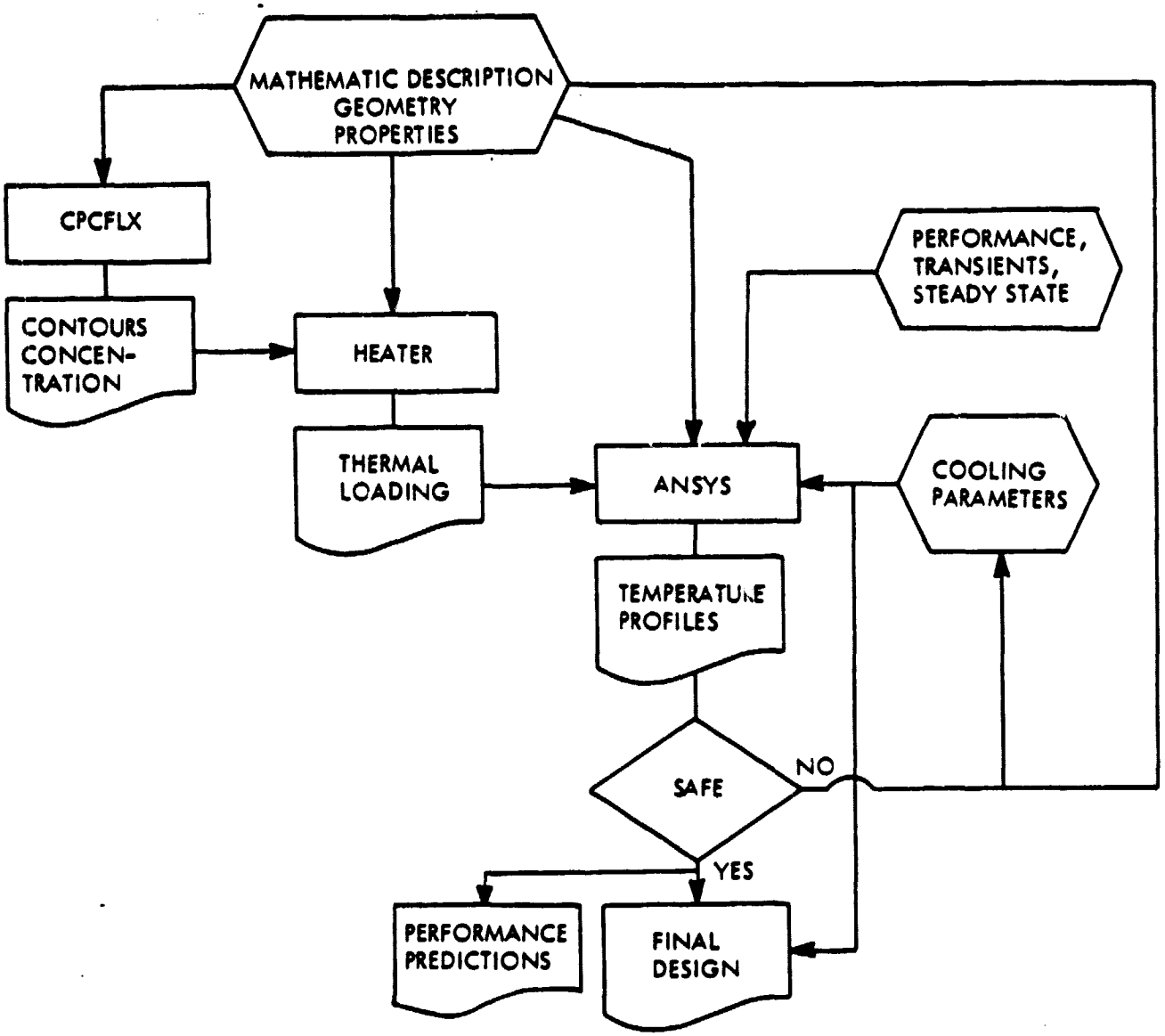

Figure 2. Methodology Flow Chart

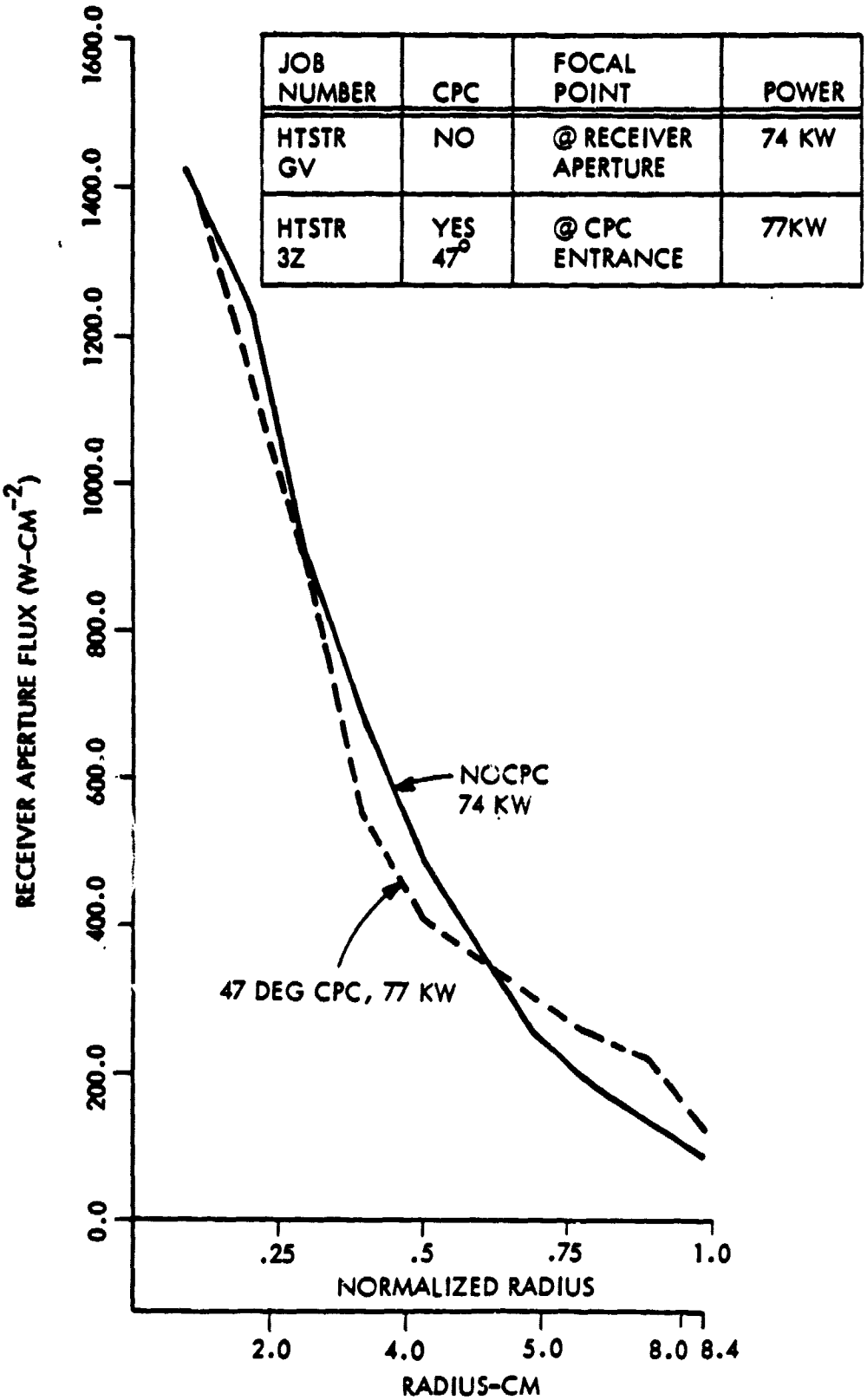

Figure 3. Typical Flux Distribution Flux vs Radius @ Window

SECTION 2
TECHNICAL DISCUSSION

2.1 FINDINGS OF THE PARAMETRIC ANALYSIS

2.1.1 General

The complete Parametric Analysis Report (82 pp) was submitted in September 1979 under separate cover. The principal recommendations from that analysis are iterated in the following paragraphs.

2.1.2 Parametric Analysis Recommendations

The windowed receivers are recommended for their superior capabilities. The two windowed concepts are very comparable in their overall evaluation but the balance favors the matrix receiver for the following reasons:

- The matrix receiver panels are fully within present day production capabilities.
- Thermal buffer material can be optionally installed or omitted.
- Thermal buffer material can be a less expensive material (Mullite, Alumina) than the receiver matrix (silicon carbide) because it is not exposed to step transients.
- Radiation losses from the thermal buffer are trapped by the receiver matrix and are returned to the airstream; the energy cannot escape through the aperture.

A review of the major points of the parametric analysis is presented below as they comprise the start point for the design and analysis work which was performed during Tasks 2, 3, and 4 of the study. The parametric analysis report itself should be referred to for a definitive description of the Task 1 work.

The subtasks (A-D) below are taken from the statement of work for Task 1. The results and findings from these subtasks are presented here as background for the subsequent sections of this report.

(a) Preliminary receiver performance calculations and graphs related to thermal efficiency, pressure drop, cavity temperature and flux distribution

The conversion efficiency is given in Table 1 for the baseline, 70 kW receiver/CPC combination with and without window as a function of temperature. Efficiency (η) is defined as power in (delivered to cavity) less reradiated power loss divided by power in:

$$\eta = \frac{P_{in} - P_{loss}}{P_{in}} = 1 - \frac{P_{loss}}{P_{in}}$$

TABLE 1. CAVITY EFFICIENCY

Temperature	Open Aperture	Windowed*
2000	0.912	0.937
2200	0.897	0.915
2400	0.891	0.895
2600	0.880	0.889
2800	0.864	0.874
3000	0.849	0.856

Table 2 summarizes the pressure drop data. Figure 4 depicts total flux versus position.

(b) A material selection based upon thermal cycling, life-cycle requirements, cost fabrication considerations and experience in similar or comparable technologies

Table 3 summarizes the physical characteristics of the materials examined. Table 4 shows material costs.

*Does not include 8% (dielectric) reflection at window surfaces. Thus overall radiative efficiency at 2000°F is 0.92 x 0.937 = 0.862.

TABLE 2. PRESSURE DROP SUMMARY

PHYSICAL PARAMETERS			WORKING FLUID		
Property	Symbol,	Units	Air	Nitrogen	Helium
Inlet Temp	T_I,	^oF	1750.0	1750.0	1750.0
Output Temp	T_O,	^oF	2500.0	2500.0	2500.0
Mass Flow	$\dot{m}$,	lb/sec	0.250	0.241	0.0853
Specific Heat @ 1750°F	Cp_I,	Btu/lb	0.279	0.288	1.25
Specific Heat @ 2500°F	Cp_O,	But/lb	0.289	0.301	1.25
Enthalpy Change	ΔH,	Btu/lb	213.	221.	624.
Power	P_M,	kW	56.2	56.2	56.2
Power	P_E,	Btu/hr	1.92E5	1.92E5	1.92E5
Pressure	p,	lb/ft^2	6480.	6480.	6480.
Gas Constant	R,	$ft/^oF$	53.4	55.2	386.
Density @ 3 ATM, 1750°F	ρ_I,	lb/ft^3	0.055	0.053	0.0076
Density @ 3 ATM, 2500°F	ρ_O,	lb/ft^3	0.041	0.040	0.0057
Volumetric FLow, 1750°F	$\dot{V}_I$,	ft^3/sec	4.54	4.55	11.2
Volumetric Flow, 2500°F	$\dot{V}_O$,	ft^3/sec	6.10	6.02	15.0
Tube ID	D_H,	inches	0.5	0.5	0.5
Number of Tube Pairs	N,		96.0	96.0	96.0
Total Flow Area	A,	ft^2	0.131	0.131	0.131
Velocity, RMS	$\bar{V}$,	ft/sec	41.0	40.7	101.0
Viscosity	μ,	lb/hr	4.39E2	4.13E2	4.76E2
Reynold's Number	N_R		6.72E3	6.87E3	2.12E3
Convective Film Coefficient	h,	$Btu/hr\ ft^2/^oF$	8.57	9.15	8.00
Active Length of Tubes	ℓ,	ft	5.0	5.0	5.0
Active Area of Tubes	A_c,	ft^2	62.8	62.8	62.8
Film Drop	ΔT	^oF	356.0	334.0	382.0
Friction Factor	f,		0.0091	0.009	0.0075-0.011
Pressure Drop	Δp,	lb/ft^2	88.0	83.0	61.0-90.0
% Pressure Drop	$\Delta p/p$,	%	1.4	1.3	.94-1.4

This table applies to the tube-header type receiver analyzed during Task 1. Pressure drops for the matrix receiver are smaller by at least one order of magnitude. Temperature, pressure and flow conditions correspond to design point for Task 2.

FLUX CONTOURS OVERLAYED ON
SCALE CROSS-SECTION OF SiC
RECEIVER PANEL

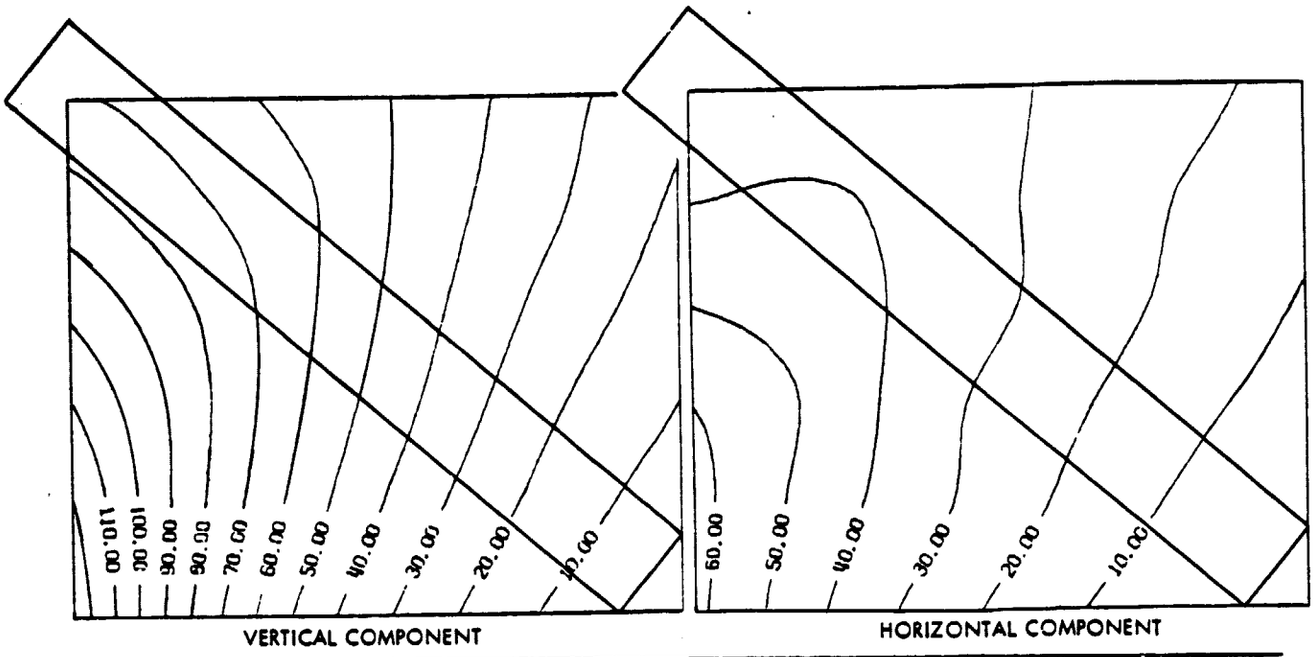

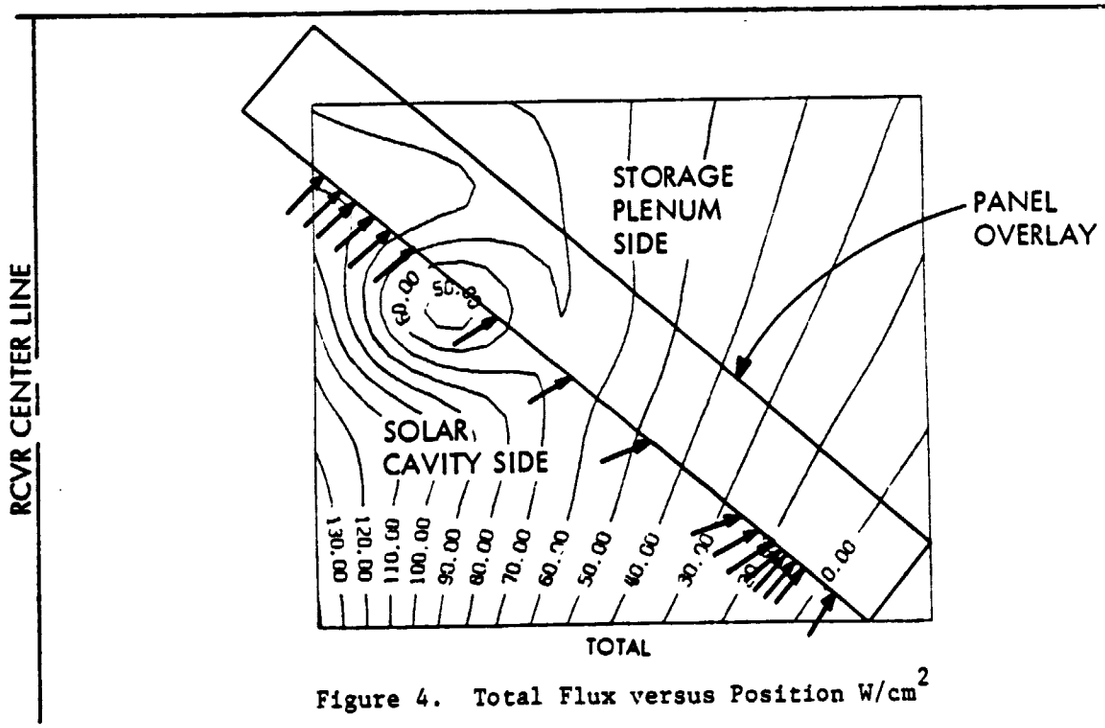

Figure 4. Total Flux versus Position W/cm^2

TABLE 3. HIGH TEMPERATURE PROPERTIES OF CERAMICS

MATERIAL	MAXIMUM TEMP (^{o}F)	ATMOSPHERE	THERMAL EXPANSION x$10^{-7}/^{o}$C	THERMAL CONDUCTIVITY @1000^{o}C (W/cm^{o}K)	THERMAL SHOCK RESISTANCE
SiC	2700	Air	50	0.3	Good-Fair
	2950	N_2,He			
Si_3N_4	2220	Air	40	0.06	Fair
	2750	N_2,He			
BN	2220	Air	68	0.2	Fair
	3000	N_2			
	2900	He			
Al_2O_3 (99.9)	3180	Air	85	0.08	Poor
	3025	N_2,He			
Cordierite	2200	Air	25	0.02	Excellent
	2025	N_2,He			
Mullite	2900	Air	50	0.03	Fair-Poor
	2700	He,N_2			
Fiber (Nextel 312)	2500	Air, N_2,He			Excellent

TABLE 4. MATERIALS RELATIVE COST

	RAW MATERIAL	PROCESSING
Lowest Cost	Cordierite	Cordierite
	Mullite	Mullite
	Alumina	Zirconia
	Zirconia	Alumina
	Silicon Carbide	
	Refractory Metals	
	Other Carbides	
Highest Cost	Nitrides	Silicon Carbide
		Refractory Metals
		Nitrides
		Other Carbides

Based on Sanders' operating experience over the past three years, silicon carbide and cordierite are known to be well suited to application in matrix or windowed extended surface receivers where thermal diffusivity and expansion are the controlling parameters. In these concepts, radiant energy is absorbed on the surface of a thin ceramic section. The energy is then convected off the same surface. Thermal stresses in these applications (based on modeling performed under prior contracts) are approximately an order of magnitude smaller, than in alternate materials.

Mullite is known to be a well-suited, sensible heat storage media and has been used in the steel industry (blast furnaces) for decades. It exhibits long life in those applications. Mullite could be used in the matrix receiver as the auxiliary thermal buffer mass where it would be isolated from radiantly and convectively induced thermal shocks.

(c) Weight estimate and space envelope diagram with identification of major components, physical arrangement, necessary supporting devices and auxiliary equipment

The four configurations with options were analyzed to provide a weight and center of gravity estimate. Figures presented in Table 5 refer to the 70 kW baseline design.

TABLE 5. WEIGHT ESTIMATES
(from Table 1)

Configuration	Storage	Weight, lbs	CG, inches*
Matrix, Windowed	No	180	12.7
Matrix, Windowed	Yes	310	14.1
Extended Surface, Open	No	131	15.8
Extended Surface, Windowed	Yes	337	13.9
Tubed	Yes	287	15.2

*Distance behind window, on axial centerline.

(d) The merits of various thermal energy storage systems shall be assessed with respect to thermal efficiency, size, weight, cost and material compatibility. Storage time to be considered should be up to 3 minutes

Thermal buffer material can be optionally installed or omitted. Thermal buffer material can be a less expensive material (Mullite, Alumina) than the matrix (silicon carbide) because it is not exposed to step transients. Radiation losses from the thermal buffer are trapped by the matrix and are returned to the airstream; the energy cannot escape through the aperture. The 70 kW model (Figure 5) weighs 180 pounds as shown or 310 pounds with additional thermal buffer.

2.2 CONCEPTUAL DESIGN

2.2.1 Introduction

The work performed in Tasks 2, 3, and 4 of the contract has been performed in accordance with the contractual statement of work and by subsequent JPL Technical Direction Memoranda 001 and 002. These requirements are presented below.

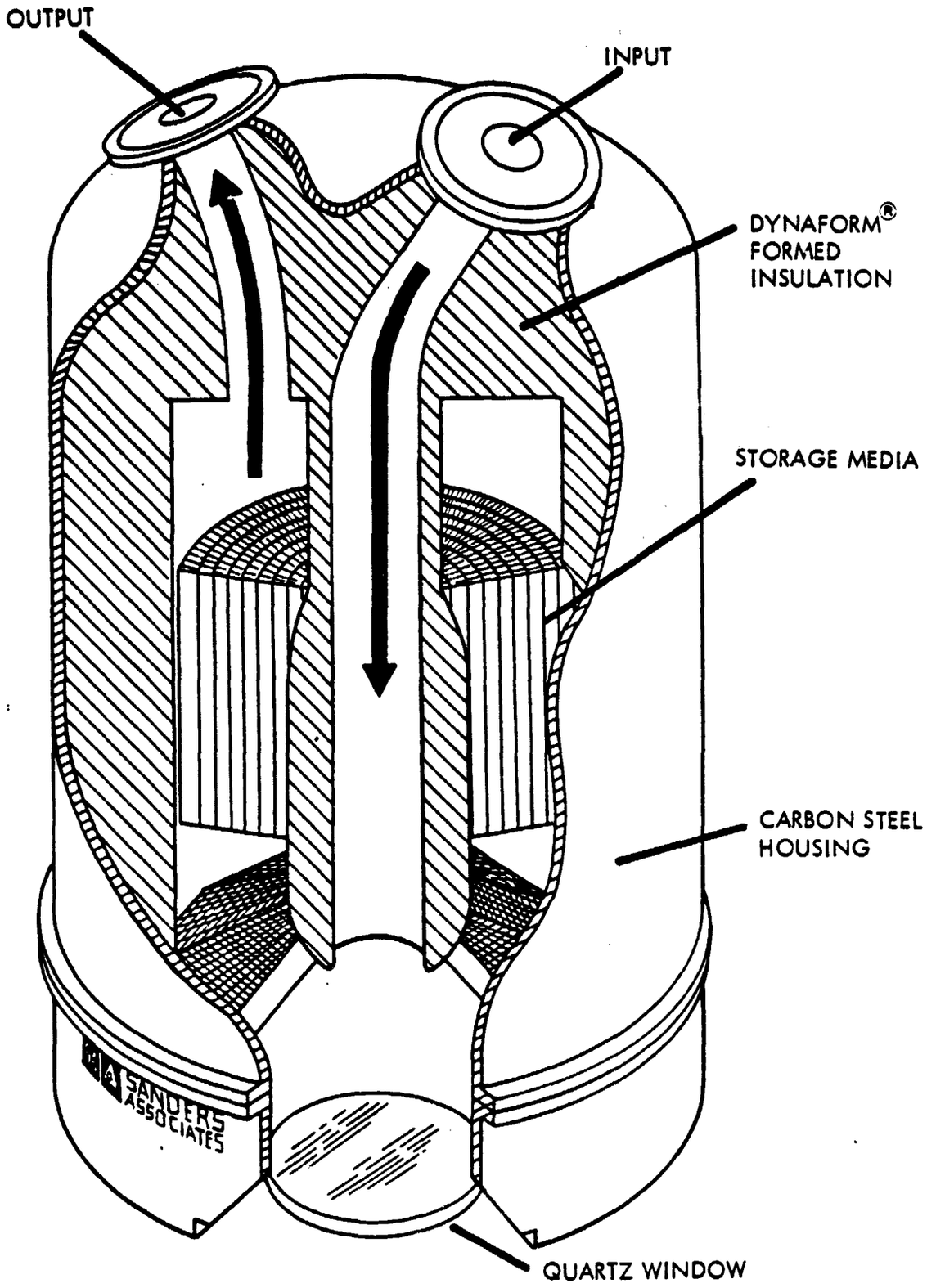

Figure 5. High Temperature Solar Thermal Receiver

2.2.2 Statement of Work Contents

Task 2 - Conceptual Design

Prepare a conceptual design for the engineering definition and preliminary performances established in Task 1. The conceptual design shall be of sufficient detail to provide the basis for engineering cost estimates and preparation of prototype of production versions of the component design indicated in Task 4. The results of this effort shall include the following:

(A) Complete receiver performance analysis including heat losses. Computations of efficiency over range of stated power inputs given in Exhibit I.

(B) Pressure drop of working fluid through the receiver for the inlet pressures given in Exhibit I (not to exceed 4% of inlet pressure).

(C) Materials selection and rationale for selection.

(D) Conceptual design drawings.

(E) Narrative explaining the receiver design, operation and salient features.

(F) Engineering analysis, assumptions and rationale in the following areas:

(i) Concentrator optical quality, thermal, and mechanical design aspects including special seals.

(ii) Structural analysis to indicate adequate strength and rigidity.

(iii) Fluid flow analysis of heat transfer capability to meet the energy, temperature, pressure, and other operational requirements.

(iv) Control system schematic and analysis to assure stability under all conditions of operation.

(v) Weight estimates, envelope diagram and an estimate of the center of mass.

Task 3 - Receiver Operation and Performance Requirements

Characterize operational and performance requirements associated with the receiver design, especially those items or operational considerations that are necessary for successful operation of the entire solar concentrator including the receiver design. In the performance of this task, the Contractor shall:

(A) Identify any special requirements related to preferred receiver orientation and position, etc.

(B) Identify requirements or interfaces needed to mount and connect the receiver to the concentrator.

(C) Indicate preferred receiver hook-up with heat engine or heat exchange equipment which circulates chemical or toxic materials.

(D) Indicate the receiver response capability at step inputs from zero to 50% and zero to 100% insolation. (See Figure 4 of Exhibit I for maximum insolation value.) The temperature rise versus time of the critical components should be characterized.

(E) Estimate the maximum duration and temperature that the receiver can tolerate without permanent damage with maximum solar input and no fluid flow in the heating passages. (See Figure 4 of Exhibit I.) Assume maximum operating temperatures prior to fluid flow interruption within the receiver.

(F) Identify special problems or considerations due to transients as a result of start-up, shutdown or intermittent cloud cover.

(G) Indicate any special safety considerations to receiver and personnel during the start-up, operational or shutdown phases.

Task 4 - Production Cost Estimates

Furnish a cost estimate related to mass producing the high temperature receiver described in this Statement of Work. The estimates should include producing 1,000, 10,000, 100,000 and 1,000,000 units per year on a continuous basis. The following information is required:

(A) Mass production techniques and processes associated with the various assembly operations.

(B) Existing major equipment within the plant to be used and equipment that must be developed for production operations. Capital investments should include tooling, facilities and other related items.

(C) Graphs showing cost per unit as a function of number of units.

(D) Key design features enhancing the receiver subsystem operating life and maintenance requirements during its lifetime.

Contents of TDM 001

The contractor is directed as follows:

The options and recommendations presented at the reveiw following Task 1 of the subject contract have been re-examined and discussed. Consideration has inlcuded the effects of work from other programs and contracts. As a result, I concur with your recommendation to proceed to a more detailed analysis and design of Concept Number 1 (i.e., matrix type with window and thermal storage matrix).

The following design point has been selected for the high temperature receiver operation. It assumes operation in conjunction with an advanced high temperature Brayton engine (20 kWe).

Working fluid-air	Mass flow	- 0.25 lbs/sec.
Inlet temperature - 1750°F	Inlet pressure	- 45 psia
Outlet temperature - 2500°F	Pressure drop ($\Delta p/p$)	- 0.04 max.

Assume the use of a concentrator with a 2 mrad slope error.

I will discuss with you the off design range of operation that should be analyzed in the near future.

Contents of TDM 002

The contractor is directed as follows:

Design point definition for the high temperature solar receiver has previously been provided to the contractor (TDM 001). The purpose of this directive is to define the possible off-design operation regimes by specifying the appropriate range expected in the following parameters:

mass flow	0.2 - 0.3 lb m/sec
pressure ratio	2 to 8
inlet temperature	$\pm$ 150°F
outlet temperature	$\pm$ 150°F

The entire envelope of operating states described above may not be practically attainable by the specific concept design selected. Therefore, at his discretion, the contractor may limit his analysis and exclude certain regimes defined above. However, such curtailment of the operation range(s) should be discussed and rationale presented.

2.2.3 HTSTR Design

The Sanders High Temperature Solar Thermal Receiver (HTSTR) has been designed as a production - oriented, high volume device with a design goal price of $25/per kWt. As such the design utilizes materials and fabrication processes well within the present manufacturing state-of-the-art. Intrinsically expensive materials

have been avoided. Accessories (particularly a terminal concentrator) have been discarded when their cost increment exceeds their performance benefits. Design-to-cost principles were vigorously pursued through all phases of the design with the result that the receiver satisfies not only its performance requirements but offers a low cost alternate to other receivers designed for the under 1100°C(2000°F) temperature regimes.

The active receiver elements within the cavity, which provide substantial cost savings, are the thin walled (non-pressurized) receiver and storage matrices. Use of these simple and inexpensive components is made possible by pressurizing the entire reciever housing. Solar energy is admitted to the receiver cavity through a fused quartz (General Electric Type 124) window which functions as a transparent pressure bulkhead. In view of: (a) the key role which the window plays in the receiver operation, and (b) the high solar concentration, the window has emerged as the prominent technical issue affecting receiver viability.

In response to this fact and frequent informal reviews and discussions with JPL regarding the window issue, a very thorough and conservative engineering analysis of the window heating and cooling requirements was performed through several refinements and iterations. Detailed results of this study are presented later (Section 2.3) in this report, but the window (and hence the receiver) are shown to survive even in light of the extreme conservatism exercised during the analysis.

The analysis in its extremism has described a worst case performance environment for the window. Deviations of the real world from the assumptions used in the analysis are likely only to reduce window temperatures from the maximum indicated by the analysis (980°C).

The assumptions, used in the window analysis are listed in Tables 6 and 7 with a brief estimate of their impact on the analysis. The sensitivity of the window to several of these parameters has not been quantitatively determined due to time and budget constraints. Additional work in the form of a scientific research experiment (SRE) as part of the receiver development contract is clearly warranted.

TABLE 6. ASSUMPTIONS AND RATIONALES

	Assumption	Rationale	Impact
1.	Solar Energy Extends from 0.28 to 15μ.	NASA/Theakara 1971 Extraterrestrial Modified by Air Mass 1 absorptivity. Daylight and its Spectrum	Adds 2.5 percent beyond 2.8μ in a highly absorptive window band. This light would normally be absorbed on the second surface mirror. Adds 10% to solar absorption.
2.	Light in "opaque" bands is absorbed in first incremental layer of window rather than on surface.	Consistent with requirments of selected finite element model. Reduces convection off both surfaces.	Imposes additional temperature gradient over both front and rear increment of window thickness. Estimated impact is about 25°C of maximum temperature rise.
3.	Mean path length of light was determined by ray tracing and index of refraction data.	Models rays impinging window from primary concentrator.	
4.	Window loading determined by spectral iteration and spatial integration.	Models real case.	Distributes heat exponentially within window and significantly increases temperatures over less rigorous methods.
5.	Solar flux modeled assuming 2 mrad slope error on primary.	By TDM direction. This is probably an optimistic estimate of mirror accuracy.	Results in sharp peaking of solar flux at center of window.
6.	Air mass 1.0 absorption characteristics assumed.	Directed by contract insolation reference data. Generally an extreme not often encountered except at solar noon on clear days with low sky turbidity.	Increases solar loading by 10-20% over normal maxima.

TABLE 6. ASSUMPTIONS AND RATIONALES (CONTINUED)

Assumption		Rationale	Impact
7.	Thermal conductivity of quartz used, does not specifically include internal radiation effects. (Figure 6)	Any internal radiation effects (as used in JPL analysis) will reduce thermal gradients.	Factor of 2 in the used conductivities would reduce window temperatures by about 250°C.
8.	Window edge was assumed to be adiabatic.	Simplifies model but increases calculated temperatures.	Likely a second order effect but should be investigated later. Inclusion of a radiating window edge would slightly lower window temperatures.
9.	IR radiation is completely absorbed by the quartz without reflection due to dielectric and reststrahlung effects. (Figure 7)	A sample of fused quartz was tested for IR reflectivity and reststrahlung was found to be important only in the 7.5 to 10μ range.	Increases IR loading by only a small fraction of a percent.
10.	Optimum window geometry has not been identified, but a working solution has been found.	A trade-off exists between pressure stress and temperature rises as a function of thickness. In addition window curvature would reduce stresses.	The solution presented represents a severe case which can be mitigated by more favorable geometry.
11.	Obvious cooling enhancement techniques such as use of cooler convection fluid temperatures have not been evaluated on a system basis.	Maximum simplicity is achieved by using inlet air at 955°C (1750°F) for internal cooling/ and compressor bleed air at 149°C (300°F) for external cooling.	Temperature Sensitivity to Cooling Air Changes: $\frac{\Delta t \text{ internal air}}{\Delta t \text{ window}} = \frac{100^{\circ}C}{80^{\circ}C}$, and $\frac{\Delta t \text{ external air}}{\Delta t \text{ window}} = \frac{100^{\circ}C}{25^{\circ}C}$

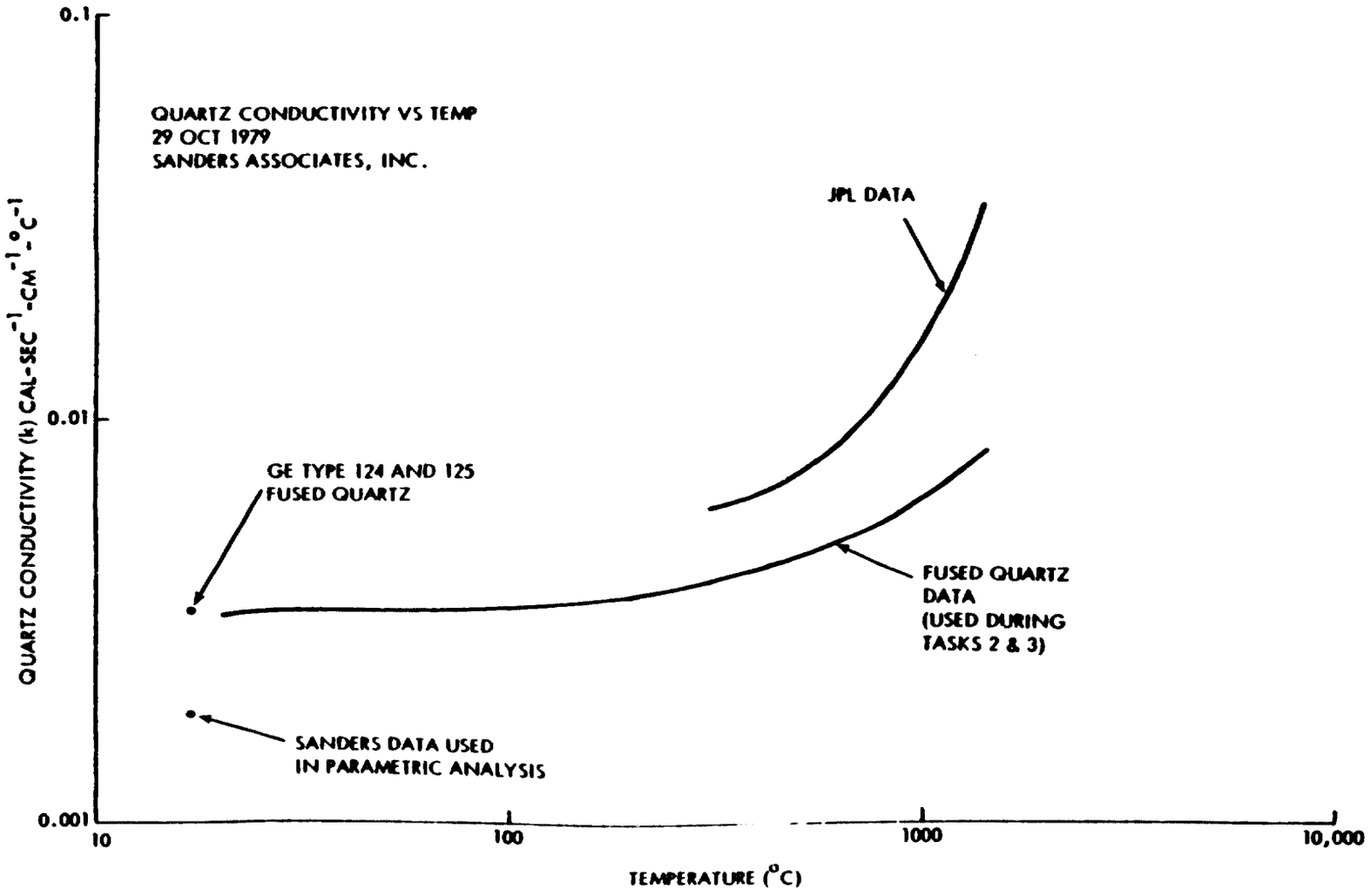

Figure 6. Quartz Conductivity versus Temperature

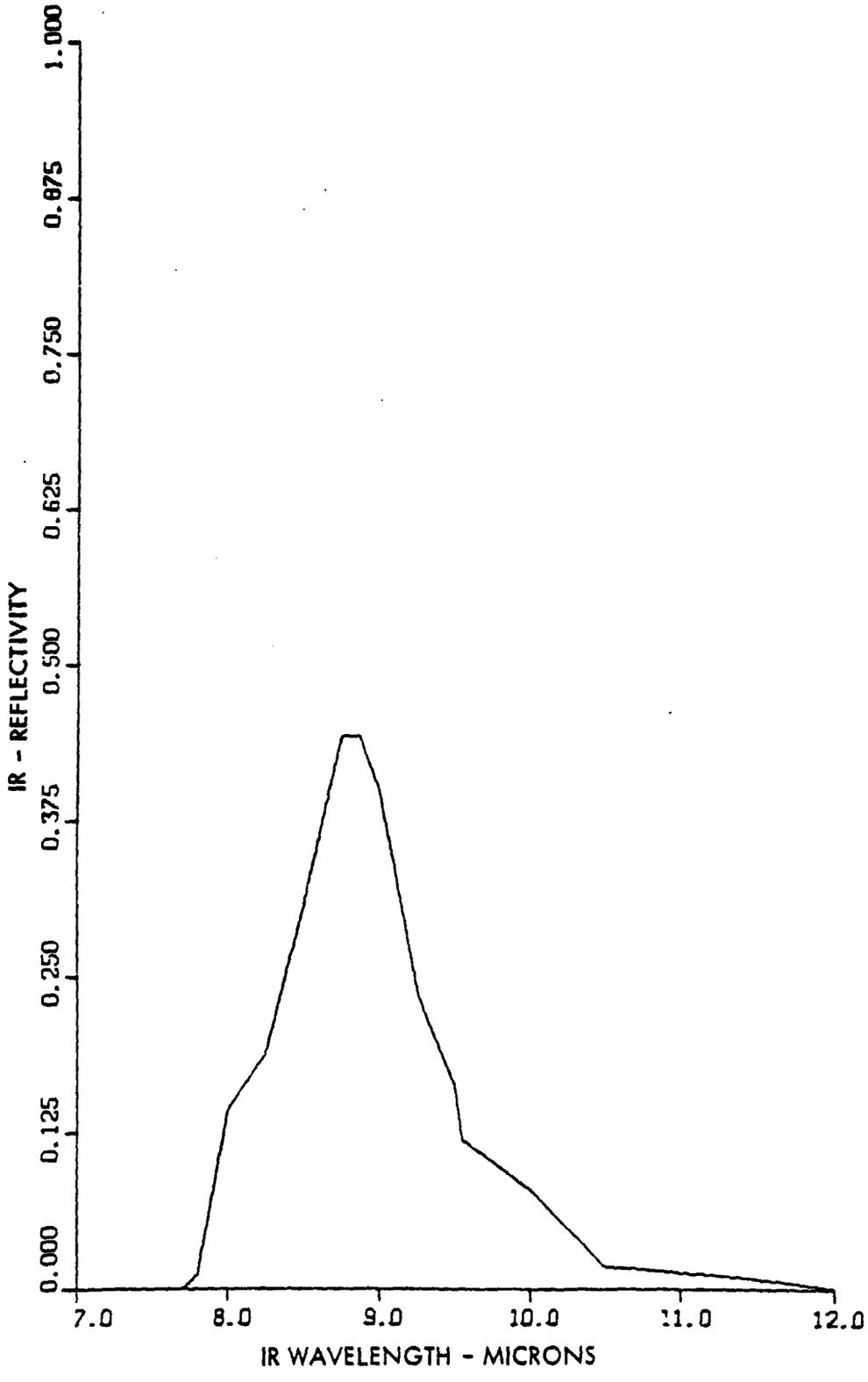

Figure 7. Reststrahlung Diminution of IR Absorption

TABLE 7. GENERAL ASSUMPTIONS

Assumption	Justification
1. Inlet Air: 1750	Contract & TDM
2. Outlet Air 2500	Contract & TDM
3. Mass Flow 0.2 - 0.3 lb sec^{-1}	Contract & TDM
4. Pressure Ratio 3:1	Contract & TDM
5. Input Power: 100% - 73.8 kW	Flux Analysis
6. Window cooling film coefficients Internal: 50 BTU HR^{-1} Ft^{-2} $^{o}_{\iota}{}^{-1}$ External: 100 BTU HR^{-1} Ft^{-2} $^{o}_{F}{}^{-1}$	Achievable with impingement cooling
7. Ambient air: $75^{o}F$	Maximizes Losses
8. Mirror reflectivity: 0.90	Contract Exhibit
9. Mirror slope error: 2 mrad	Contract & TDM
10. Working fluid: Air	TDM 001

2.3 RECEIVER PERFORMANCE ANALYSIS

The HTSTR was analyzed with a finite element model of a solar receiver that was developed at Sanders and has been in continuous evolution since 1976. The advantage of such a finite element program based on currently available software (the same goes for finite differences) is its flexibility. Thus, while a specialized program can always be developed for a given model that runs more efficiently than our model, the inherent flexibility of the commercial software makes it possible to investigate variations, such as addition or deletion of terms from the heat balance equations used, or in the refinement or subdivision of thermal nodes, with a relatively small programming and verification effort. This saving in analysis time more than offsets computer run costs. Of more importance, it encourages exploration of design variations that allow a model to evolve toward a good balance of complexity with experimental measurement accuracies in test equipment. Sanders' model has been correlated with tests of developmental receivers at scales from 10 kW to 250 kW of insolation in all of the respects that have been found significant, without being too cumbersome or costly to run.

As in any analysis used for design purposes, model complexity is kept within bounds by selection of a number of reasonable physical approximations which enter implicitly in the correspondence between the actual configuration and the selected modeling representation, as well as in several choices that are more directly visible. While many of the choices are technically hypothetical, and therefore subject to judgment and questioning, good correspondence to test data circumvents many potential arguments and tends to validate a model more firmly as a greater variety of tests meet with reasonable correspondence.

To the extent the approximations are established and agreed upon, the numerics are objective, and can be arrived at by any of a variety of currently available computer-software combinations. For the present program, all the physical effects judged to be important in a solar receiver in the appropriate temperature range have been presented and all the model parameters have been estimated to a reasonable degree to match the approximations inherent in Sanders' basic model. The derivation of the input information which the model calls upon from the selected design configuration will be discussed.

2.3.1 Inputs

The organization of a finite element model requires statements of: (a) geometry, (b) material properties and (c) boundary and initial conditions in different sections of the program. While some of the distinctions are arbitrary, consistency is most essential. We shall follow the separation made in our model.

2.3.1.1 Geometry

In the present model, the inlet and outlet chambers are represented with relatively coarse refinement compared to the honeycomb, where much more detail is used. At the temperatures involved, radiation effects are of major importance. As such, they are represented for each zone of subdivision (node) by appropriate emissivity, surface area and radiation configuration factor. Since many of the radiating surfaces have emissivities significantly less than unity, and since they interact in groups of three or more, a number of "graybody radiation effects" must be accounted for.

Kreith shows how the net heat transfer between two gray cylindrical surfaces, one enclosing the other, is given by:

$$q_1 = \frac{A_1(E_{b1} - E_{b2})}{\frac{1}{\varepsilon_1} + \frac{A_1}{A_2}\left(\frac{1}{\varepsilon_2} - 1\right)}$$

where A_2 is the outer and A_1 the inner surface. Along with a lengthy derivation based on simultaneous equations of heat balance, he shows a network analog, top of Figure 8 that would yield the same solution for this two-body radiation exchange. He further extends it to a four body exchange. What we have done is replace the concepts of blackbody radiation potential E_b and radiosity, J with a "real node" at temperature T, as measured by all but radiative effects at the body itself, and a "phantom node" at T' which is only involved in radiation exchanges. If we use Kreith's "resistance" term,

---

(1) F. Kreith, "Principles of Heat Transfer", Textbook Co., 1973, pp 255-286.

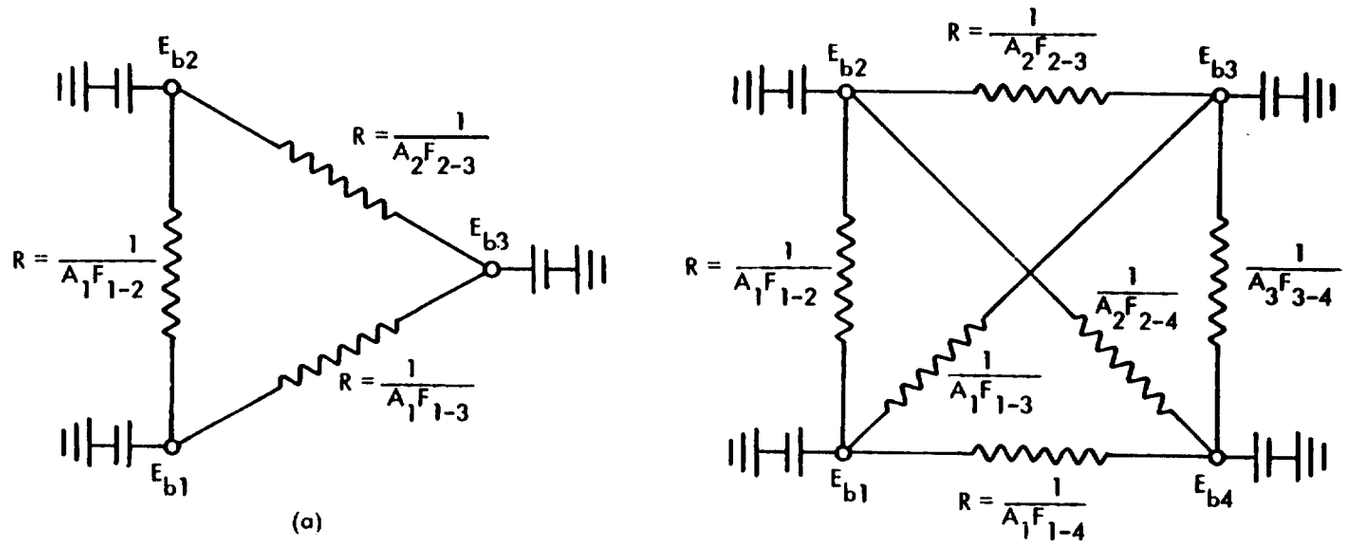

Figure 8. Equivalent Networks for Radiation in Gray Enclosures Consisting of Two and Four S
(a) Two Gray Body Surfaces, (b) Four Gray Body Surfaces

$$\frac{1-\varepsilon_i}{\varepsilon_i A_i},$$

to account for the temperature difference between real and phantom nodes as

$$T_i^4 - (T_i')^4 = q_i \frac{1-\varepsilon_i}{\varepsilon_i A_i}$$

and equate the right hand side to a standard form of the Maxwell-Boltzmann equation:

$$T_i^4 - (T_i')^4 = q_i \frac{1}{\sigma \varepsilon_{eff} A_{eff} F_{eff}}$$

we see that if we made the choices

$$A_{eff} = A_i$$

$$\varepsilon_{eff} = \frac{\varepsilon_i}{1-\varepsilon_i}$$

$$F_{eff} = 1$$

for the link between T and T′, we would get the same resistance as Kreith,

$$R = \frac{1-\varepsilon_i}{A_i \varepsilon_i} \quad .$$

If, further, we made the choice for the link between the "phantom nodes" T_i' and T_j' linking two different areas

$$A_{eff} = A_i \qquad \text{or} \qquad A_{eff} = A_j$$
$$\varepsilon_{eff} = 1 \qquad\qquad \varepsilon_{eff} = 1$$
$$F_{eff} = F_{i-j} \qquad\qquad F_{eff} = F_{j-i}$$

we would get the "resistance"

$$R = \frac{1}{A_i F_{ij}} = \frac{1}{A_j F_{ji}}$$

as does Kreith.

So far, we have done nothing materially different from Kreith's illustration except made one set of choices among others possible. We have also been consistent between our rules and Kreith's four-gray--body interaction, also in Figure 8, which shows how a network-solving computer could save much algebra.

What we add by our interpretations may be placed in perspective by noting that Kreith's discussion applies to a network representation that deals with radiation only, with T^4 as the potential, $\sigma\, \varepsilon_{eff}\, A_{eff}\, F_{eff}$ as 1/R and heat flow, $\dot{q}$ as current. In other parts of his book, he treats linear thermal networks where T represents a potential, UA,(K/Δx)A, or $\dot{m}\ c_p A \sim 1/R$ and $\dot{q}$ is current. Our hypothesis is that we can deal on a single, comprehensive basis with a network solving computer, such as a finite element or finite difference software system can provide, treating radiation together with other heat transfer in terms of simple elements that solve

$$q_{ij} = \sigma\, \varepsilon_{eff}\, A_{eff}\, F_{eff}\, (T_i^4 - T_j^4)$$

for radiations

$$q_{ij} = hA(T_i - T_j) \text{ Convections}$$

$$= \frac{k}{\Delta x} A(T_i - T_j) \text{ Conduction}$$

$$= \dot{m}\ c_p A\ (T_i - T_j)$$

fluid heat transport and solve them all together provided we model gray body radiation with pairs of elements using the above rules.

We give an example in which a blackbody case is broadened to cover a gray body situation. Black body radiation impedances can be network modeled as shown in excerpted Figure 9(b). Node radiation potentials (E_{b1}, E_{b2},.....) occur at the

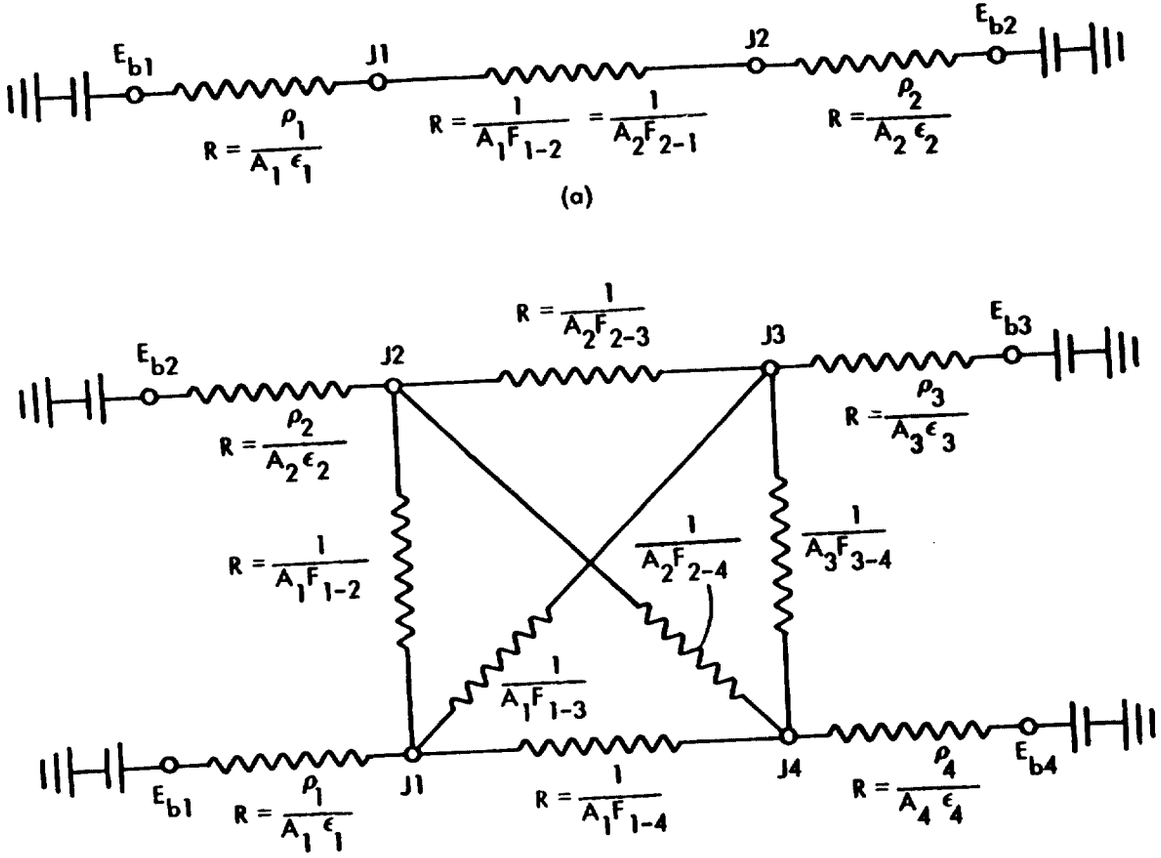

Figure 9. Equivalent Networks for Radiation in Black Body Enclosures consisting of three and four Surfaces

respective node temperatures. The node to node impedances are inversely proportional to the product of source area and source to sink view factor; e.g.,

$$R = \frac{1}{A_2 F_{2-3}} \quad .$$

Figure 8(b) from Kreith shows a network equivalent of gray body radiation impedances. Node radiation potentials (E_{b1}, E_{b2},....) again occur at the respective node temperatures. However, the actual radiosity of the nodes (J_1, J_2, ...) is reduced by the gray surface impedances,

$$R = \frac{1-\varepsilon_2}{A_2 \varepsilon_2} \quad .$$

In Figure 8(b), reflectivity is complementary to emissivity, that is $\rho = 1 - \varepsilon$. Then the actual radiation which occurs from surface to surface ($J_2 \rightarrow J_3$), for example is inversely proportional to the product of the source area and source to sink view factor,

$$R = \frac{1}{A_2 F_{2-3}} \quad .$$

Note that the intersurface impedance is of the same form in both black and gray network models, but that the radiosity between gray surfaces are closer together than the radiation potentials of black nodes. If E_{b1} is at maximum temperature and E_{b4} is at minimum temperature it should be intuitively obvious that

$$E_{b1} > J_1 > J_4 > E_{b4} \quad .$$

The radiation potentials, according to the Stefan-Boltzmann law, is $E_{b1} = \sigma T_1^4$. Considering now that the radiation between surfaces 1 and 4, as defined by the surface radiosities, J_1 and J_4 and the intersurface radiation impedance,

$$R = \frac{1}{A_1 F_{1-4}}$$

is of the same form as for the black body network shown in Figure 9(b), it is perfectly consistent to define the radiosities in accordance with the Stefan-Boltzmann, if we use an effective surface temperature, T'. Then, for example, $J_1 = \sigma (T_1')^4$.

We have applied this concept to the ANSYS modal of the receiver by use of "phantom"nodes. In our model the physical node 1 has a radiation potential E_{b1}. The corresponding "phantom" node, 101, has radiosity J_1. There exist similar mode/"phantom"node pairs 4, 104 and so forth. The finite element program can then calculate equivalent black body radiation temperatures for the physically grey nodes. Heat transfer between nodes 1 and 4 are then modeled as shown below.

Convection $$\dot{Q}_H = HA\ (T_1 - T_4)$$

Conduction $$\dot{Q}_K = \frac{bA}{x}\ (T_1 - T_4)$$

Radiation $$\dot{Q}_{R_{1-101}} = \sigma(T_1^4 - T_{101}^4) \cdot \frac{A_1\epsilon_1}{1-\epsilon_1}$$

$$\dot{Q}_{R_{101-104}} = \sigma(T_{101}^4 - T_{104}^4) \cdot \frac{A_1F_{1-4}}{1}$$

$$\dot{Q}_{R_{104-4}} = \sigma(T_{104}^4 - T_4^4) \cdot \frac{A_4\epsilon_4}{1-\epsilon_4}$$

Note that all internodal radiation is channeled through the associated phantom nodes, but conduction and convection internodal transfer passes directly from physical node to physical node.

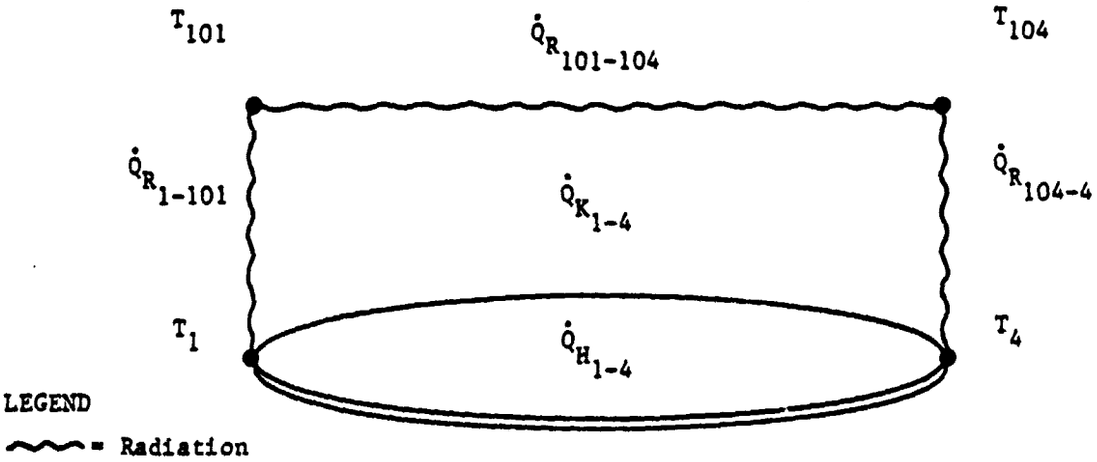

LEGEND

~~~ = Radiation

——— = Conduction

▬▬ = Convection
~~~

These expressions, plus Kirchoff's laws lead to the familiar results in Kreith's examples, as well as other test cases.

One further adaptation in modeling windows that are transparent at some wavelength ranges, and absorbent (or reflective) elsewhere is to modify the configuration factor for elements connecting two solid nodes through the window by $F_{X\text{-window}} \longleftarrow \tau_{window} F_{X\text{-window}}$ where τ_{window} is the transmission averaged over the spectrum at approximately the node temperatures:

$$\tau_W = \frac{\int \tau(\lambda) R(\lambda;T) d\lambda}{\int R(\lambda:T) d\lambda}$$

where $R(\lambda;T)$ is the Planck radiation spectrum, a function of wavelength, λ. Parameter T is the "average" temperature of the pair of nodes involved.

Similarly, when modeling emissivity in the element connecting the window in its emitting band (or absorption band) replace $\varepsilon/(1-\varepsilon)$ by $(1-\tau_W)/\tau_W$, assuming negligible reflection in $\alpha + t + r = 1$.

The values used for the various constants in the model will be tabulated without further comment or justification at this time. It is understood that any of these selections can be further expanded upon to any degree judged essential, but a complete enumeration of all these selections and their bases would draw upon a considerable body of experience in modeling and on comparison with test results. All the geometric constants have been methodically arranged so that any desired change in Table 8 can be carried out by modifying the corresponding entry in the model card deck. Figure 10 illustrates schematically where the elements are in the model.

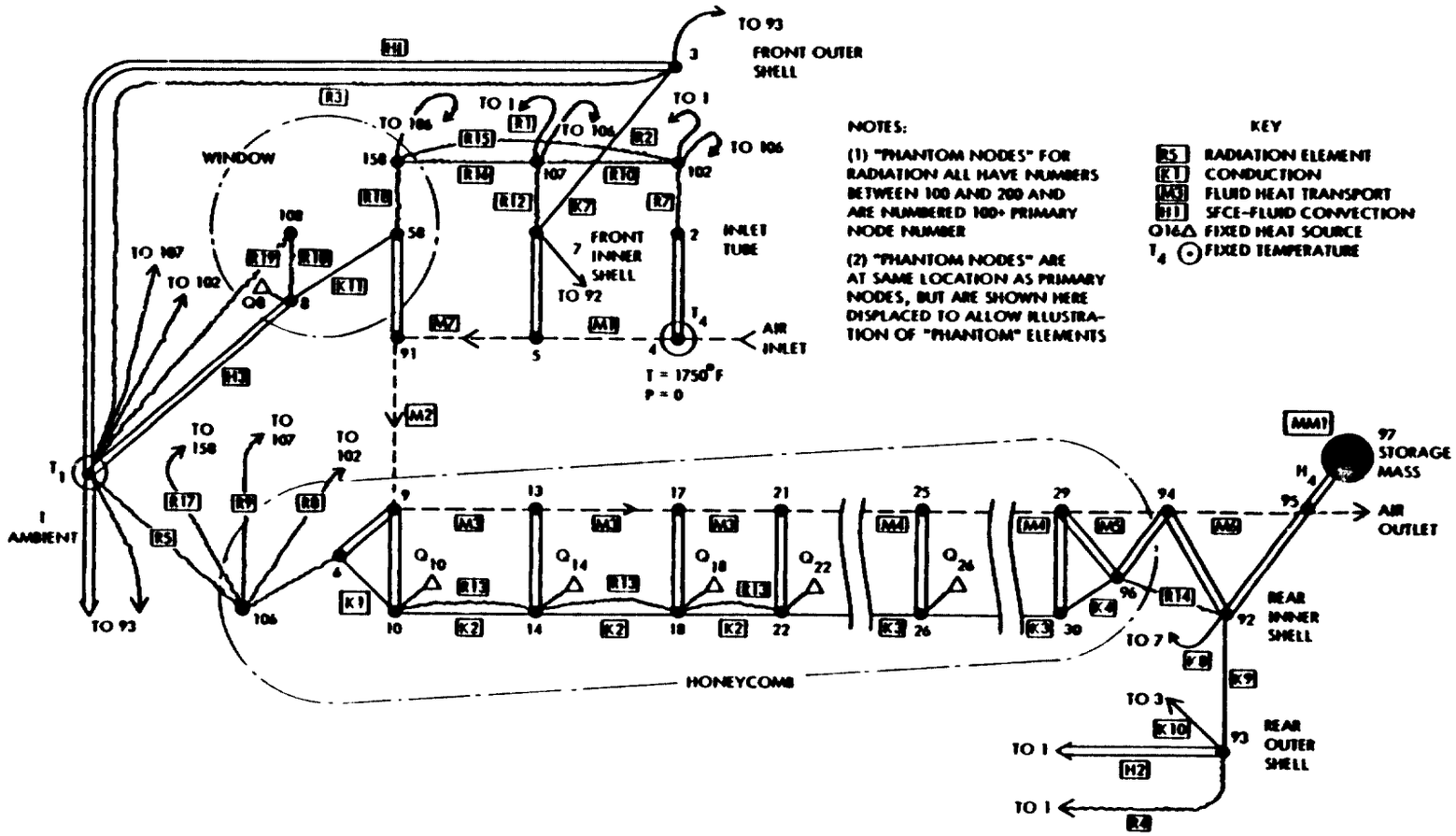

Figure 10. Thermal Schematic of Receiver Model Showing Relation of "Geometric" Constants to Nodes and Elements

TABLE 8. VALUES OF "GEOMETRY" CONSTANTS USED IN SOLAR RECEIVER MODEL [illegible]MP

A. RADIATION ELEMENTS*

	Emissivity	Area (Ft^2)	View Factor F	Comments
R1	1.0 E_7	0.135 A_7	0.0270 $\tau_W \times F_{7-\infty}$	Coupling through transmitting window
R2	1.0 E_2	1.25 A_2	0.0109 $\tau_W \times F_{2-\infty}$	Coupling through transmitting window
R3	0.3 E_{SKIN}	5.28 $A_{FRT\ SHELL}$	1.0	
R4	0.3 E_{SKIN}	17.7 $A_{RR\ SHELL}$	1.0	
R5	1.0	1.28 A_{HCOMB}	0.027 $\tau_W \times F_{HCOMB-\infty}$	Coupling through transmitting window
R6		NOT USED		
R7	0.25 $E_7/(1-E_7)$	0.135 A_7	1.0	2-102 Phantom
R8	1.0	1.28 A_7 or A_{HCOMB}	0.217 F_{7-H} or F_{H-7}	
R9	1.0	1.28 A_2 or A_{HCOMB}	0.770 F_{2-H} or F_{H-2}	
R10	1.0	0.135 A_2 or A_7	0.03157 F_{2-7} or F_{7-2}	
R11	9.0 $E_H/(1-E_H)$	1.28 A_{HCOMB}	1.0	6-106 Phantom

*Refer to schematic diagram, Figure 10 for specific location in thermal network.

TABLE 8. VALUES OF "GEOMETRY" CONSTANTS USED IN SOLAR RECEIVER MODEL HTEMP (Continued)

	Emissivity	Area (Ft^2)	View Factor F	Comments
R12	0.25 $\varepsilon_7/(1-\varepsilon_7)$	1.25 A_7	1.0	7-107 Phantom
R13	1.0	8.36	0.1628 $144N \times A_{HCOMB} \times \pi \times d_H \times \Delta L$	Specific to SiC Honeycomb
R14	1.0	1.28 A_{HCOMB}	1.0	
R15	1.0	0.135 A_7	1.0	
R16	1.0	1.25 A_{HCOMB}	1.0	
R17	1.0	1.28 A_W	1.0	
R18	3.15 $(1-\tau_W)/\tau_W$	0.0238 A_W	1.0	Coupling from absorbing window

---

† $F_{INTERSEGMENT} = \frac{d_H}{4\Delta L}\left[F_D\left(E\text{-}9, \frac{d_H}{2}, \frac{d_H}{2}\right) - F_D\left(\Delta L, \frac{d_H}{2}, \frac{d_H}{2}\right) + F_D\left(2\Delta L, \frac{d_H}{2}, \frac{d_H}{2}\right) - F_D\left(\Delta L, \frac{d_H}{2}, \frac{d_H}{2}\right)\right]$

where $F_D(\Delta L, R_1, R_2) = 1/2\left[X - \sqrt{X^2 - 4\left(\frac{R_2}{R_1}\right)^2}\right]$ and $X = 1 + \frac{1 + \left(\frac{R_2}{\Delta L}\right)^2}{\left(\frac{R_1}{\Delta L}\right)}$

TABLE 3. VALUES OF "GEOMETRY" CONSTANTS USED IN SOLAR RECEIVER MODEL HTEMP (Continued)

B. CONDUCTING ELEMENTS

	Cross Section For Conduction	Formula	Comments
K1	0.256	$A_{HCOMB} \times (1-f)$	
K2	0.256	$A_{HCOMB} \times (1-f)$	
K3	0.256	$A_{HCOMB} \times (1-f)$	
K4	0.256	$A_{HCOMB} \times (1-f)$	
K5	1.0	---	Not used
K6	1.0	---	Not used
K7	5.28	$A_{FRT\ SHELL}$	Insulation
K8	0.916	$\pi D \times$ (thickness 1)	Inner Shell
K9	17.7	$A_{RR\ SHELL}$	Insulation
K10	0.144	$\pi D_o \times$ (thickness 2)	Outer Shell
K11	0.238	A_W	Window Front - Rear

C. CONVECTION ELEMENTS

	Surface Area	Formula	Comments
H1	5.28	$A_{FRT\ SHELL}$	
H2	17.7	$A_{RR\ SHELL}$	
H3	0.238	A_{WINDOW}	
H4	288.0	$A_{STORAGE\ SFCE}$	

TABLE 8. VALUES OF "GEOMETRY" CONSTANTS USED IN SOLAR RECEIVER MODEL HTEMP (Continued)

D. FLUID FLOW AND CONVECTION ELEMENTS

	Hydraulic Diameter d_H	Flow Cross Section	Convection SFCE 1	Convection SFCE2	Comments
M1	$\frac{0.3524}{\sqrt{D_{INL}\ D}}$	0.0976 $\frac{\pi}{4} D_{INL}\ D$	0.135 A_2	1.25 A_7	
M2	0.007 d_H	1.024 $(1-f)A_{HCOMB}$	1.E-10 1.E-10	0.256 fA_{HCOMB}	
M3	0.007 d_H	0.717 $(1-f)A_{HCOMB}$	1.63 $\frac{1}{2}144\pi NA_H d_H \Delta L_1$	1.63 $\frac{1}{2}144\pi NA_H d_H \Delta L_1$	
M4	0.007 d_H	0.717 $(1-f)A_{HCOMB}$	8.15 $\frac{1}{2}144\pi NA_H d_H \Delta L_2$	8.15 $\frac{1}{2}144\pi NA_H d_H \Delta L_2$	
M5	0.007 d_H	0.717 $(1-f)A_{HCOMB}$	0.256 fA_{HCOMB}	1.E-10 1.E-10	
M6	0.479 D	1.474 $\frac{\pi}{4} D^2$	5.96 $\frac{1}{2}\pi DL_{OUT}$	5.96 $\frac{1}{2}\pi DL_{OUT}$	
M7	$\frac{0.3524}{\sqrt{D_{INL}\ D}}$	0.0976 $\frac{\pi}{4} D_{INL}\ D$	1.E-10 1.3-10	0.238 A_W	

E. MASS ELEMENTS

	Thermal Mass	Formula
MMI	21.72	$M_{STORAGE} \times C_{P,\ STORAGE}$

2.3.1.2 Material Properties

Material properties used in the model were obtained from handbook data on the materials involved.* Table 9 presents the values used in Sanders' model. Where the data has shown temperature variation, this model can use a polynomial in temperatures of up to fourth degree (five coefficients). In most of our calculations to date, we have not gone beyond second degree polynomials (three coefficients). In our tabulation, one coefficient listed for a property implies it is constant with temperature. Where we have three coefficients tablulated, a_0, a_1 and a_2, this signifies that the property involved is represented by:

$$p = a_0 + a_1 T + a_2 T^2$$

where T is the temperature in degrees F. For fourth degree polynomial representation:

$$p = a_0 + a_1 T + a_2 T^2 + a_3 T^3 + a_4 T^4$$

TABLE 9. MATERIAL PROPERTIES USED IN HTEMP SOLAR RECEIVER MODEL

AIR		
Conductivity, K	= 1.337E-2, 2.037E-5, -1.751E-9	(BTU/HR-FT-^{o}F)
Heat Capacity, Cp	= 0.2357, 2.531E-5, -1.938E-10	(BTU/LB-^{o}F)
Density/G	= 3.262E-10, -2.183E-13, 5.35E-17	((LB/FT^3)/(FT/HR^2))
Viscosity/G	= 9.861E-11, 1.350E-13, -1.862E-17	((LB/FT-HR)/(FT/HR^2))
Gravitation Accel, G	= 4.173E8	(FT/HR^2)
CONVECTION COEFFICIENTS		
Air Inside Window H	= 5	(BTU/HR-FT^2)
Air Outside Window H	= 100 (Effective value for impingement cooling)	(BTU/HR-FT^2)
Air in Honeycomb Ducts		
$H = \frac{K_{AIR}}{d_H}$	(Appropriate for laminar flow in long ducts, Graetz number <10)	

*While no particular items are expected to be critical for model results, it would be good practice in a design to be used extensively to measure many of these properties and verify the handbook results for specific samples of some of the materials involved. We expect properties of air to be well established and culled of any inadvertant errors. Insulating materials and ceramics, however, may vary in properties such as thermal conductivity from sample to sample. Other properties, such as heat capacity, are generally insensitive to methods of preparation and thus tend to be constant between samples.

TABLE 9. MATERIAL PROPERTIES USED IN HTEMP SOLAR RECEIVER MODEL (Continued)

SILICON CARBIDE		
Conductivity, K	= 1.4237E2, -8.868-2, 1.447E-5	(BTU/HR-FT-^{o}F)
Heat Capacity, Cp	= 0.1824	(BTU/LB-^{o}F)
Density	= 193.44	(LB/FT^3)
INSULATION		
Conductivity, K	= 0.01780, 1.312E-5, 2.920E-8	(BTU/HR-FT-^{o}F)
Heat Capacity, Cp	= 0.1828	(BTU/LB-^{o}F)
Density	= 8.0	(LB/FT^3)
STAINLESS STEEL		
Conductivity, K	= 7.896, 6.576E-3, -1.915E-6	(BTU/HR-FT-^{o}F)
Heat Capacity, Cp	= 0.11	(BTU/LB-^{o}F)
Density	= 488.0	(LB/FT^3)
QUARTZ		
Conductivity, K	= 0.75147, 5.5083E-4, -5.9530E-7, 6.1488E-10, -1.757E-13	
Heat Capacity, Cp	= 0.179	
Density	= 137.3	

2.3.1.3 Heat Inputs

Heat source terms treated in our model are represented by triangles in Figure 6 and are tabulated in Table 10. The window loading, at node 8, was calculated from window material transmissivity data. The heat loading on the honeycomb was based on a Monte Carlo calculation of flux distribution appropriate to honeycomb geometry and to silicon carbide (absorptivity = 0.9).

TABLE 10. HEAT SOURCE VALUES USED IN HTEMP MODEL AT 252767 BTU/HR TOTAL INSOLATION

Node	Heat Input (Btu/hr)	Comments
8	840.	Front of Window
6	69532.	Front Face of Honeycomb
10	64911.	Inside Honeycomb Tube
14	76257.	Inside Honeycomb Tube
18	13777.	Inside Honeycomb Tube
22	4865.	Inside Honeycomb Tube
26	2431.	Inside Honeycomb Tube

2.3.2 Efficiency, Heat Losses and Conditions

Representative model output data is provided in Table 11. Certain values are very close for all nominal runs at rated output temperatures, and these values are mentioned below, outside the tabulation.

2.3.2.1 Wall Losses

Heat losses through the walls are typically 892 Btu/hr at full insolation and with flow adjusted to yield nominal output temperatures of 2500°F. These tend to be constant for most conditions studied.

2.3.2.2 Radiation Losses

Because of the basic dependence on T_{ABS}^4, radiation losses are the most sensitive to cavity and honeycomb temperature. With the large honeycomb surface area, the honeycomb temperature does not exceed the outlet air temperature by more than 430°F at the nominal flow rate of 830 lb/hr. Thus, the outlet temperature plus 430°F crudely determines radiation losses. The model proper accounts for any nonuniformity in the cavity, but model runs show the cavity and honeycomb face temperatures to be within about 20°F of each other.

2.3.2.3 Window Cooling

The impingement forced air cooling, which limits maximum window temperatures, extracts typically 15850 Btu/hr, or 30% of the total loss from the cavity. Radiation from the window to ambient totals to 618 Btu/hr, relatively negligible, but almost as large as the total losses from the walls of the receiver.

2.3.3 Pressure Drops

Included in the finite element model is an element that models the D'Arcy-Weissbach relationship between pressure drop and fluid flow. The temperature dependent properties of air are accounted for, also friction factor as a function

TABLE 11. OUTPUT TEMPERATURES, ENERGY DELIVERED AT OUTLETS, AND LOSSES AT VARIOUS FLOW CONDITIONS, CONSTANT INSOLATION AT 232606 BUT/HR

Case	Inlet T_o (^oF)	Outlet T_o (^oF)	Flow Rate $\dot{M}$ (LB/HR)	Energy Out (Gain in Air Enthalpy) (BTU/HR)	Energy Losses (Radiation + Window + Walls) (BTU/HR)	Net Efficiency (%)
A	1750	2835	550	173155	58675	75%
B	1750	2615	700	174527	56827	75.5%
C	1600	2502	700	180740	51510	78%
D	1900	2729	700	168280	62538	73%
E	1750	2596	720	175464	56158	76%
F	1750	2517	810	178605	53302	77%
G	1750	2451	900	181080	50973	78%
H	1750	2395	990	183150	49058	79%
I	1750	2348	1080	185004	47453	79.5%

Average Total Input: $\frac{\Sigma \text{ Energy out} + \Sigma \text{ Energy Losses}}{n} = 231830$

of Reynolds number. At the sublaminar flow in the ducts, this amounts to $f_{fric} \sim 64/N_{Re}$. "Fitting Coefficients" are not added for honeycomb end effects at the $N_{Re} < 15$ conditions typical of the honeycomb ducts. Typical steady state pressure drop at 830 lb/hr is under 6.5 lb/ft^2.

Predicted wall losses from the receiver performance model are ≈0.3 kw. Aperture losses are ≈3.7 kw including convection and radiation. These findings coupled with window flux modeling lead to receiver and system efficiencies shown below in Table 12.

TABLE 12. COMPLETE RECEIVER EFFICIENCY COMPARISON INCLUDING PRIMARY MINOR EFFECTS

Case	Net Efficiency	1) Net + Reflection	2) Net + Reflection + Spillage	3) Overall Solar to Air Stream
	*1.0	*1.0*0.92	*1.0*0.92*0.905	1.0*0.92*0.905*0.90
A	0.750	0.690	0.625	0.562
B	0.755	0.695	0.629	0.566
C	0.780	0.718	0.649	0.584
D	0.730	0.672	0.608	0.547
E	0.760	0.699	0.633	0.569
F	0.770	0.708	0.641	0.577
G	0.780	0.718	0.649	0.584
H	0.790	0.727	0.658	0.592
I	0.795	0.731	0.662	0.596

NOTES

1. Accounts for window reflection, 8%

2. Accounts for additional losses caused by rays outside diameter of aperture; 11.02 kw or 9.5%

3. Accounts for additional losses caused by primary mirror reflectivity, 90%

2.3.4 Material Selection and Rationale

The designed operating parameters of the HTSTR, including temperatures ranging from 2000° to 3000°F, and the possibility of reactive atmospheres, requires the use of high refractory ceramic materials as heat exchanger components. The generalized properties of these materials include high temperature stability in oxidizing and chemically active atmospheres, thermal shock resistance, capability of fabricating general shapes and scaling in size, and relative feasibility of material cost and availability.

2.3.4.1 Heat Exchanger Material

Sanders chose silicon carbide (SiC) as the heat exchanger material in the HTSTR receiver based on its known properties, success in previous applications and survival in adverse environments. The high thermal conductivity and emissivity of SiC make it an excellent heat exchanger material. The strong covalent bonding of the carbide gives it a very high melting point, and generally high temperature corrosion and erosion resistance. State of the art fabrication techniques make SiC available as a high density, impermeable body suitable for pressurized systems.

Sanders used a form of SiC in its highly successful 1/4MWt receiver experiment tested at Georgia Institute of Technology in 1978. In that case low density SiC material was impregnated with more silicon to form densified α-sintered silicon carbide.

2.3.4.2 Receiver Shell

Carbon steel was selected for the HTSTR receiver shell. Carbon steel can be used instead of 316 stainless because the receiver cavity is so well insulated that the shell temperature will not exceed 200°F. The temperature limit of carbon steel is 600-800°F, far above the shell temperature. The use of carbon steel reduces costs substantially.

2.3.4.3 Thermal Storage Material

Sanders has chosen mullite, an alumino-silicate, as the heat exchanger material for the integral thermal storage area of the HTSTR receiver. Mullite is much less expensive than SiC and has a higher operating temperature than cordierite, which are the alternate material choices. The mullite storage area is shielded from radiation to prevent rapid thermal degradation since mullite has poor thermal shock resistance. Thus mullite performs very well in this environment and has the added benefit of being economical.

2.3.4.4 Window Material

The solar receiver window is made from GE124 quartz. Parametric analysis on the solar window for the HTSTR was performed and a window approximately 8 inches in diameter and 0.4 inch thick was indicated. The receiver design included a Compound Parabolic Concentrator (CPC) to increase the power captured.

A materials search was then conducted to find the optimum window material that could both tolerate the expected temperatures (under 1000^{o}C) and that has very good optical tranmission. The higher the tranmission of the window, the lower the absorption, thus the window would stay cooler.

The following materials were considered for the HTSTR window: Tyco sapphire, GE124 quartz, GE125 quartz, Amersil Suprasil W-2 quartz, and Crystal Systems sapphire. Of these materials only Tyco's sapphire is not manufactured in a large enough boule.

Of the materials mentioned, Amersil Suprasil W-2 has the highest minimum internal transmission (96%) from 0.27μ to 2.7μ, but is by far the most expensive, \$17.45 per cm^3. GE124 quartz's external transmission is 89% to almost 94% in the 0.27μ to 2.5μ range, at a cost under \$0.37 cm^3. This maximum of 7.0% reduction in the optical transmission is accompanied by a price reduction of nearly 98%. The HTSTR window of GE124 is approximately \$165.00 vs. a window of Amersil Suprasil W-2 for approximately \$8000. Clearly, economics do not warrant the selection of

Suprasil W-2 for the HTSTR window for a maximum spectral transmission difference of only 7.0%. The spectrally integrated transmission varies less than 1%. Delivery time of GE124 quartz in the desired size is approximately four weeks.

2.3.4.5 Insulation

Dynaform® is a castable, high temperature insulation manufactured by Johns-Manville. Dynaform® can withstand temperatures up to 2700°F and has thus been chosen as the best insulation for the HTSTR system whose operating temperatures range from 2000-3000°F. Dynaform® is relatively inexpensive and yet has its own structural integrity. It may be vacuum-formed, which substantially reduces machining costs, and lends itself very well to the many complex shapes required. Dynaform® is ideally suited as the insulation material of the HTSTR system due to its high temperature insulation and ease of fabrication.

2.3.4.6 Gasketing

The chosen gasketing for the window is a thin-walled hastelloy C-ring with high temperature integrity. A face seal will be used rather than a gland seal since a face seal is less impacted by the thermal expansion difference between the hastelloy flange and quartz window.

2.3.4.7 Compound Parabolic Concentrator (CPC) Trade-off

An in depth parametric trade-off of the HTSTR receiver was performed consequent to discussion at the October design review at JPL. Receiver cone angles from 43-54 degrees were compared. The maximum flux level and flux concentration occur with a 47 degree CPC acceptance angle. Trade-offs were then performed between a 47 degree receiver both with and without a CPC. The receiver without the CPC captures about 4% less energy but has a higher flux peak and the overall flux distribution is more peaked. Consequently, further analysis of the benefits of the CPC were investigated.

A CPC reduces the radiative area of the receiver; this is important at cavity temperatures of 2600°F and re-radiation loss 47 watts/cm^2. The energy capture difference (between the 47 degree receiver with a CPC and the one without) is only 2901 watts or 2.9 kW. That is only a 4.5% gain in total power with the addition of the CPC. Yet the addition of the CPC significantly increases the cost of the receiver. In addition, if a CPC were to be included, flux analysis indicates it would need its own cooling system (see Figures 11 and 12).

Sanders believes that the CPC is not warranted as part of the design due to economics.

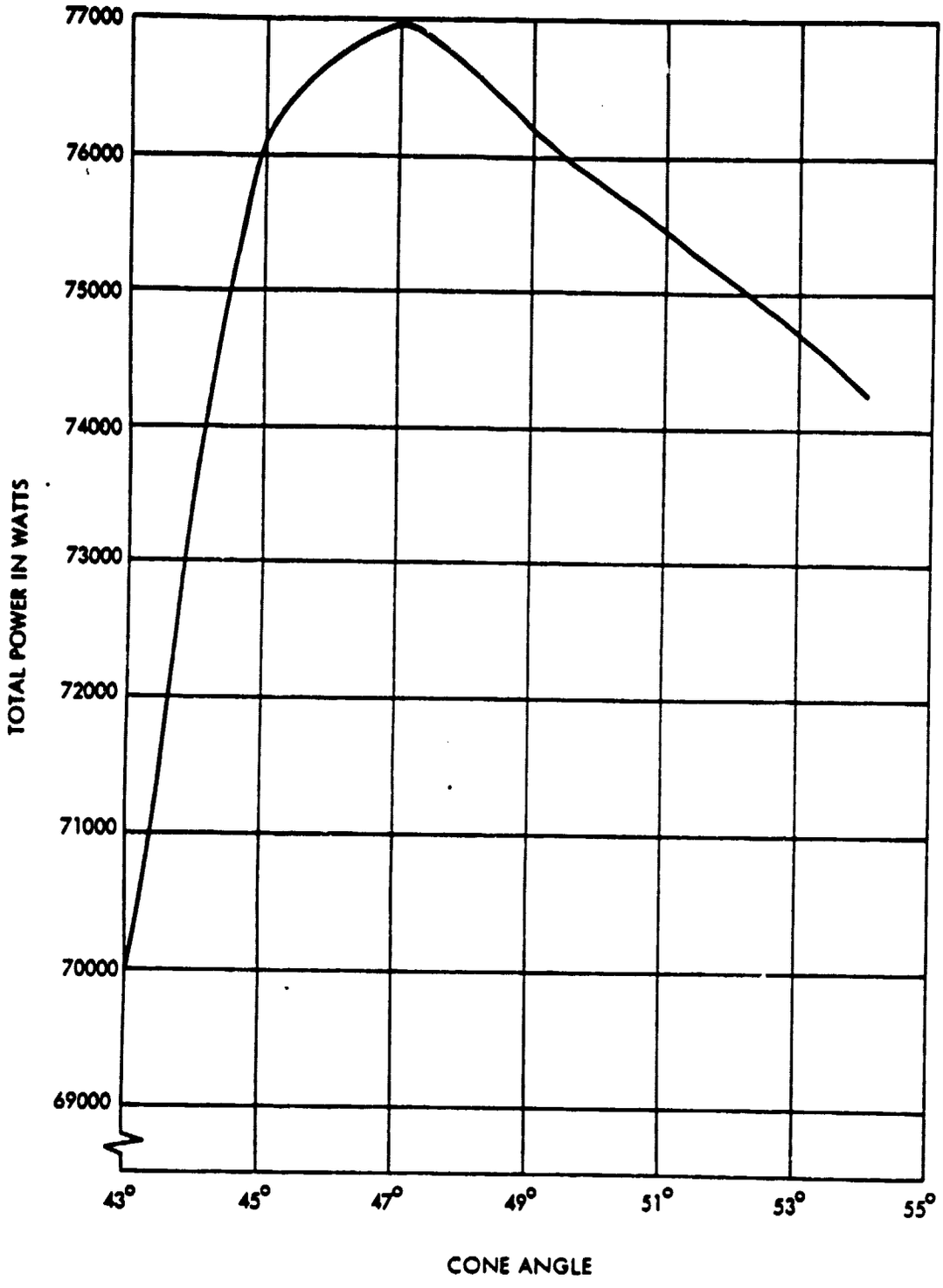

Figure 11. Total Power Into Receiver versus CPC Angle

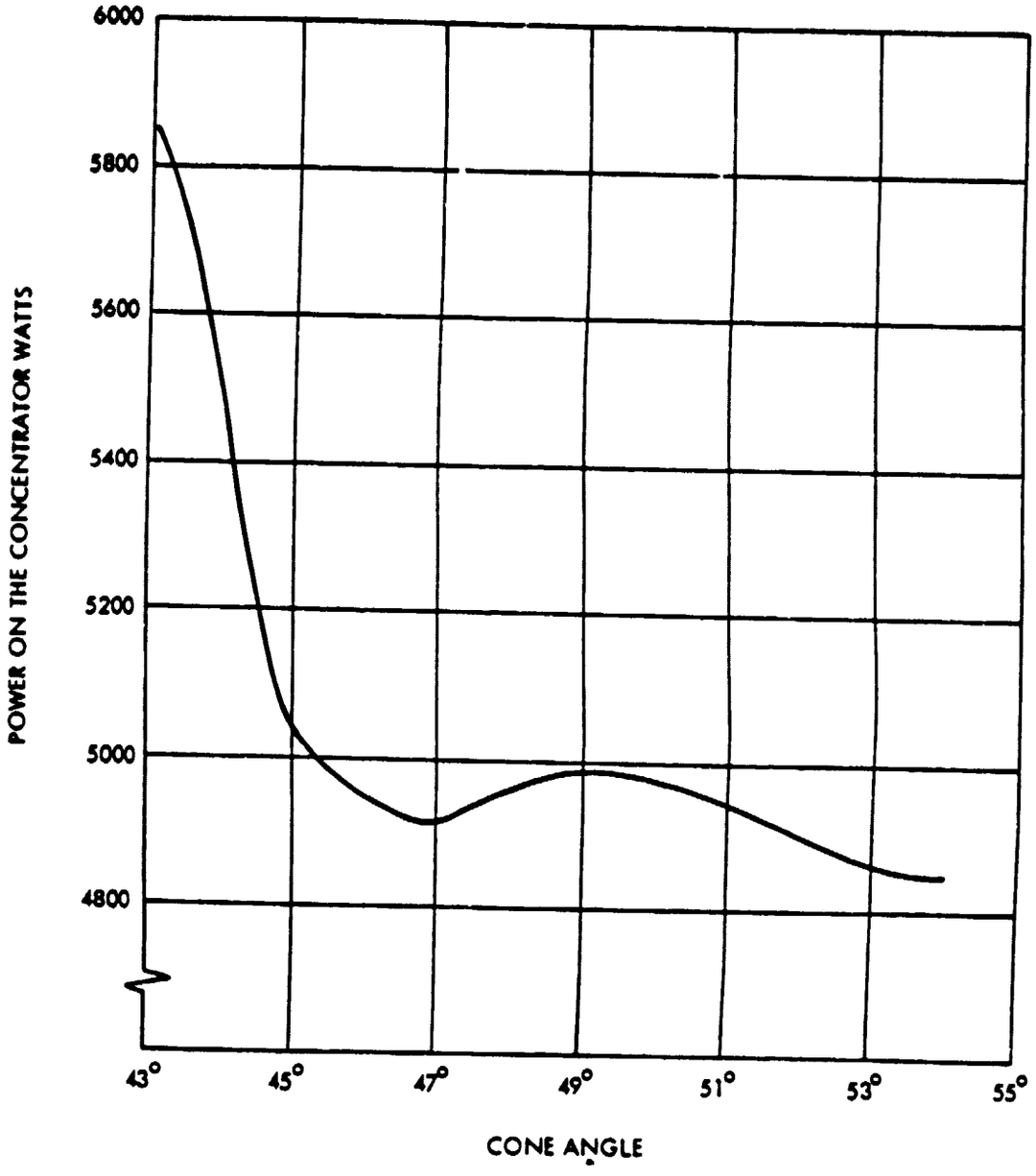

Figure 12. Total Power on Concentrator versus CPC Angle

2.3.5 Receiver Design

2.3.5.1 Description

The Sanders High Temperature Solar Thermal Receiver (HTSTR) design concept for a 70 KWt input is a compact and simple design which employs readily available production materials and developed production technologies for low cost. The Task 2 receiver is 30 inches in diameter and 36 inches long, and weighs approximately 500 pounds.

The receiver housing performs multiple functions; it is an integral housing, pressure vessel and ecto-skeleton. As a housing, its exterior is weatherproof and is finished with engine enamel to resist heat and corrosion. As a pressure vessel, it complies with Section VIII, Division I of the ASME Boiler Code. The wall is 0.25-inch thick cold-rolled low carbon steel. The vessel is split into two sections for assembly and maintenance access. The rear section includes the vessel proper and rear end dome. The front section consists of the forward (face) dome. The two sections are joined by a 150 psi flange and hardware. It is fitted with 150 psi flanges at the rear for air (the working fluid) inlet and output. A fused quartz window is fitted at the front and is retained by an air-cooled flange. Cooling air from the flange is directed by jet nozzles against the external face of the window to provide a high convective film coefficient for impingement cooling of the window.

The window acts as a transparent pressure bulkhead to admit concentrated solar flux while simultaneously containing the working fluid. Window sealing is provided by a Hastelloy C-ring face seal between the window flange and internal surface of the window.

The window flange and mounting hardware are protected from spill-over flux by air cooled stainless steel radiation shields.

Internally, preformed insulation provides thermal impedance and structural integrity. The preforms are configured to form the depicted air flow galleries. The preforms key together as they assemble to form a stable, integrated structure with the receiver panels and storage mass. The central inlet duct is similarly fabricated of the same preformed insulation material, Dynaform®, a Johns-Manville product.

The receiver panels are α-sintered silicon carbide honeycomb matrices 1.25 inch thick. The honeycomb is configured with 100 flow channels per square inch. The hydraulic diameter of each channel is 0.084 in, and mean wall thickness is 0.0164 in. This geometry ensures effective heat transfer and low pressure drops. The resulting panel solidity is 30%. Silicon carbide was chosen for the application because of its demonstrated (in Sanders Associates, Inc., airborne infrared countermeasures (IRCM) systems) ruggedness and suitability to the high temperature application. The panels are beveled and mitred in the green state (prior to firing) to fit into the receiver as trapezoidal prisms and collectively form a 12-sided pyramid (finite element cone).

The storage mass is comprised of mullite extrusions with approximately 50 channels per square inch. The channels have a hydraulic diameter of ≈0.140 inch and a mean wall thickness of 0.06 in. The resulting solidity is 50%. The coarser geometry (vis-a-vis the SiC receiver panels) of the mullite induces a thermal impedance to heat flow in and out of the mullite. Thus, the mass acts as a thermal buffer during brief sun outages rather than as a thermoclinal quasi-constant temperature heat source. The approximately 137 pounds of mullite storage mass is supported by a step in the preformed insulation. Face hydrostatic loading imposed by the mullite on the insulation is less than 5 psi.

In operation, preheated air enters the receiver and flows through the central inlet duct to the solar cavity. The flow velocity in the feed pipe is 62 feet per second. The air is accelerated through the inlet nozzle to play on the rear surface of the window. There, removal of absorbed infrared cavity reradiation occurs and the air is diverted to the SiC receiver panels where it is heated to 2500°F. The air flows serially through the solar matrix and storage mass channels. The heated air is collected in an outlet plenum and flows through the outlet port.

Cool air is routed to the exterior surface of the window via channels in the window flange. This cool air may be supplied from compressor bleed in an engine application or from house or utility air in a fossil-offset fuels or chemicals process application.

High film coefficients (5.7E-2 watts $cm^{-2}\ {}^{o}C^{-1}$(100 $Btu\text{-}hr^{-1}\text{-}ft^{-2}\text{-}{}^{o}F^{-1}$)) are required to achieve the necessary cooling; Sanders has achieved such cooling by using its patented impingement air cooling for IRCM system windows. Design implementation of this technique for the HTSTR was not undertaken as the requirement for flow modeling and experimentation was not within the scope of this study.

2.3.5.2 Salient Features

In summary, the design features which contribute to the functional success and economic viability of the HTSTR are notably:

- The use of air jet impingement cooling to remove absorbed solar and IR energy from the windo.
- The use of a Hastelloy C-ring to seal the window/cavity interface
- The application of an edge compressive pressure applied to the window by the retaining clamp and C-ring reduces maximum window stress to less than 300 psi. This is less than one-third of the maximum recommended tensile stress, 1000 psi.
- The SiC honeycomb panels and mullite storage mass are securely supported directly by the interlocking Dynaform® preformed insulation

2.3.6 Engineering; Analysis and Assumptions

2.3.6.1 Introduction

During the Parametric Analysis (Task 1) substantial effort was directed to the modeling of the flux incident at the aperture and within the cavity. The baseline primary mirror was considered to have a 2-mrad (one standard deviation) surface slope error. Preliminary work during the proposal had shown significant advantages to the use of a compound parabolic concentrator. Work during the parametric analysis led to the identification of optical CPC geometry and focus location to maximize energy capture.

Manual calculation of spectral energy distribution and spatial integration of solar radiation absorption in the window indicated maximum temperature rises of 500°C would be generated. Quartz thermal conductivity was assumed to be linear, that is not a function of temperature.

Based on the findings of the Parametric Analysis, Sanders predicted the viability of the design and recommended subsequent work in Tasks 2, 3 and 4 be directed to a receiver of the following configuration:

- Input: 70 KWt
- Inlet: 1750°F
- Output: 2500°F
- Absorber: SiC Honeycomb
- Pressure: 3 atmospheres$_{abs}$
- Storage: Mullite honeycomb extrusion
- Aperture: Windowed (GE Quartz 124)

The performance recommendations were accepted and Sanders continued work on their recommended configuration.

2.3.6.2 Key Technical Issue - Window

The window was identified as the key technical issue in the Sanders receiver. Specific technical questions identified were:

- What is the impact of cavity IR radiation on the window?
- What is the temperature distribution of the window?
- What is the spectral absorptivity of the window material?
- What material is best suited to the application?
- What is the thermal conductivity of the window?

An iterative engineering and analysis process began wherein the issues were closely scrutinized. Numerous sessions of mutually informative and constructive criticism occurred between Sanders and the technical monitor and his staff at JPL.

Window Transmissivities

A detailed materials information search led to the identification of GE Quartz 124 (versus 125) as the best material to use. It has higher transmissivity in the visible than does 125, but is more absorptive in the near IR. This difference in spectral characteristics results in cavity radiation becoming a major heat source to the window, but intense solar loading is avoided.

Comparative plots of the log (base 10) of the absorption coefficients are shown in Figures 13 and 14. The Suprasil W data is less detailed, but the curve represents the guaranteed minimum absorptivity throughout the range. Manufactured by Amersil, the material has tight quality control and excellent imaging qualities; but it is expensive and does not offer apparent transparency advantages.

Solar Radiation

The spectral distribution of solar energy was researched at length with the resulting identification of the NASA-Theakara extraterrestrial (air mass = 0) distribution of 1971, tabulated below and shown graphically in Figure 15.

Air mass 1 spectral transmissivity[1] is shown graphically in Figure 16.

The convolution of these data represents terrestrial solar irradiance which are tabulated below and shown in Figure 17. This convoluted data multiplied by the appropriate optical concentration ratio serves as the input irradiance to the spectrally absorbing window.

---

[1]Henderson, S.T., Daylight and Its Spectrum

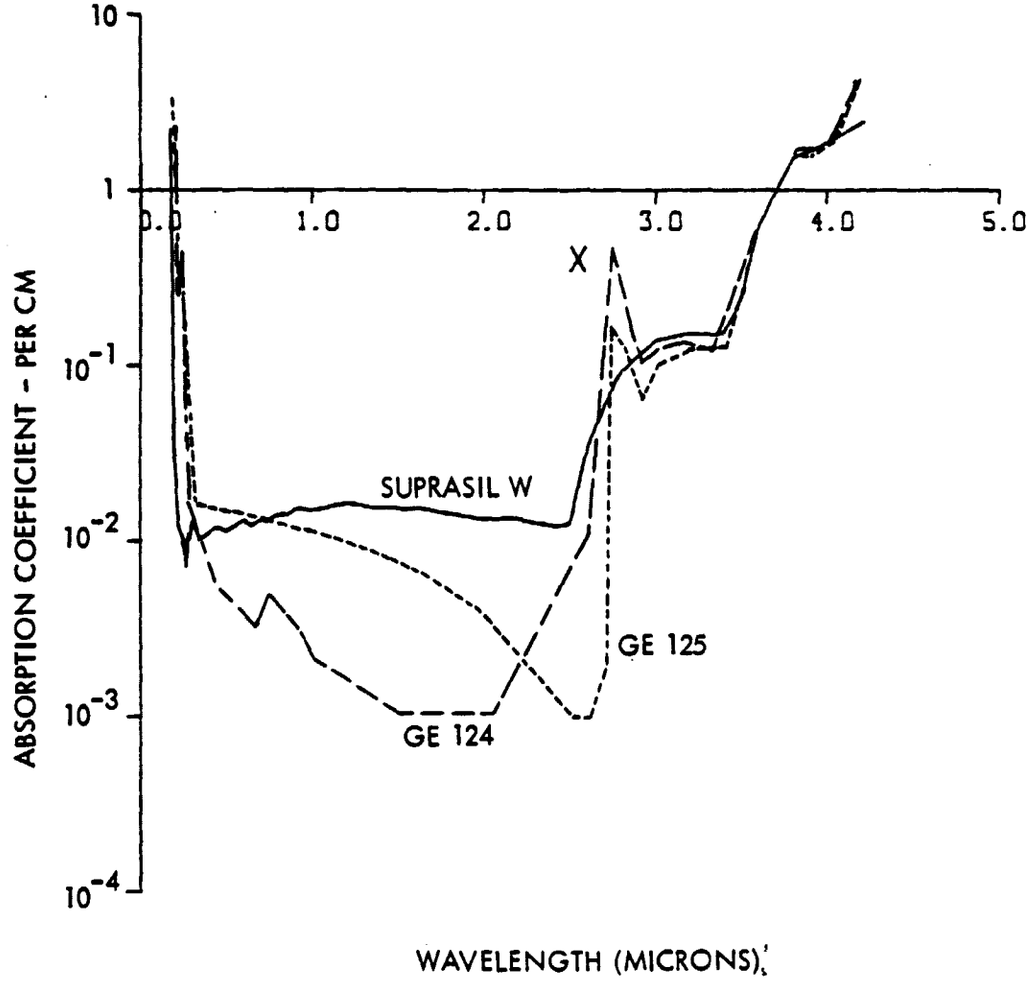

Figure 13. Absorption Coefficients for Candidate Window Materials

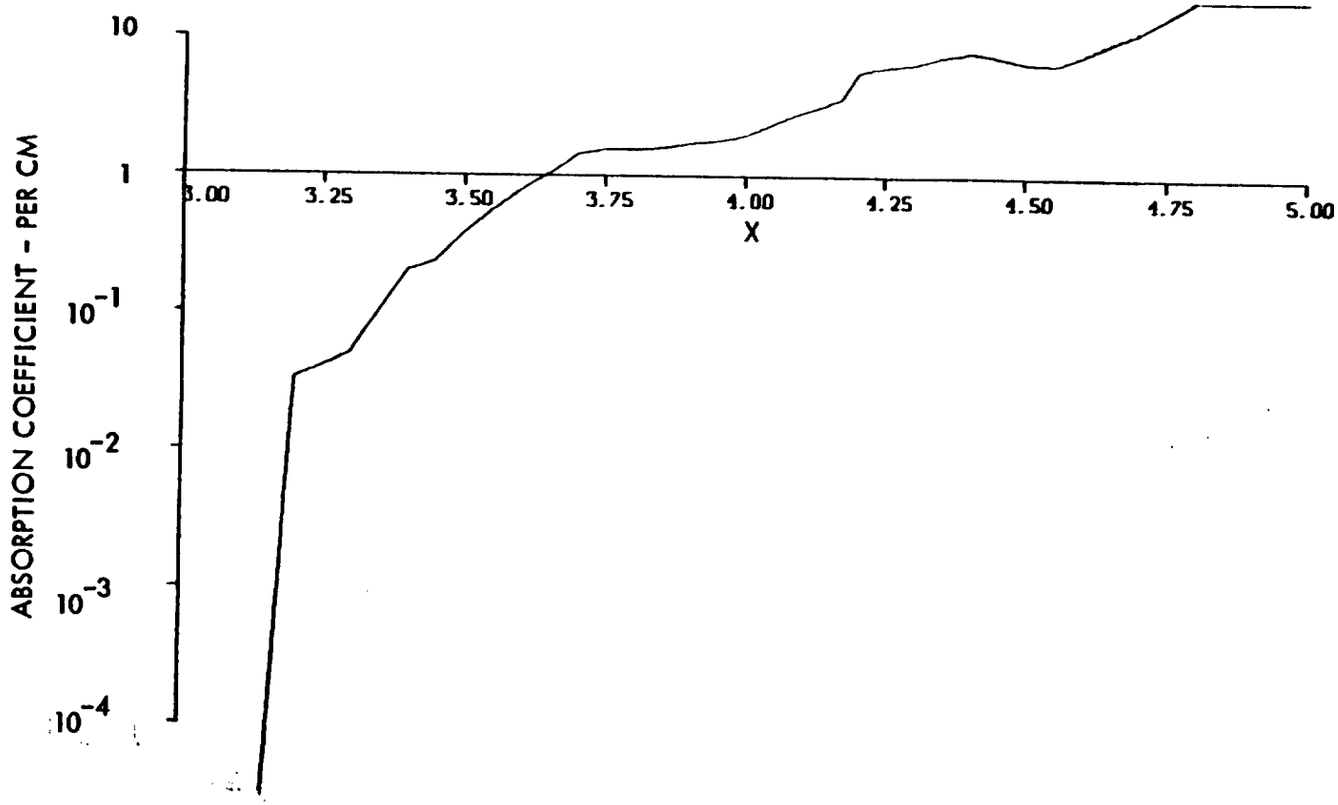

Figure 14. Measure Absorption Coefficient versus wavelength for Quartz, GE 124

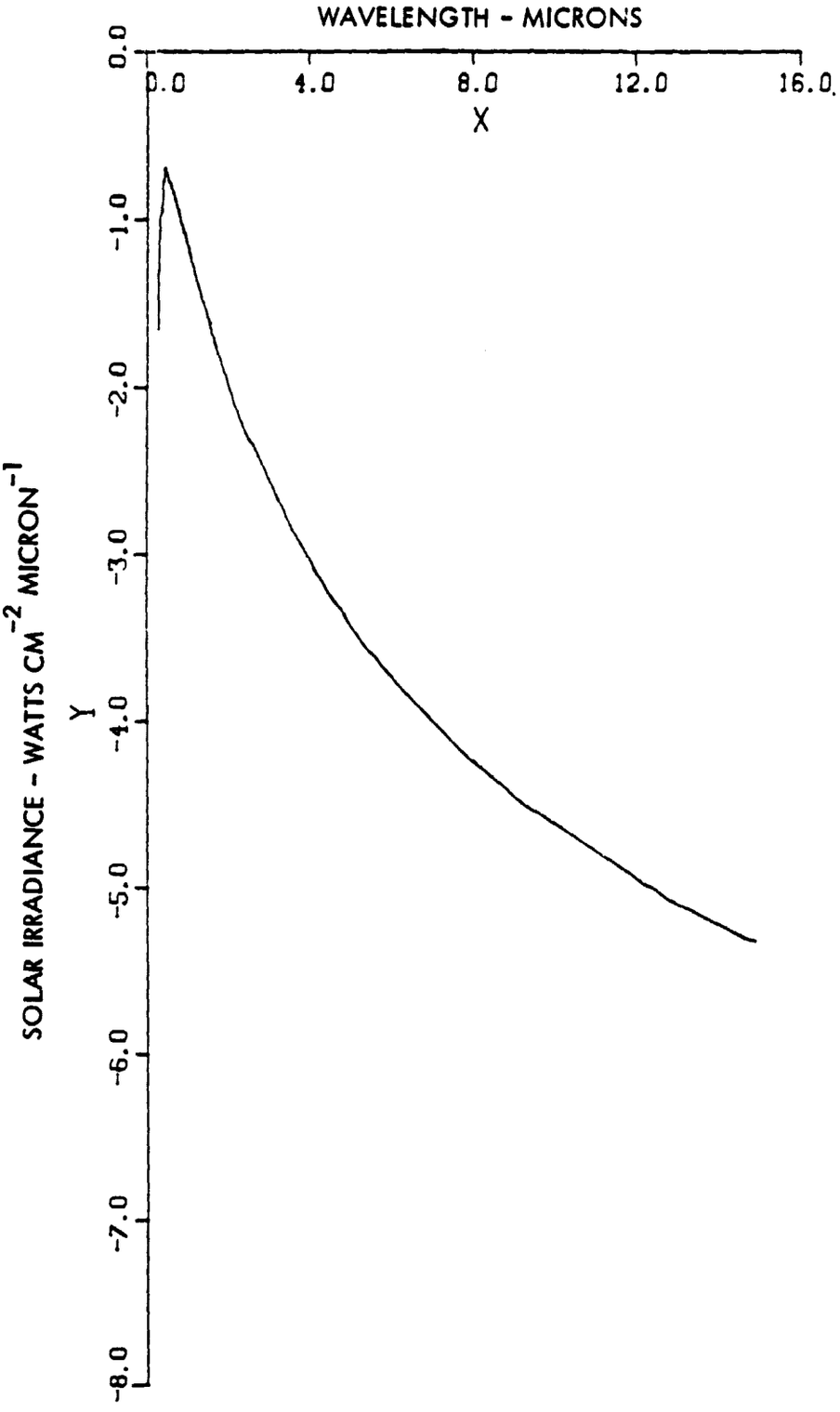

Figure 15. Spectral Distribution of Solar Energy; Air Mass = 0

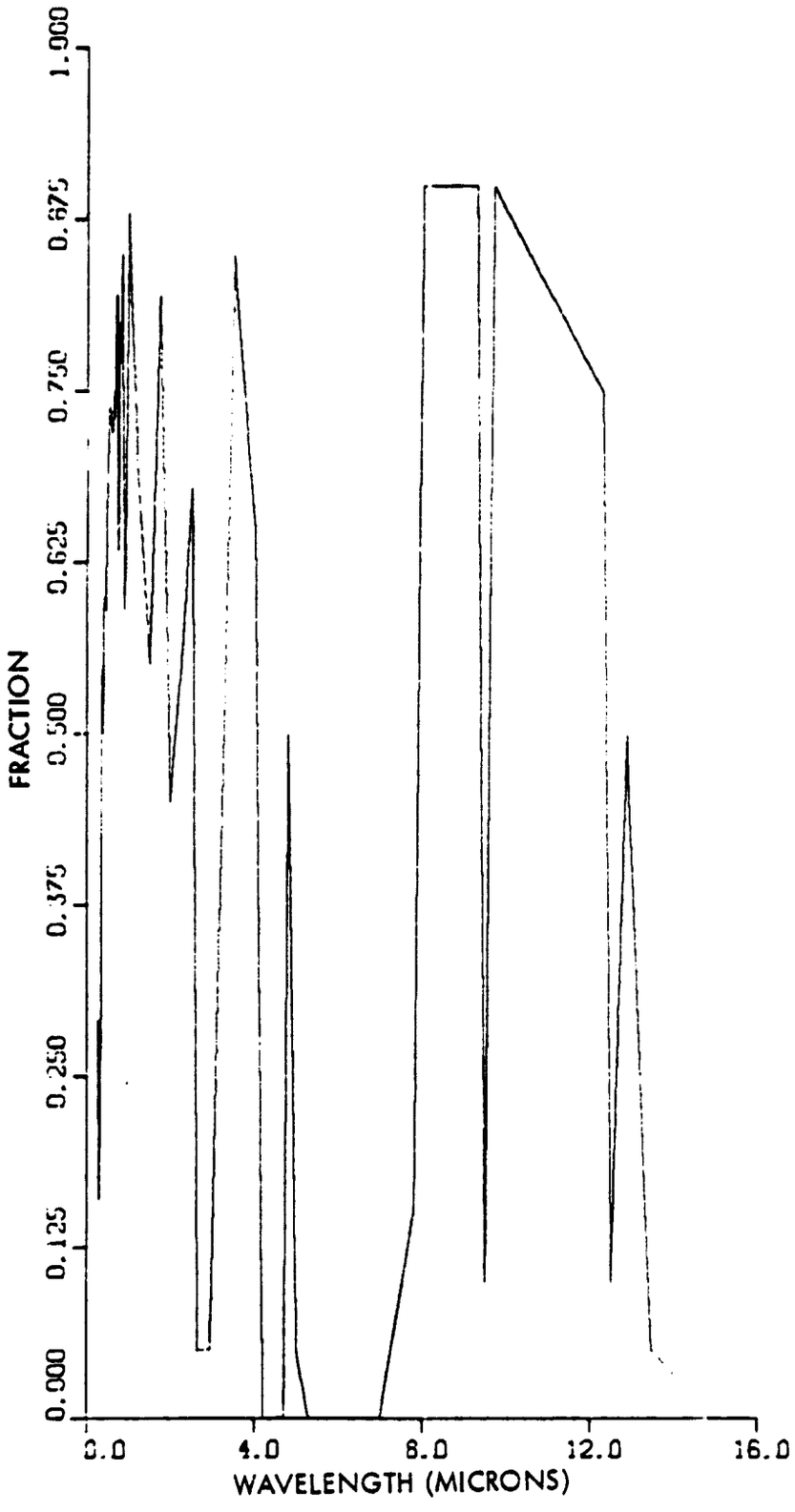

Figure 16. Spectral Transmissivity; Air Mass = 1

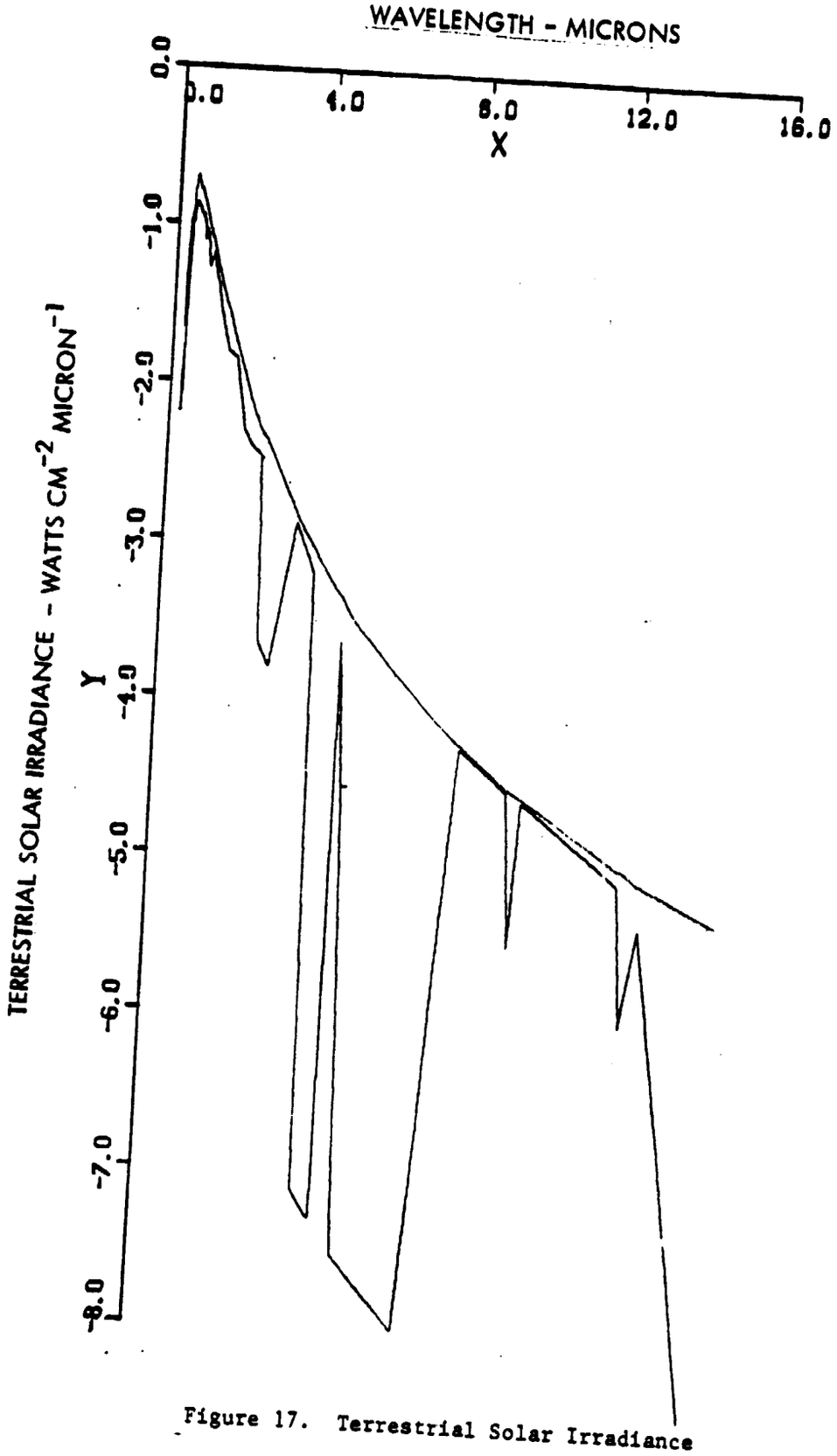

Figure 17. Terrestrial Solar Irradiance

Flux Distribution

The flux loading at the window and within the receiver cavity was modeled using a Monte Carlo sampling technique to generate rays and to trace their propagation and absorption through the system. During the Parametric Analysis, Task 1, near optimum energy collection geometries and focal points were identified. Those findings remain valid; however, early window analyses using preliminary window transmissivity data indicated a need to reduce the peak flux values and to smear the flux over a large area of the window without inducing significant spillage losses. Modeling experiments with the CPC geometries (specifically theoretical throat diameter, acceptance angle, concentrator length, and the physical location of the throat (and mouth) along the concentrator axis) yielded three significant findings:

- The three-dimensional or cone-like compound paraboloidal concentrator has a much smoother acceptance cutoff than does a two-dimensional or trough-like compound parabolic concentrator

- Skew rays significantly detract from the step cutoff of the two-dimensional concept.

- The larger entrance of the CPC reduces spillage from 11.0 kW to 3.1 kW, but much of that additional power interception is offset by (a 6% to 10%) absorption of the general population of rays and by skew ray rejection

- Absorption on the CPC is important because in small f/number applications (large source angle) nearly 75% of the captured rays must bounce at least once on the concentrator. Even with high surface reflectivities 90% to 92% the CPC absorbs about 5 kW on a 70-kW receiver

- Significant flux distribution changes can be effected by extending the CPC to a point where its slope is negative. This effect offers marked flexibility in window design, but infers a very expensive concentrator

- Maximum capture of 77 kW for this application occurs when the CPC has the following parameters
  a. acceptance angle, θ = 0.82 radians
  b. throat radius, Y_0 = 0.084 meter
  c. length, Z_{max} = 0.221 meter

- Energy capture without a CPC is 74 kW

- For the 70 kW receiver operating at the focal point of a σ = 2 mrad primary reflector, the CPC offers 4% greater input with the incurred cost of the CPC itself, mounting hardware, and greater cooling requirements

The predicted flux intensities at the window for the receiver with and without a CPC are shown in Figure 3. The peak flux intensity differs little but the CPC does direct an additional 3 kW through the outer reaches of the window.

Energy Absorption

Window heating results from the distributed absorption of energy throughout the window. The extent and severity of the window heating was evaluated using developed finite element software (ANSYS). The degree of fineness to which one properly divides a model depends mainly on the nonlinearity of the problem. In this case, the structure (window) is plane and symmetrical but the thermal loading is highly curved in both the axial and the radial directions. The window was then modeled as a circular sector 5 degrees wide with edge conditions of circular symmetry. The thickness and radius were each divided into 10 increments; the window model is comprised of 100 solid elements for thermal and structural evaluation. The absorbed solar radiation flux inputs are tabulated below in a matrix corresponding to thickness and radius increment position within the window. The infrared absorption is constant across the radius of the window but does vary throughout the thickness of the window.

Three graphs are included. Figure 18 shows absorption through the thickness of the window on axis. This depicts peak solar plus cavity IR loading on the window. Second, Figure 19 shows absorption through the thickness of the window at the

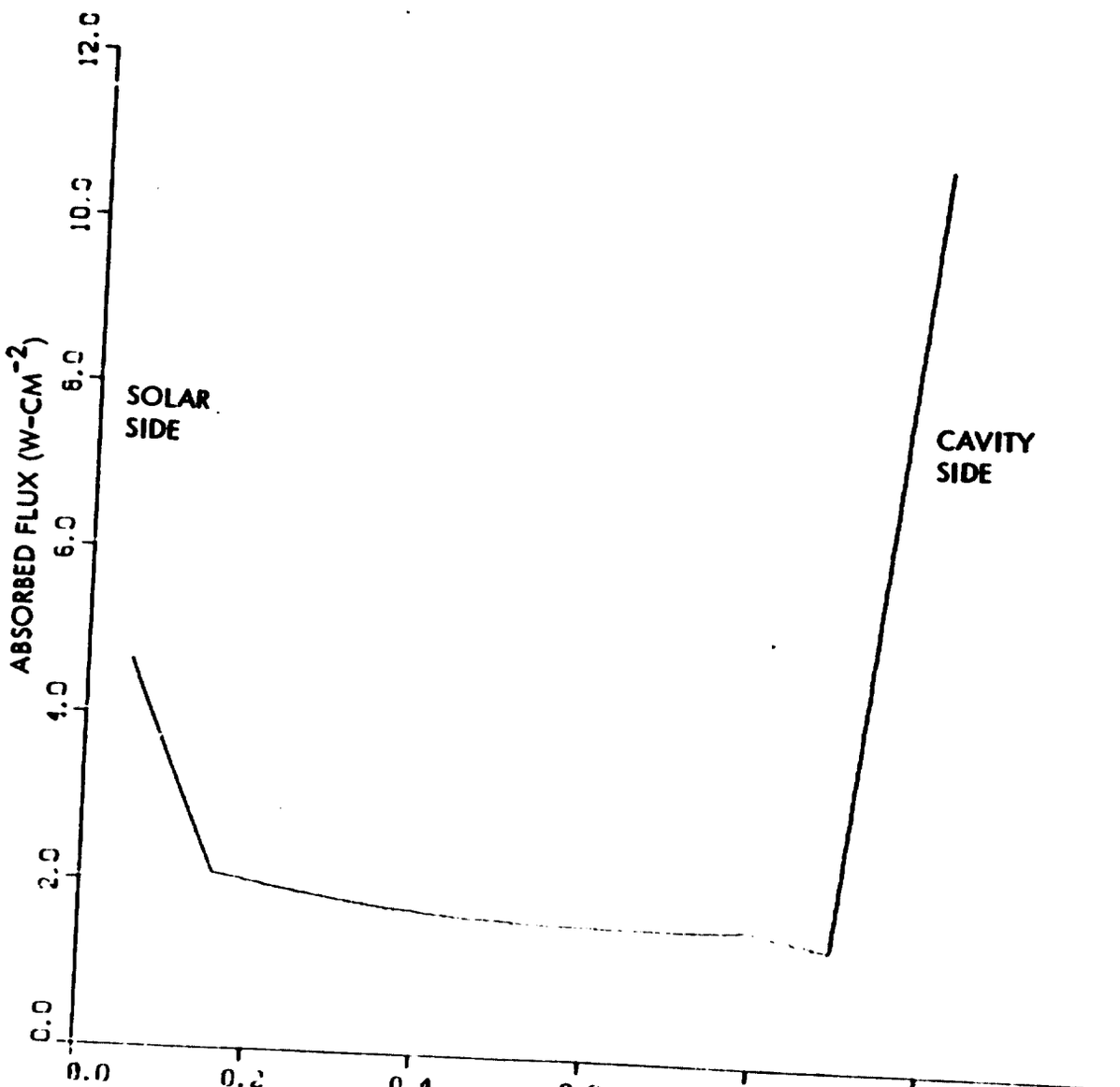

Figure 18. Absorption Through Thickness of the Window On-Axis

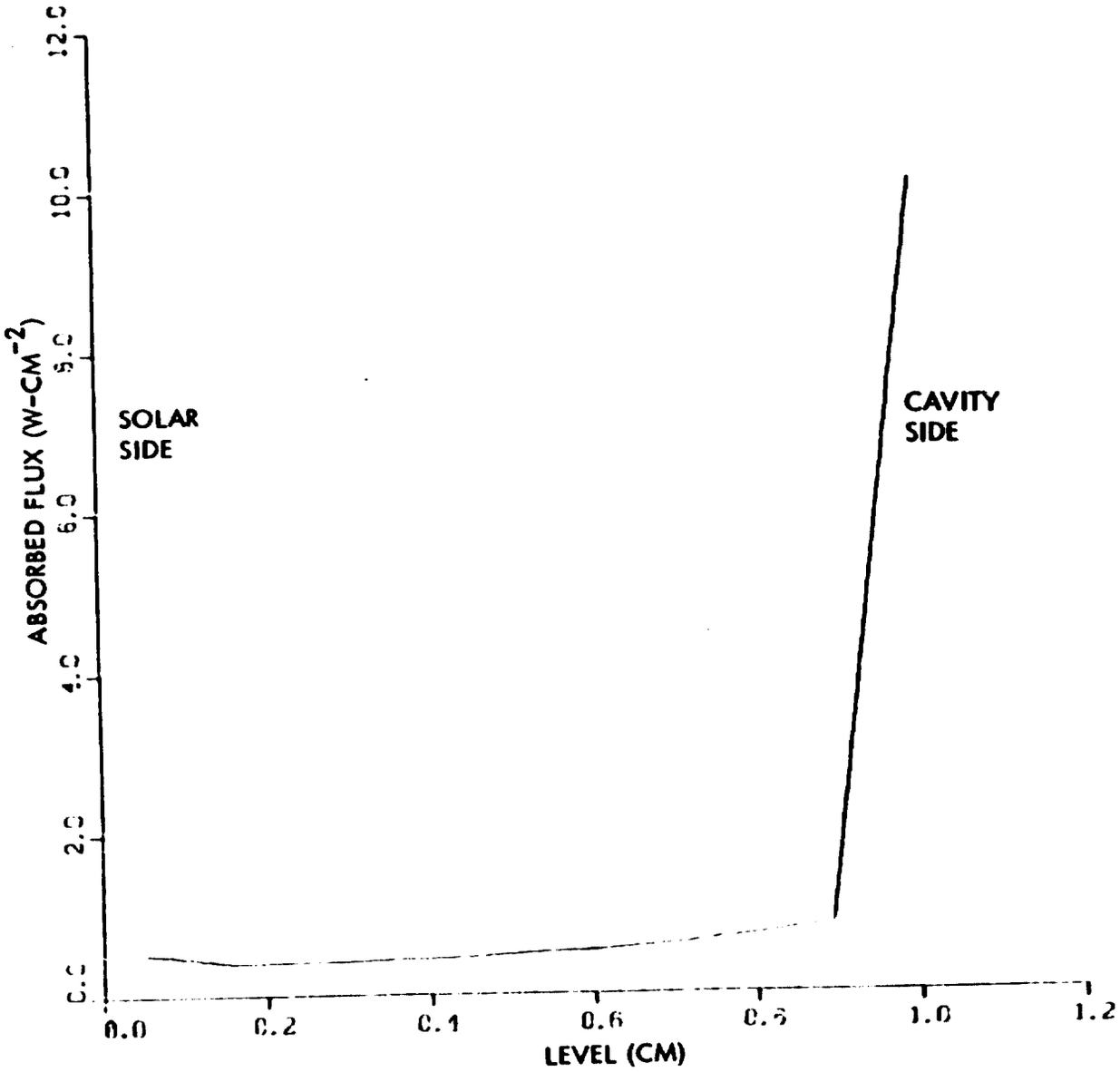

Figure 19. Absorption through Thickness of the Window at Outermost Region of Window

outermost region of the window and depicts minimum solar plus cavity IR loading on the window. The third, Figure 20 shows absorption across the window from centerline axis to edge.

Temperature Distributions

A series of thermal load cases were analyzed to predict window temperature profiles and temperature rises with solar loading and with both radiative and forced convective cooling. The series of calculations showed that film coefficients of 0.057 watts cm^{-2} C^{-1} (100 Btu-hr^{-1}-ft^{-2}-$^{o}F^{-1}$) on the external face, and half that on the internal face, are sufficient to sustain the window under peak flux conditions. Calculations showed the window would survive in the environment specified, and that several options are available to lower window temperatures to relatively benign levels. A summary of results is given below.

Window calculations lead to a radiative efficiency prediction for the receiver as shown in Table 13.

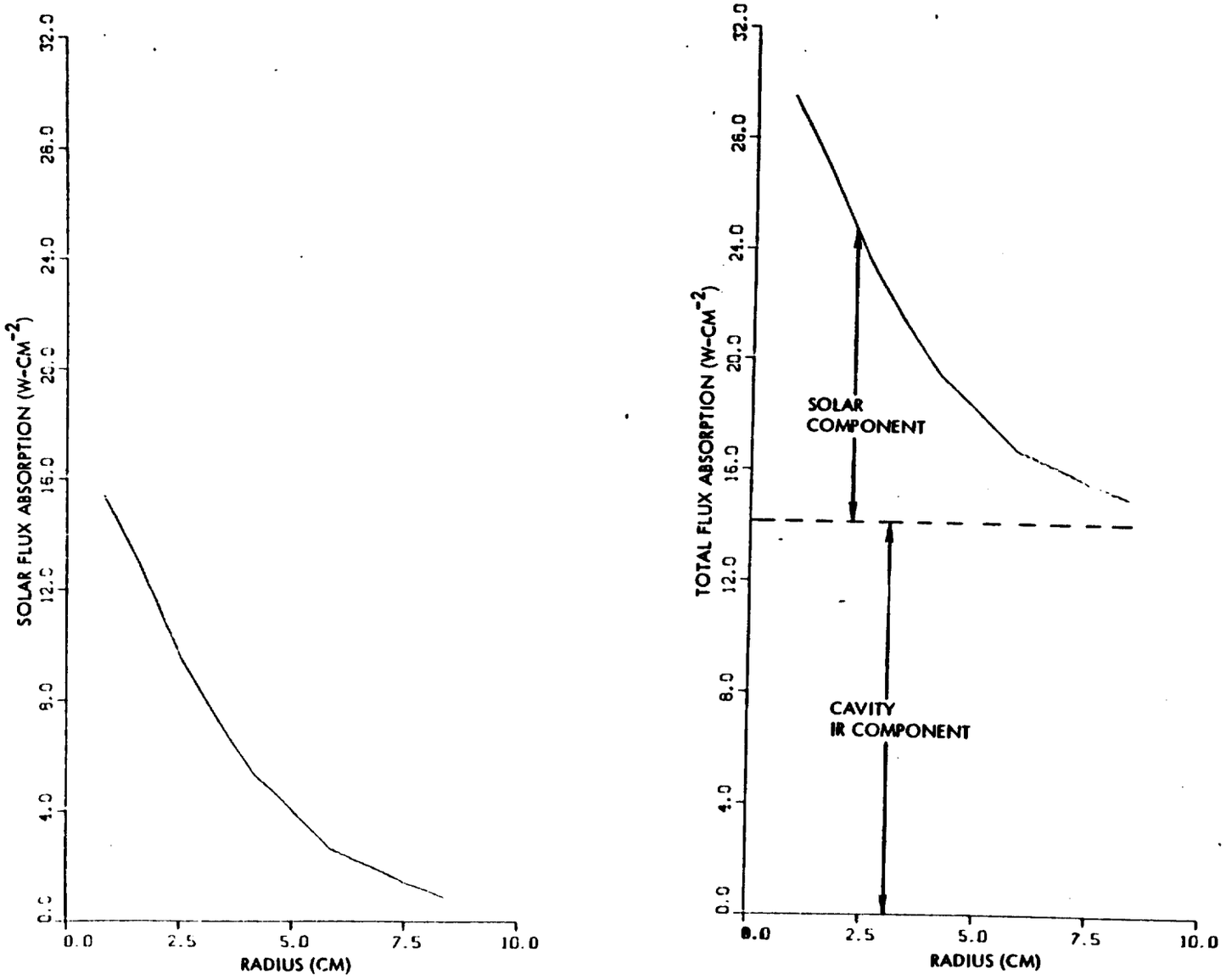

Figure 20. Absorption Across Window from Centerline Axis to Edge

TABLE 13. RECEIVER ENERGY BALANCE

Cooling Air Temperatures		Window Temperatures °C			
Internal	External	Maximum	Minimum	ΔT	Thermal Loss to Ambient
955	149	976	368	610	3.22 kW
955	50	957	288	669	3.42 kW
750	50	878	258	620	3.04 kW
500	50	778	221	557	2.56 kW
500	150	805	305	500	2.38 kW

Temperature contours are shown for windows operating in these regimes in Figure 21.

Solar absorption by the window is 0.77 kW so between 1.61 and 2.45 kW escape from the cavity through the window. This is a sharp reduction from the 6.53 kW which would escape from the aperture without a window. This "greenhouse effect" very nearly compensates for the incoming solar radiation that is lost to dielectric reflection.

An energy balance is shown below for windowed and open cavity receiver of the HTSTR sizing and temperature regime.

With Window	Effect	Without Window
74.0	Incident Power, kW	74.0
5.92	Reflection, 8%, kW	-
68.08	Input, kW	74.0
3.22	Window Loss	-
-	Aperture Convection (1%)	1.0
2.0	Aperture Radiation	6.53
62.9	Net Input	66.5
0.85	Radiative Efficiency	0.90

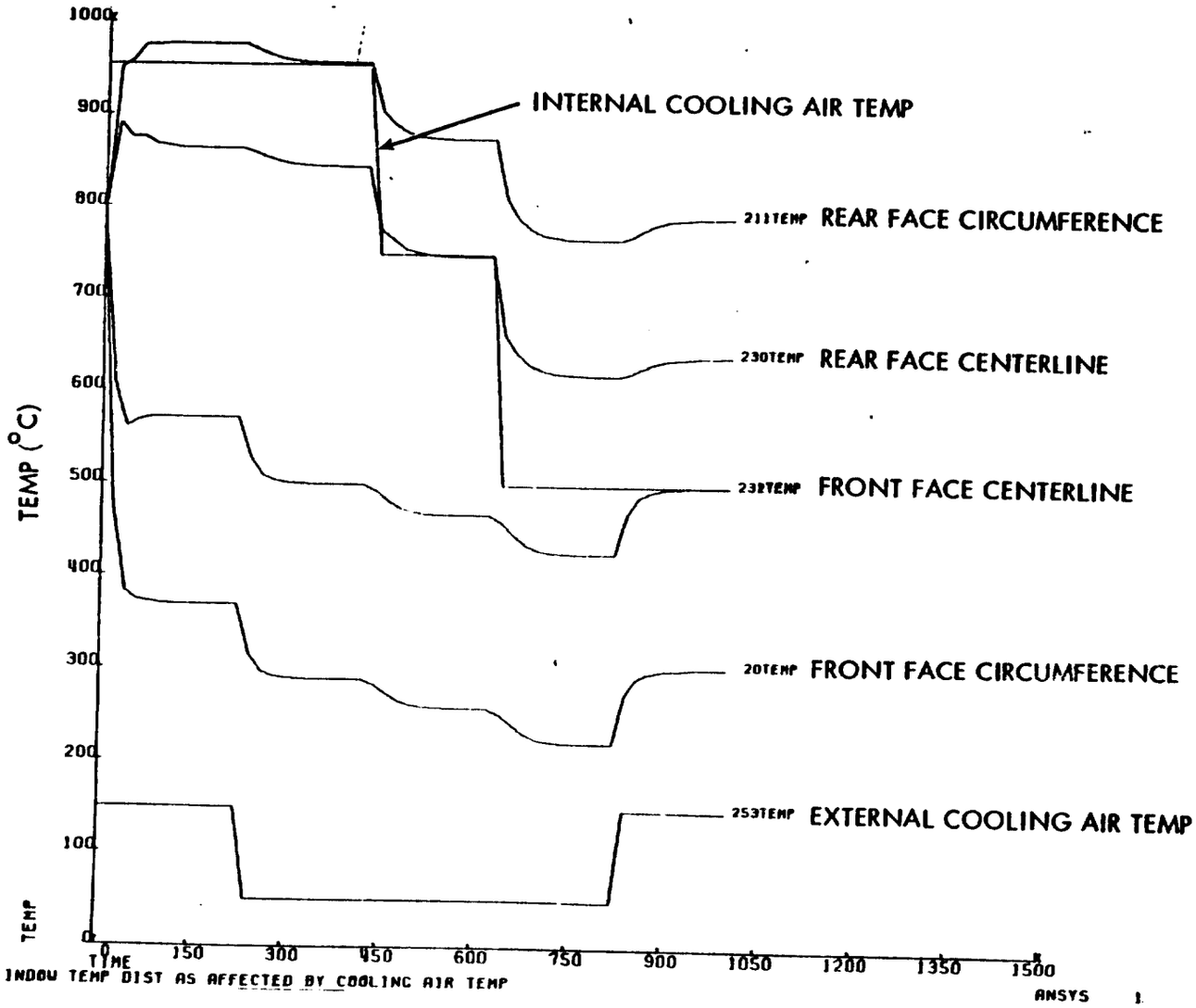

Figure 21. Temperature Contours (1 of 5)

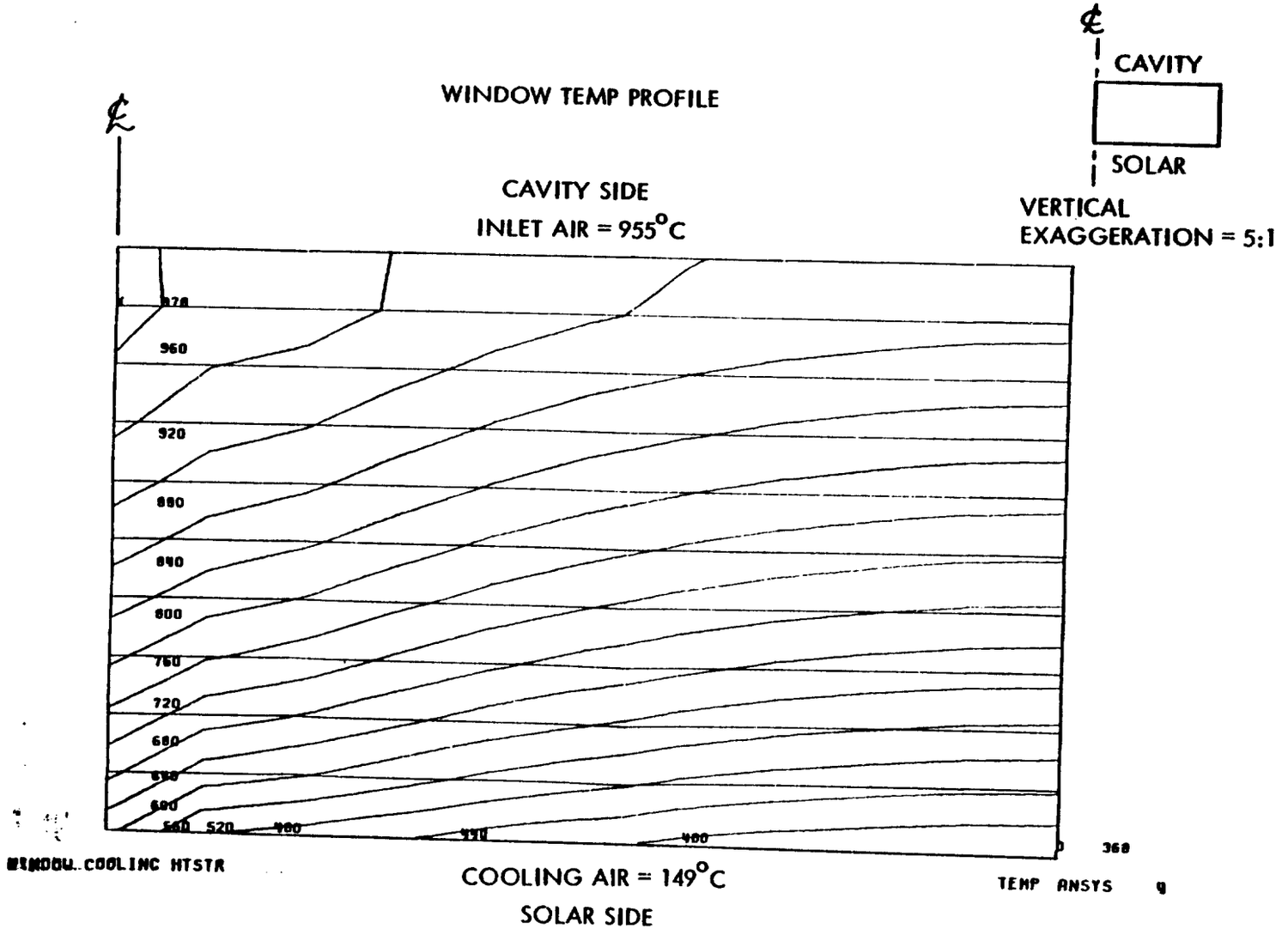

Figure 21. Temperature Contours (2 of 5)

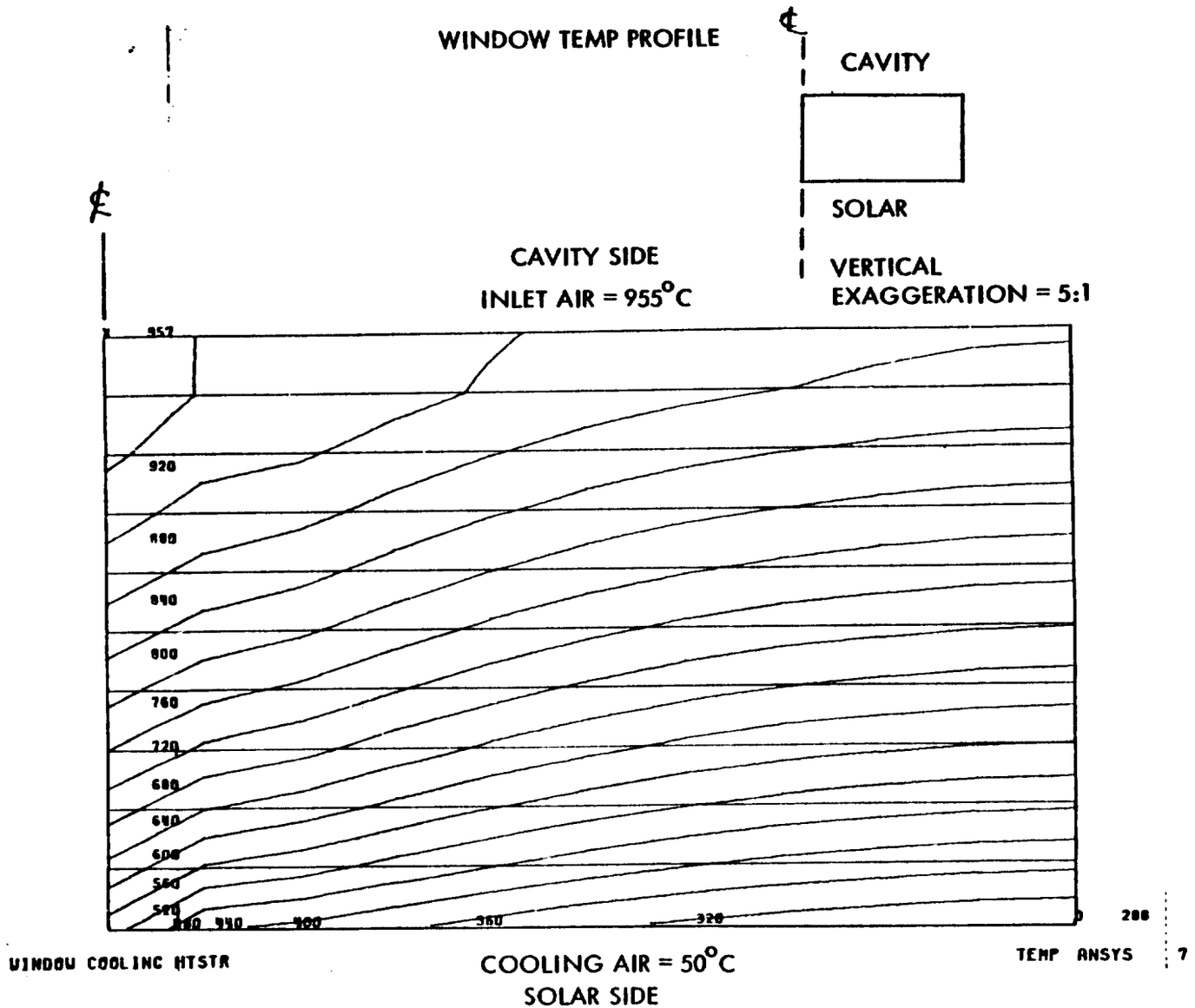

Figure 21. Temperature Contours (3 of 5)

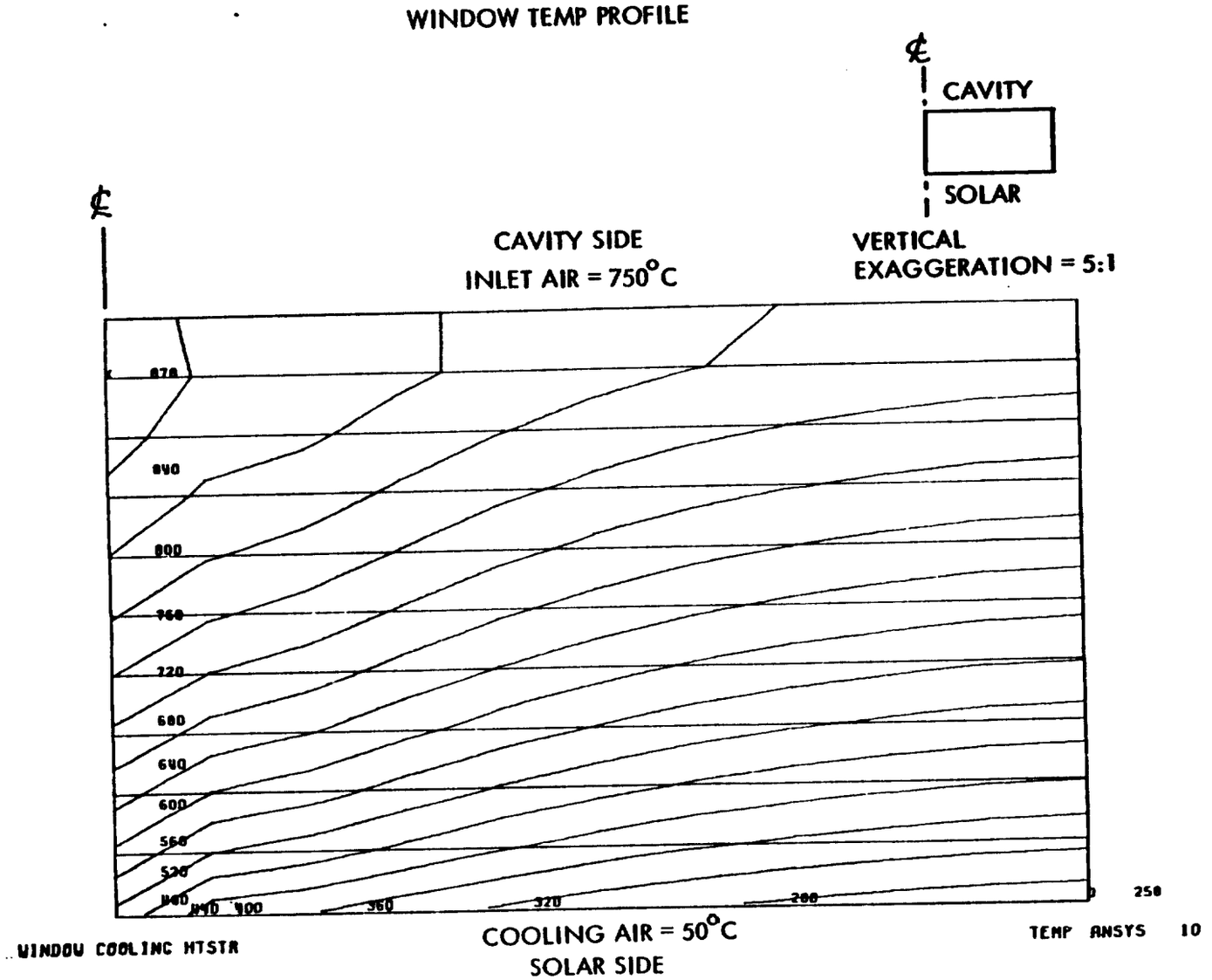

Figure 21. Temperature Contours (4 of 5)

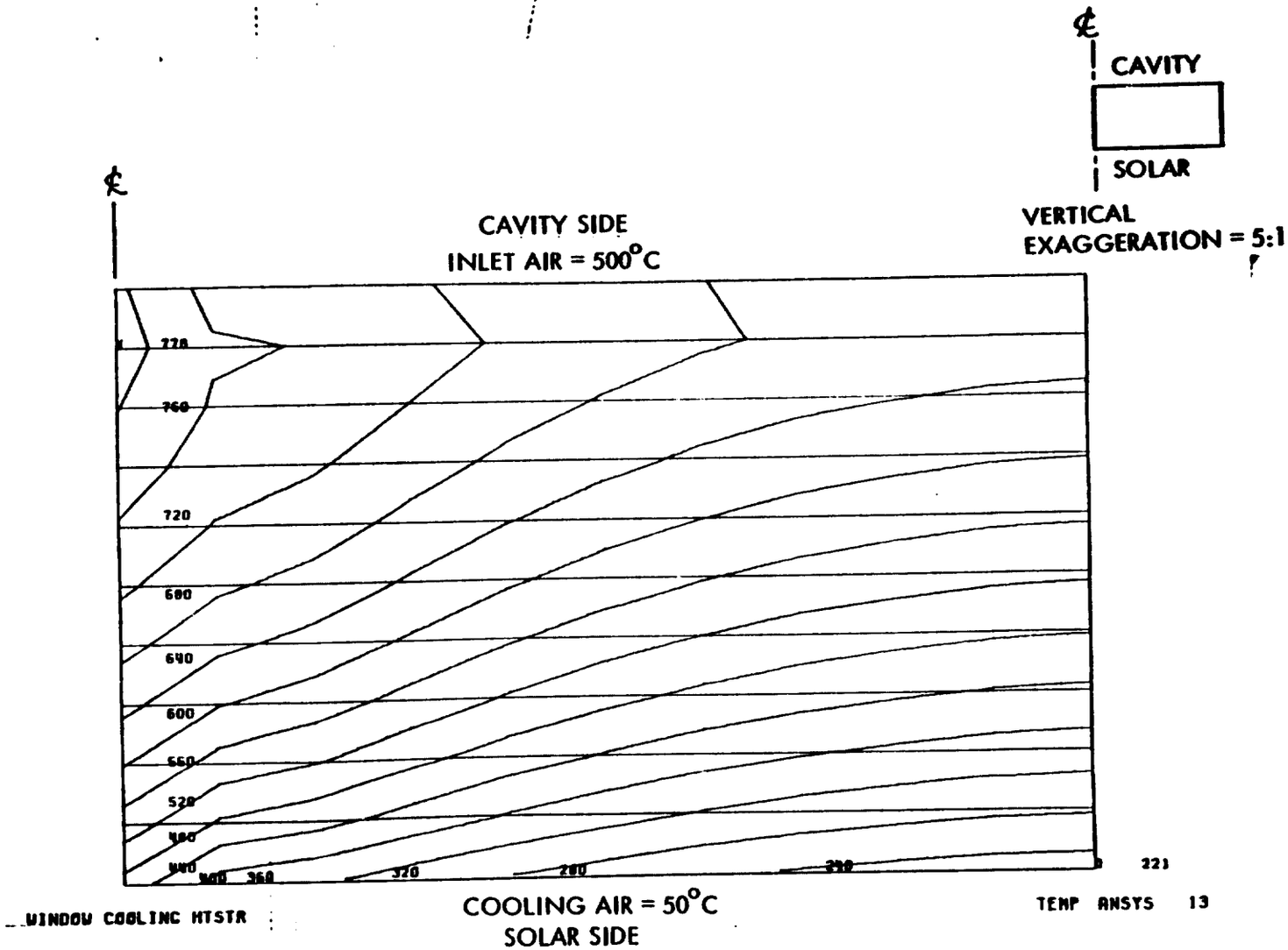

Figure 21. Temperature Contours (5 of 5)

2.3.7 Window Stress Analysis

The ANSYS finite Element Analysis Program combines structural capabilities with thermal analysis ability. The Nodel Temp Distribution Values, derived from the thermal analysis section, were input for the thermal stress component. Pressure components, equivalent to cavity pressure differential and edge loading conditions were also added to complete the necessary data input for a program solution run and post processing of resultant data for tabulation and plotting of associated stress and deflections.

The structural analysis was run to evaluate the design performance and integrity of the window when subjected to both thermal and pressure stress. The allowable stress was compared to the program resultant stress and displacement for this evaluation..

2.3.7.1 Structural Analysis Model

The ANSYS structural model continues where the thermal model ends. The structural model is the same 5 degree sector, divided into 10 radial zones by 10 layers thick, as the thermal model, having 100 elements and 231 nodal points, see Figures 22 and 23. The only differences between the models are the phantom convective and radiative elements on both sides of the window are not required, and the isoparametric solid thermal element was replaced by an equivalent 3-D isoparametric structural solid. The node numbers and locations are the same in both the structural and thermal models.

The front face of the model lies in the X-Z plane, the back face lies 5 degrees anti-clockwise from the front.

Because of the circular symmetry of the window, the analysis of only a small sector is required in order to fully analyze the entire window.

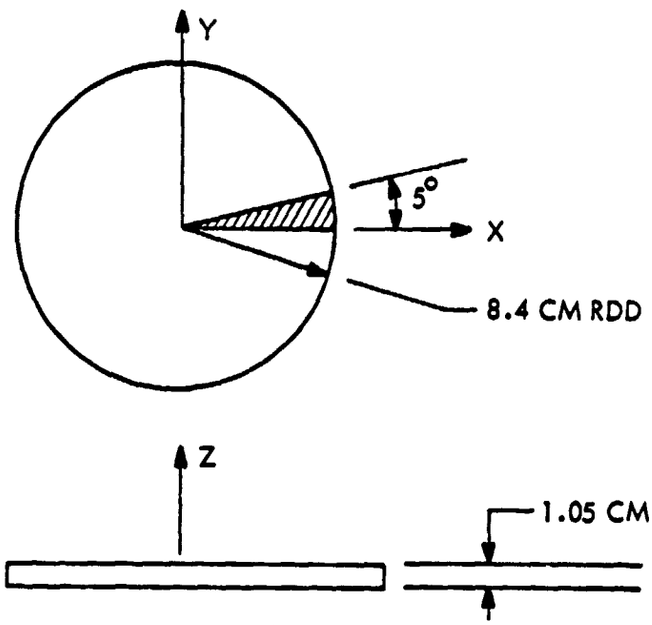

Figure 22. Structural Model

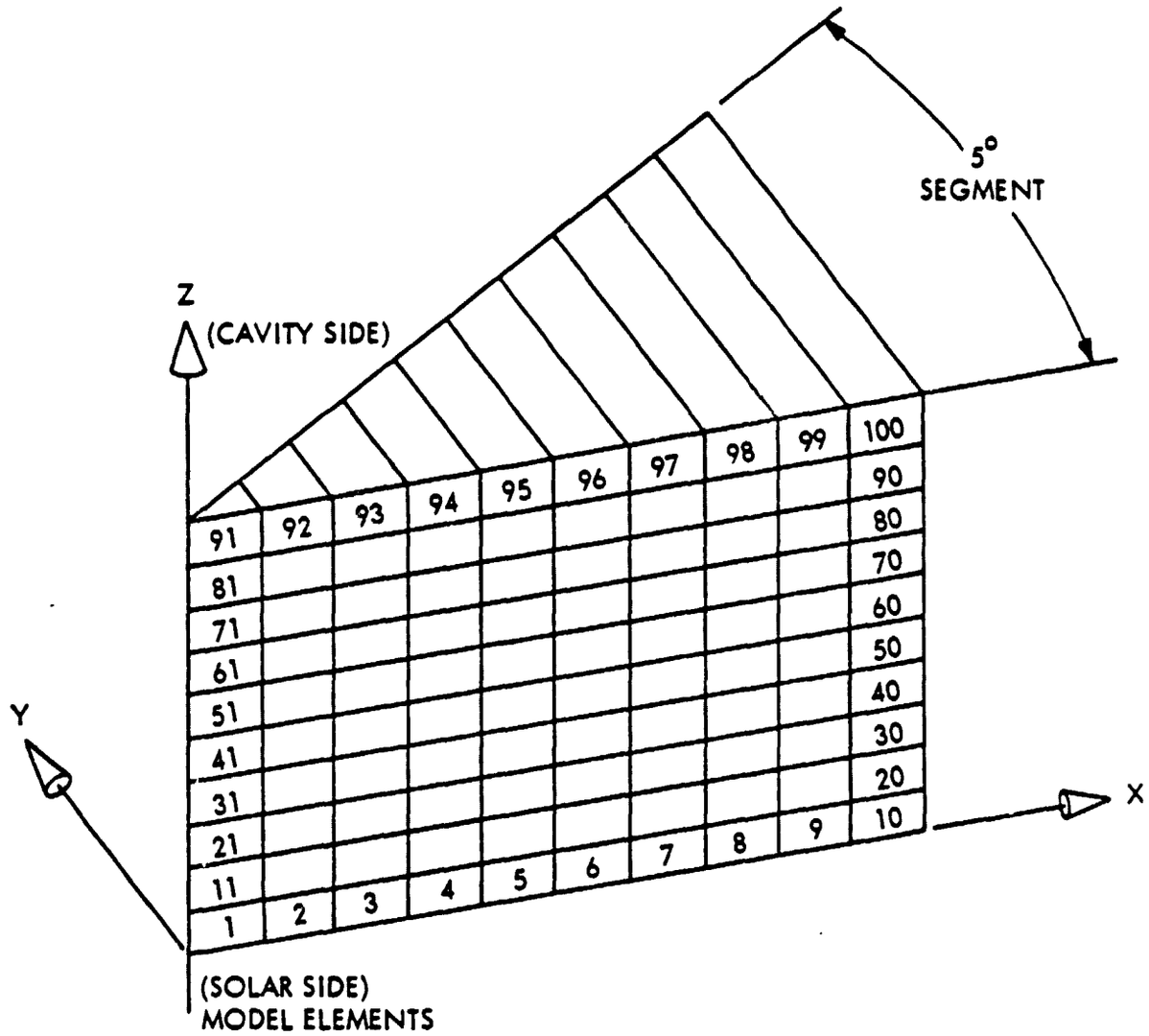

Figure 23. Structural Model

2.3.7.2 Analysis Input Data

The data input to the problem analysis is divided into different sections, those appropriate sections for the structural analysis are described below.

2.3.7.2.1 Material Property Definitions

Material property definitions are input to provide the necessary material properties for program computations requiring them. The material properties for the quartz window material are listed in Table 14.

2.3.7.2.2 Pressure Definitions

A uniform pressure load of 2 atmospheres was added to the top face of the top row of elements, element numbers 91 through 100. This represents the pressure differential on the inside of the window with the receiver operating as a closed system.

The pressure load is:

$$P = 2.0665 \times 10^3 \ GM_f/cm^2$$

2.3.7.2.3 Nodal Temperature Input

The temperature distribution results from the thermal analysis used as the nodal temperature input for the structural anlaysis, as the thermal stress component. Because the node numbers of both the thermal and structural are exactly the same, the nodal temperatures of the thermal analysis can be used as direct input.

The nodal temperature input values are shown and the resultant temperature contours as discussed in the thermal analysis section of this report.

TABLE 14. QUARTZ WINDOW MATERIAL PROPERTY DATA

Elastic Modulus

$$Ex = 7.34196 \times 10^{8}\ GM_f/cm^2$$

Coefficient of Thermal Expansion

$$ALPX = 5.5 \times 10^{-7}\ cm/cm\text{-}^{\circ}C$$

Poisson's Ratio

$$NUXY = 1.6 \times 10^{-1}$$

Mass Density

$$DENS = 2.2\ GM/CM^3$$

Maximum Allowable Compressive Stress

$$\sigma_{-LIM} = 1.19 \times 10^{7}\ GM_f/cm^2$$

Maximum Allowable Tensile Stress

$$\sigma_{+LIM} = 6.34 \times 10^{5}\ GM_f/cm^2$$

2.3.7.2.4 Boundary Conditions

Boundary conditions are specified in order to a) vary the edge conditions of how the window is supported, and (b) to give the model the realism of not just being a sector but in fact a continuous portion of the whole window.

The analysis was performed on two different boundary conditions, a simply supported edge and a semi-clamped edge condition.

The simply supported edge fixed the bottom two nodes in the Z direction (UZ = 0). The edge condition also allows translation in the X direction and rotation, of the other nodes along the edge, about the fixed nodes.

The semi-clamped edge fixes both the two bottom and two top nodes in the Z direction (UZ = 0). The nodes, however, are free in the X direction and hence allowed to translate in the X direction (grow radially).

The circular symmetry is preserved, and the model is a continuous piece of the whole window by setting all nodal displacements equal to zero (UY = 0) in the circumferential Y direction. Also UX = UY = 0 at those nodes which are coincident with the center line of the window. This assumes that under deflection the sides of the model remain parallel and the deflection at the center of the window can only be in the Z direction.

2.3.7.3 Load Cases

A total of four signficant load cases were analyzed to determine the stress and displacement levels of the window. These four load cases are shown in Figure 24 and include:

2.3.7.3.1 Load Case 1

a) Simply Supported Edge

b) Nodal Temp Input

Structural Analysis Load Cases

a) All load cases include nodal temperature input from previous thermal analysis.

b) All load cases include 2 atm pressure load on cavity side face.

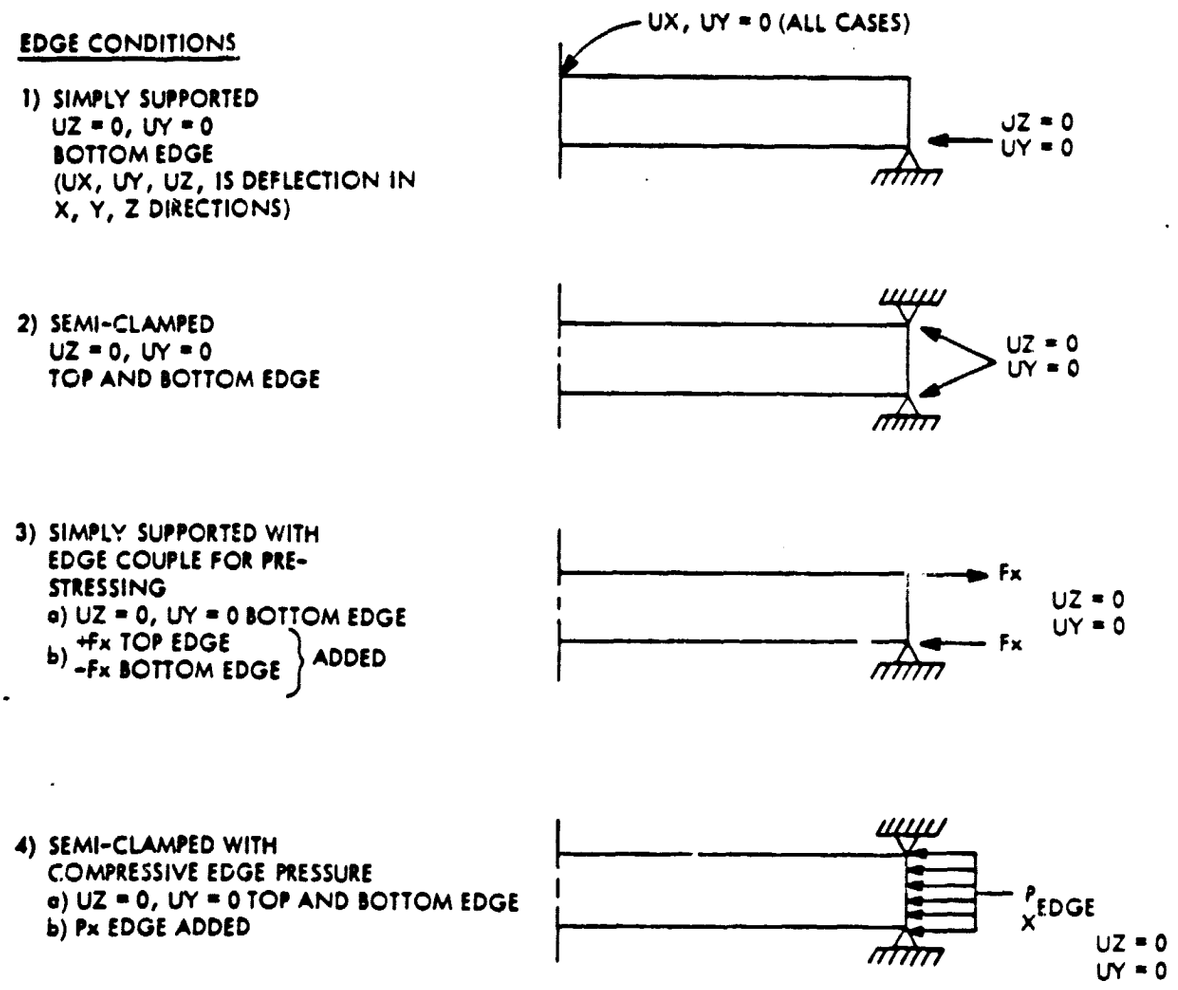

Figure 24. Load Cases

c) Pressure Load (on cavity side face)

2.3.7.3.2 Load Case 2

a) Semi Clamped Edge

b) Nodal Temp Input

c) Pressure Load (on cavity side face)

2.3.7.3.3 Load Case 3

a) Simply Supported Edge

b) Nodal Temp Input

c) Pressure Load (on cavity side face)

d) Edge couple (to add edge moment to act as prestressing component to window. The couple was added as a force (+Fx) at the top nodes and an equal but opposite force (-Fx) at the bottom nodes along the X axis.

2.3.7.3.4 Load Case 4

a) Semi Clamped Edges

b) Nodal Temperature Input

c) Pressure Load (on cavity side face)

d) Compressive Edge Pressure Load (This compressive edge load was added to act as a hoop stress to add additional compressive loading to the window. The added compressive load was intended to shift the window stress to a higher compression load and a lower tensile load. The nature of the quartz material allows much higher compressive than tensile loading.

2.3.7.4 Results

The results of the analysis of the four load cases are discussed below and also tabulated in Table 15.

For the simply supported edge load case 2.3.8.3.1, the maximum deflection is -0.0120 cm (-0.0047 in) and occurs at the window axis as might be expected for a simply supported thin disk with a uniform load on one side (positive Z is in the vert (up) direction).

The maximum tensile stress (Smax) is equal to 323,227 GM_f/cm^2 (4590 psi) and acts on the bottom surface. The maximum compressive stress (Smin) is equal to -323,464 GM_f/cm^2 (-4593 psi) and acts on the top surface.

For the semi-clamped edge load case 2.3.8.3.2 (Figure 25), the maximum deflection is -0.0053 cm (-0.0021 in) and again acts at the window axis in the vertically down direction.

The maximum tensile stress (Smax) is equal to 236,810 GM_f/cm^2 (3363 psi) and acts on the bottom surface. The maximum compressive stress (Smin) is equal to 234,837 GM_f/cm^2 (3335 psi), and acts on the top surface.

In both cases, the tensile and compressive stresses are nearly, but not exactly, equal and opposite. The difference is due primarily to the temperature gradients.

For the third load case 2.3.8.3.3, the same as the first except for an added edge moment to induce some opposite bending stress, the maximum deflection is +0.0072 cm (+0.0028 in) and acts at the top surface.

The maximum tensile stress (Smax) is 229,726 GM_f/cm^2 (3262 psi) and now acts on the top surface at the extreme edge as opposed to the nea nter for the previous two cases.

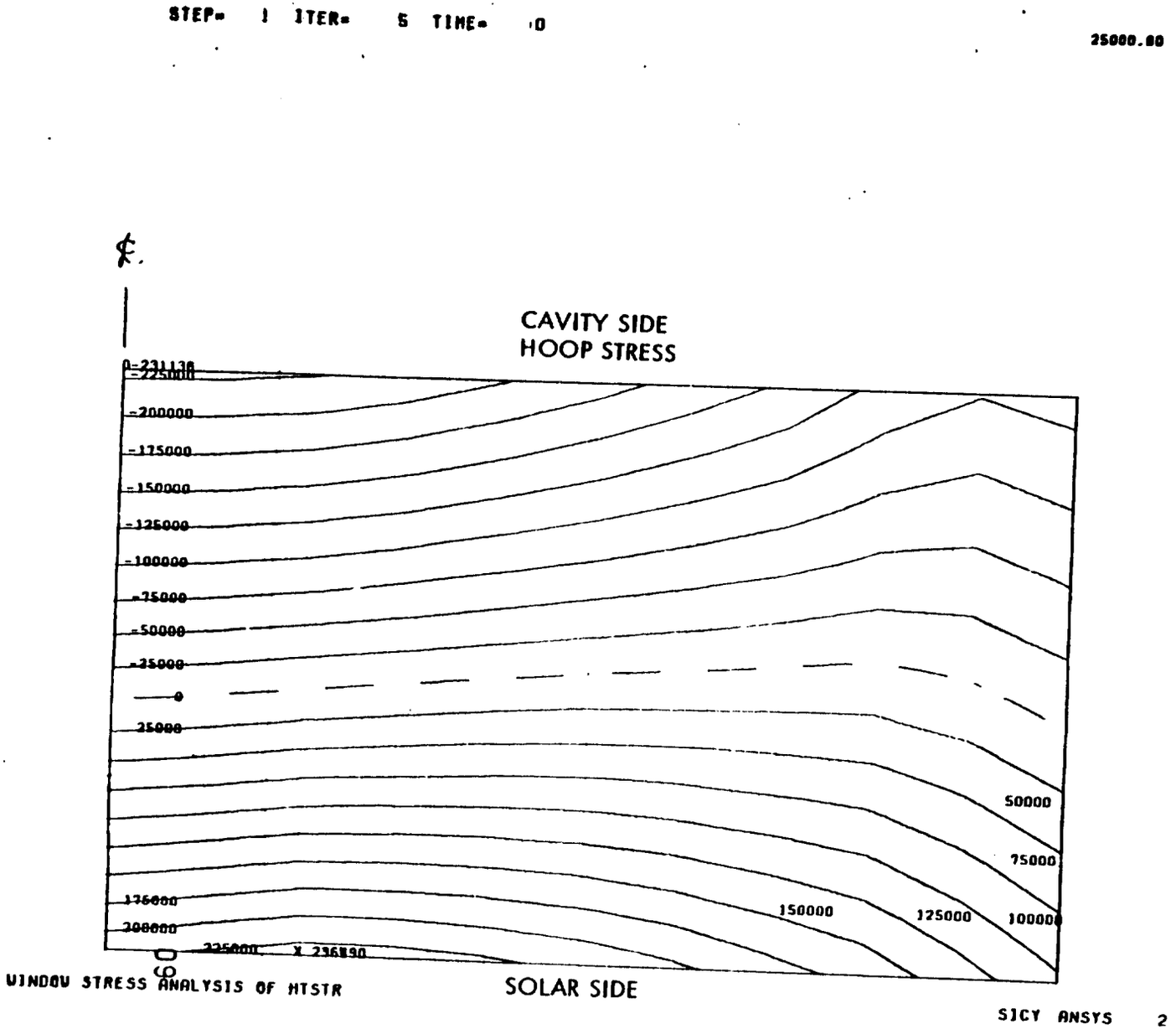

Figure 25. Load Case 2 Results (1 of 5)

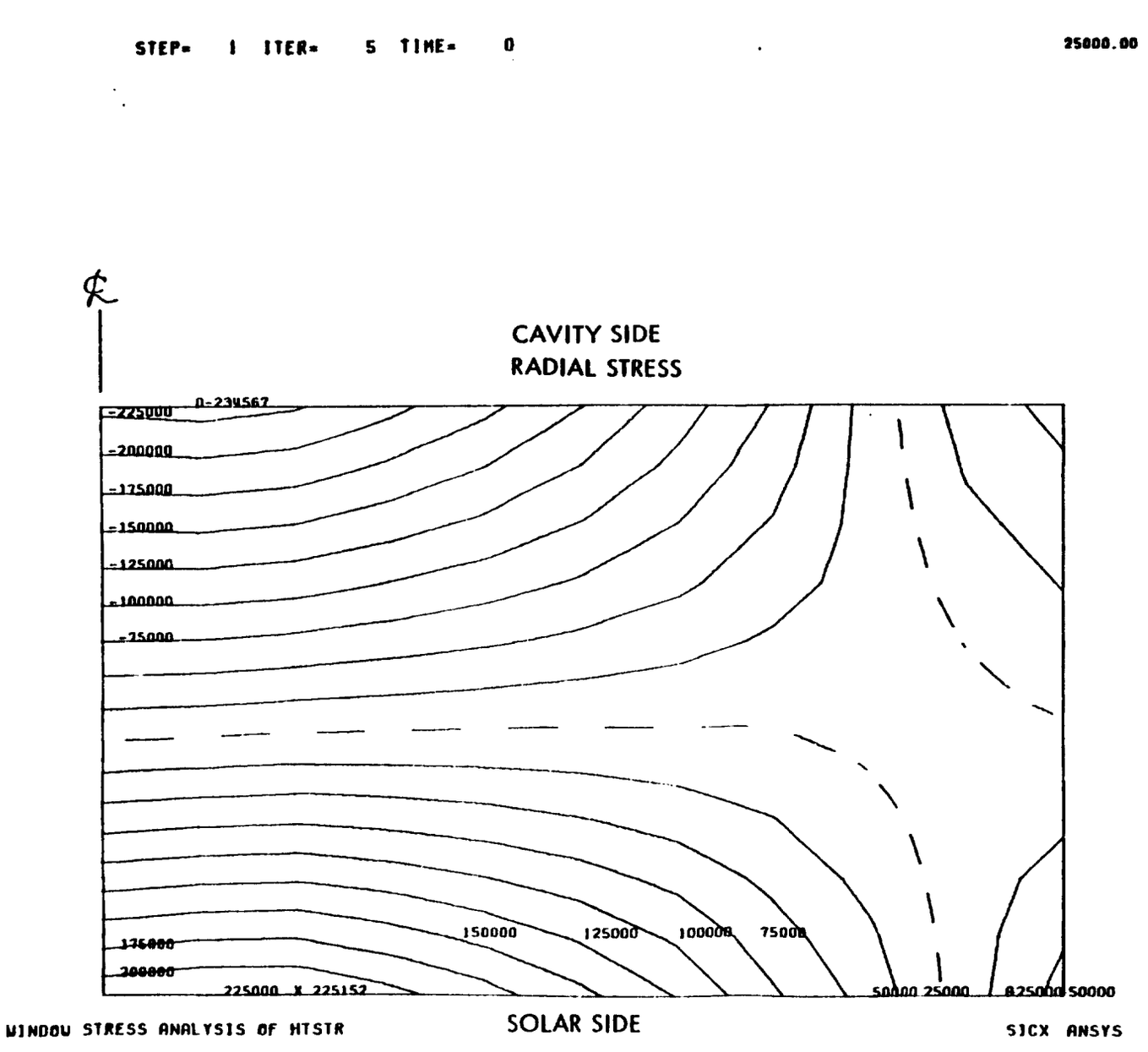

Figure 25. Load Case 2 Results (2 of 5)

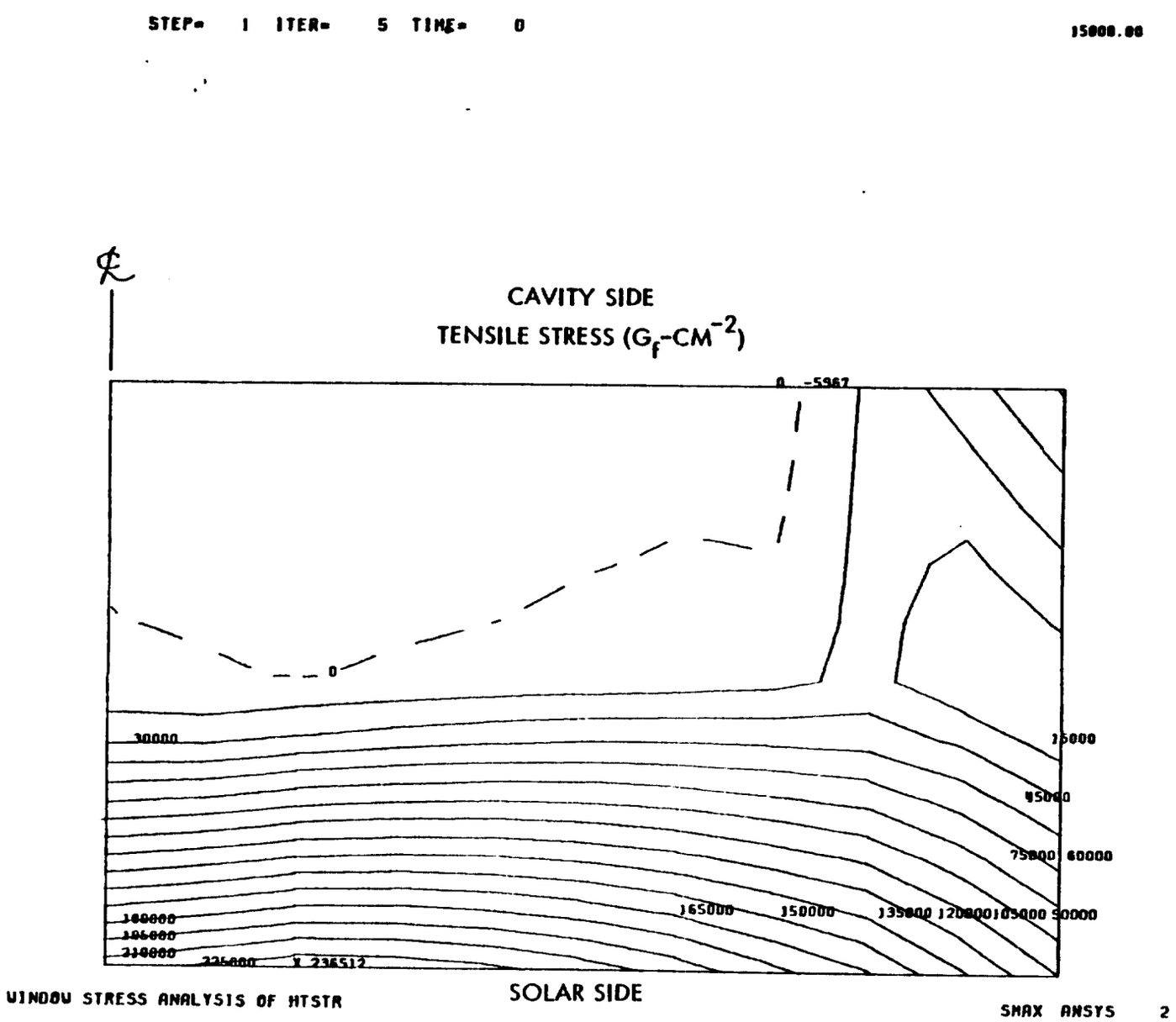

Figure 25. Load Case 2 Results (3 of 5)

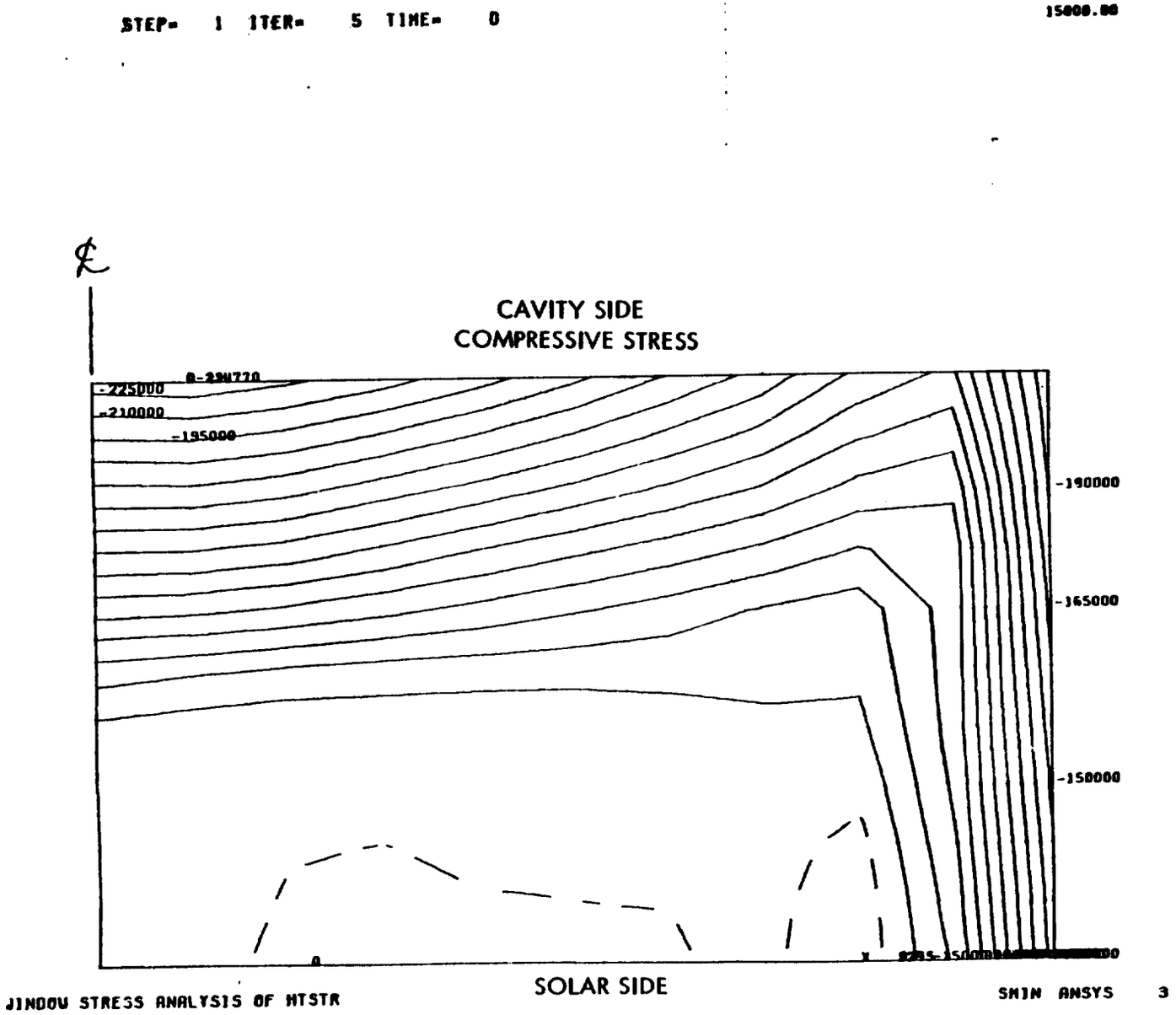

Figure 25. Load Case 2 Results (4 of 5)

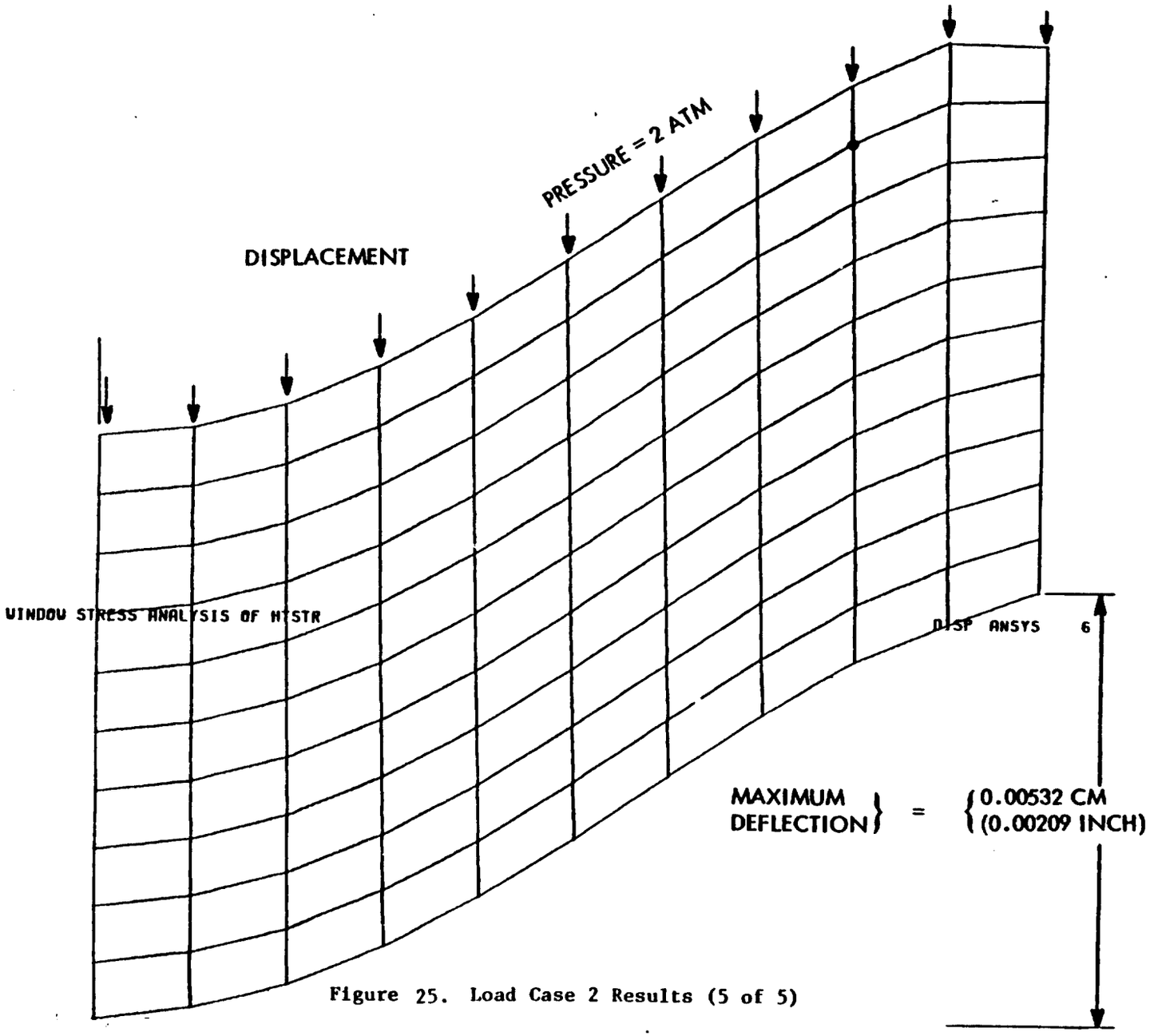

Figure 25. Load Case 2 Results (5 of 5)

TABLE 15. LOAD CASE SUMMARY

Input Conditions of Load Case	Max Displ (+Z is ↑) cm (in)	Max Ten Stress GM_f/cm^2 (psi)	Max Comp Stress GM_f/cm^2 (psi)
a) Simply Supported	-0.0120	323227	323464
b) Temp Load	(-0.0047)	(4590)	(4593)
c) Pressure Load		Acts: Bot/Cent	Acts: Top/Cent
a) Semi Clamped	-0.0053	236810	234837
b) Temp Load	(-0.0021)	(3363)	(3335)
c) Pressure Load		Acts: Bot/Cent	Acts: Top/Cent
a) Simply Supported	+0.0072	229726	221208
b) Temp Load	(+0.0028)	(3262)	(3141)
c) Pressure Load		Acts: Top/Edge	Acts: Bot/Edge
d) Edge Moment			
a) Semi Clamped	-0.0054	19097	471632
b) Temp Load	(-0.0021)	(271)	(6697)
c) Pressure Load		Acts: Top/ 2/3 Edge	Acts: Top/Cent
d) Comp. Edge Press.			

The maximum compressive stress (Smin) is equal to 221,208 GM_f/cm^2 (3141 psi) and acts on the bottom surface and also at the extreme edge.

For the fourth load case 2.3.8.3.4 (Figure 26), the same as the second except for the compressive edge pressure, the maximum deflection is -0.0054 cm (-0.0021 in) and acts at the bottom surface.

The maximum tensile stress (Smax) is 19,097.6 GM_f/cm^2 (271 psi) and acts on the top, towards the outer edge. It is likely to occur there due to the bending stress imposed by the edge compression. The maximum tensile stress on the bottom at the window axis is only 8018 GM_f/cm^2 (114 psi).

The maximum compressive stress (Smin) is 471,632 GM_f/cm^2 (6697 psi) and acts on the top near the window axis (Z axis).

In load cases 1 and 2 the stresses are considerably greater than the maximum tensile design working stress of 70,422 GM_f/cm^2 (1000 psi) with little hope of stress reduction.

Load case 3, with the edge moment shows that with some judicious tweaking of the edge moment, it may be possible to reduce the maximum tensile stress. However, it is doubtful that it could be reduced to the allowable working stress level.

Load case 4 shows the most promise and, in fact, is a workable mechanical solution. The maximum tensile stress is well below the maximum allowable, however, the maximum compressive stress is considerably higher than any of the other load cases. The nature of the quartz window material allows for a much higher compressive stress than tensile stress. The tensile strength of quartz is documented at 633,803 GM_f/cm^2 (9000 psi) and a compressive strength of 11,929,577 GM_f/cm^2 (169,400 psi). Using a comparable safety factor of 9 for the allowable compressive stress as was used for the allowable tensile stress, the allowable compressive stress is 1,323,944 GM_f/cm^2 (18,800 psi). This is well above the calculated maximum compressive stress for load case 4.

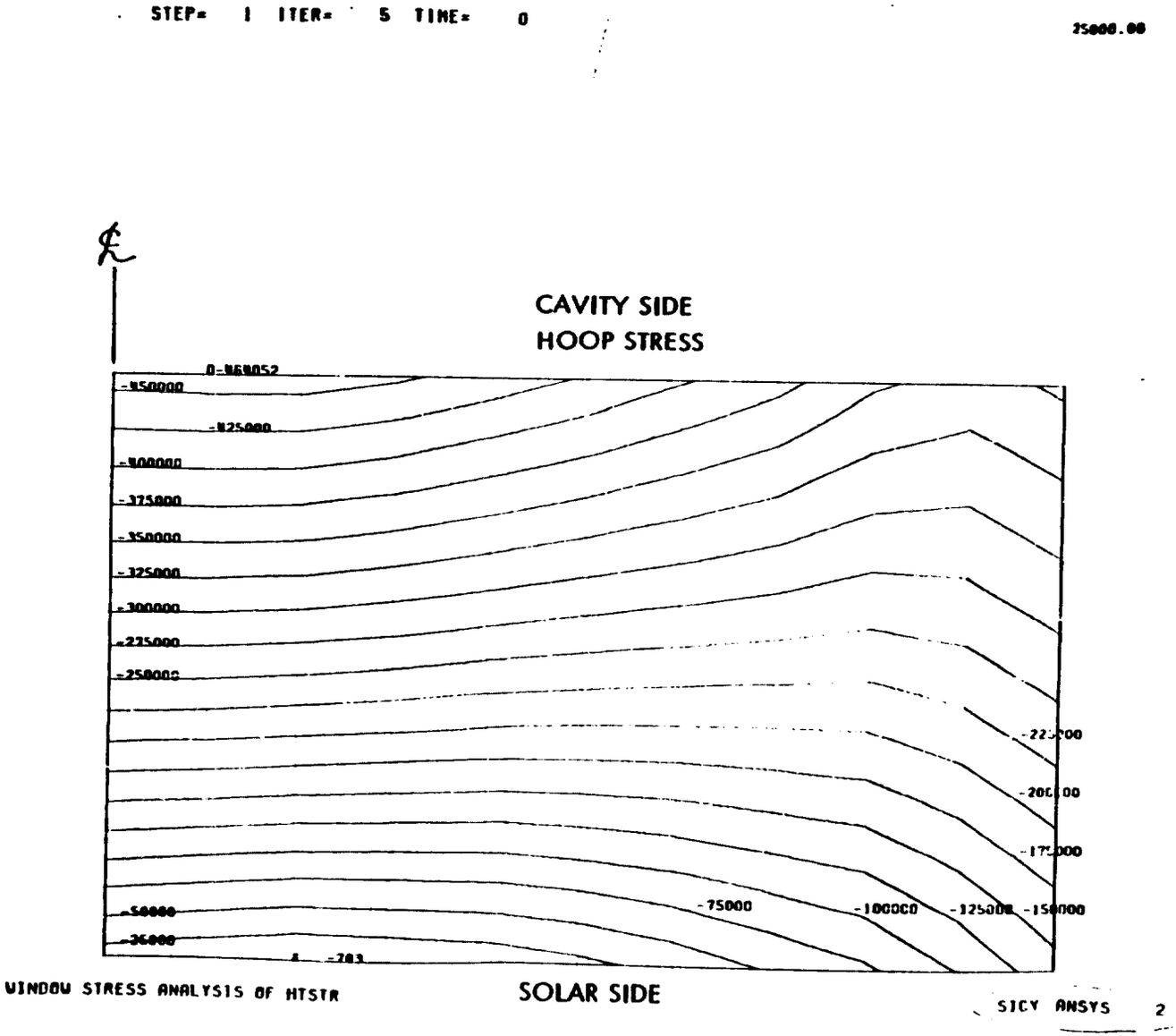

Figure 26. Load Case 4 Results (1 of 5)

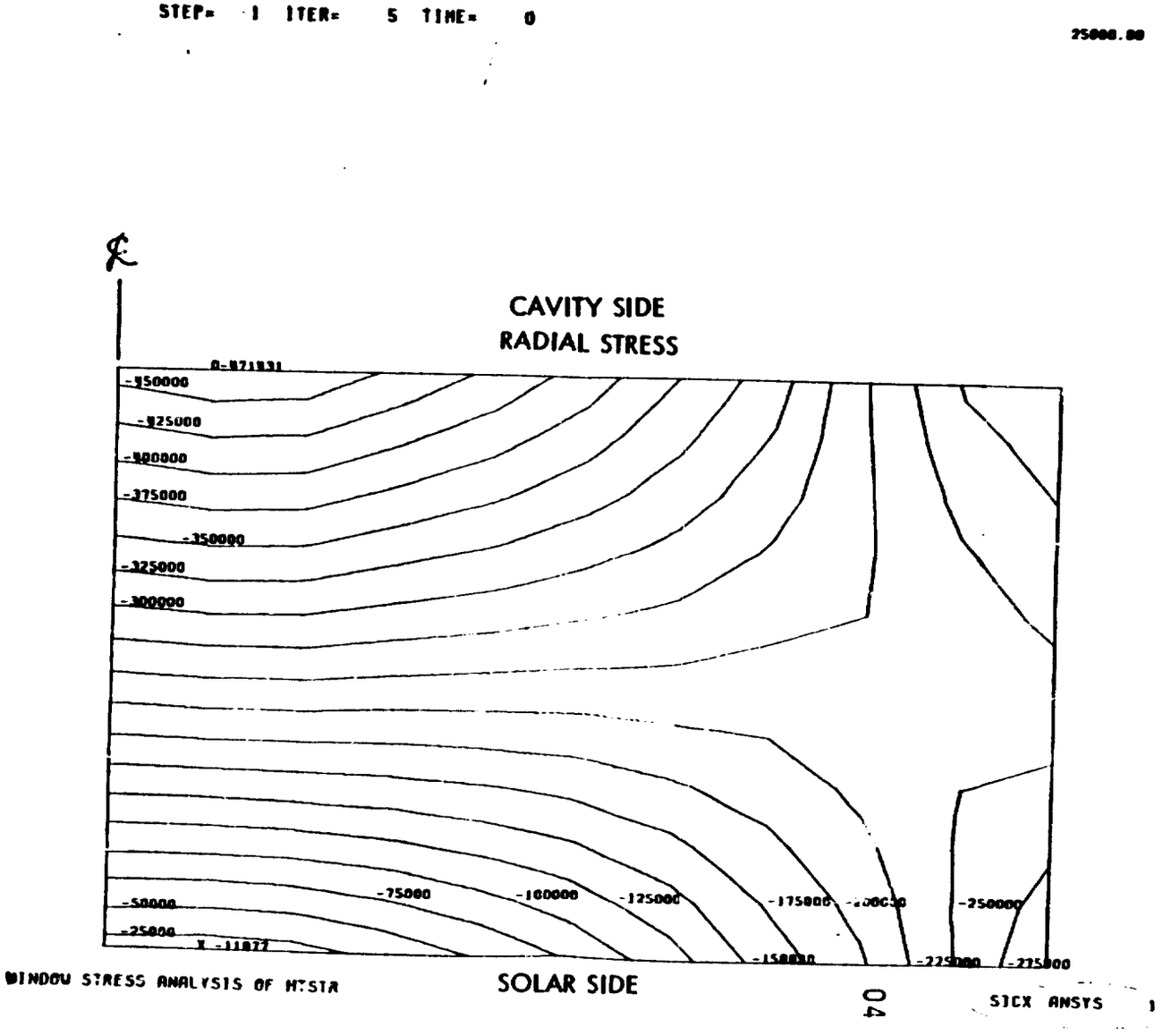

Figure 26. Load Case 4 Results (2 of 5)

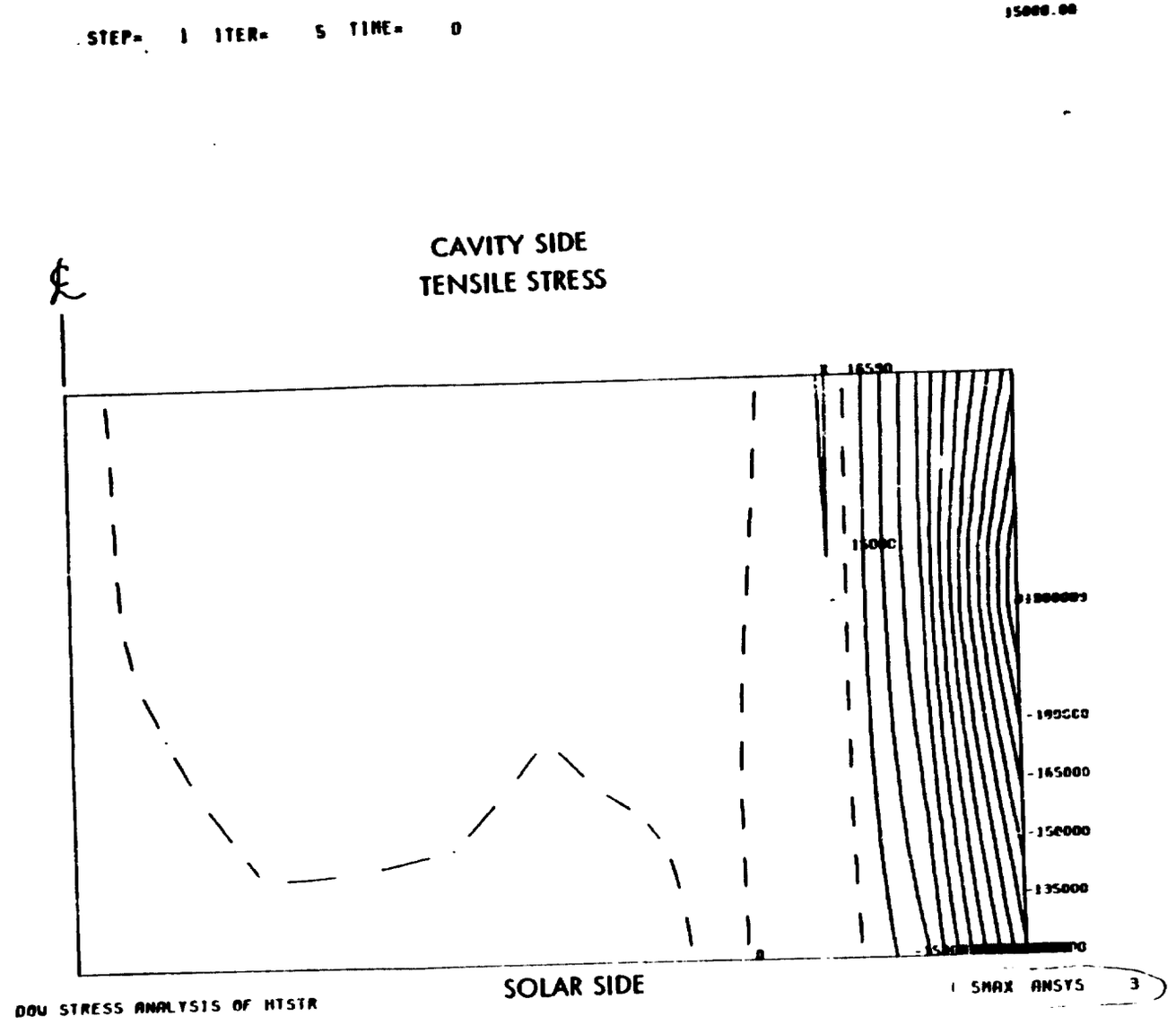

Figure 26. Load Case 4 Results (3 of 5)

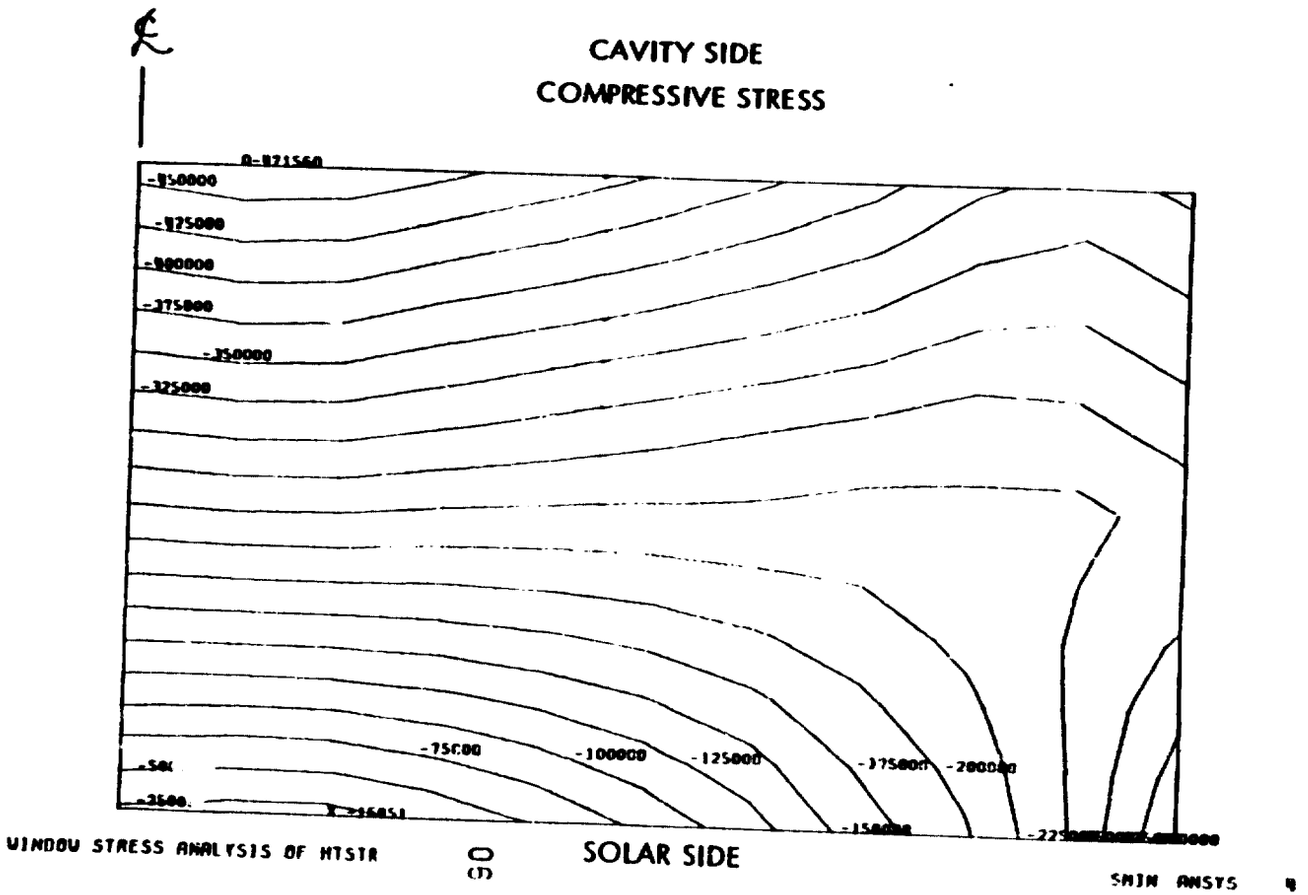

Figure 26. Load Case 4 Results (4 of 5)

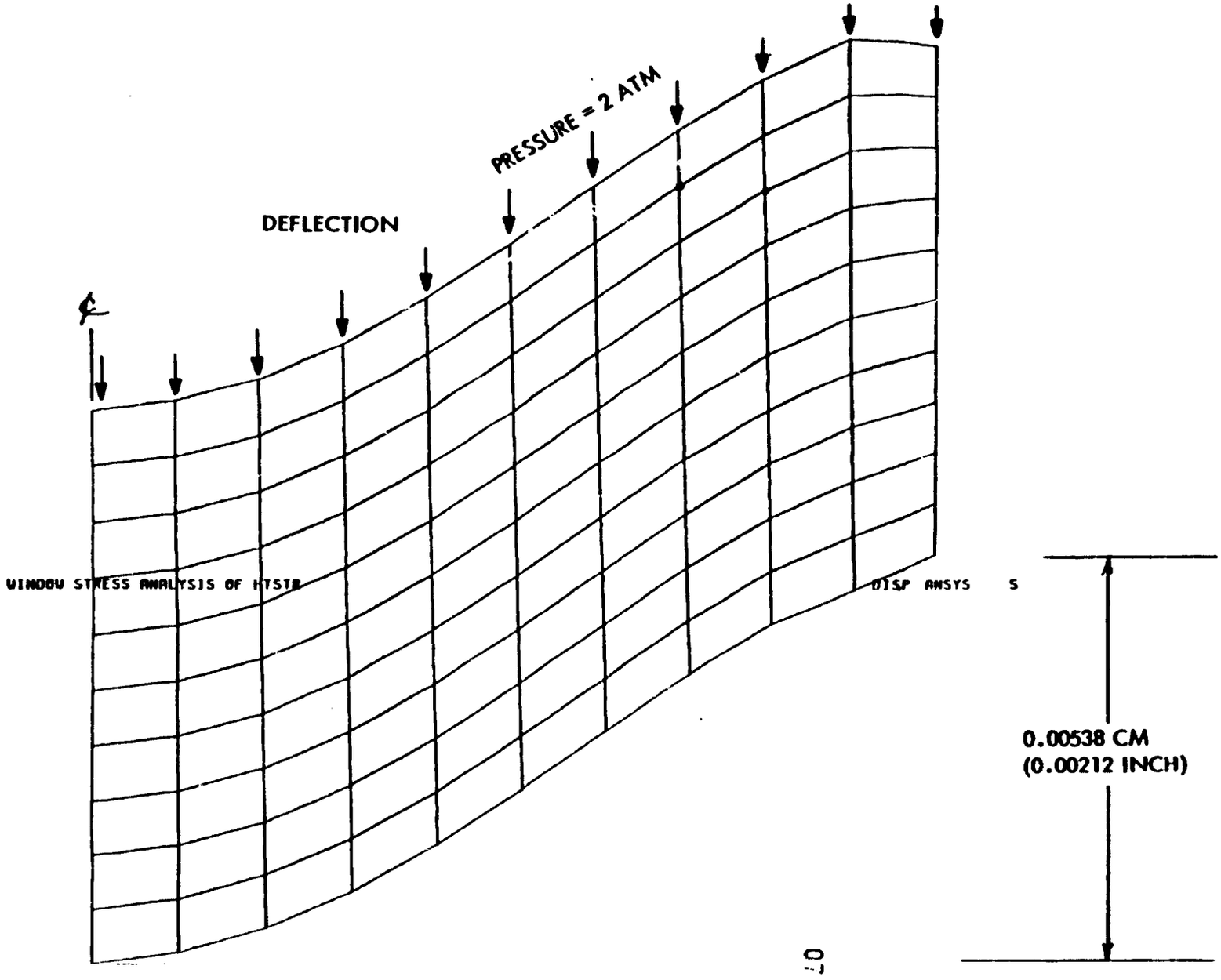

Figure 26. Load Case 4 Results (5 of 5)

2.4 RECEIVER OPERATION AND PERFORMANCE REQUIREMENTS

2.4.1 Orientation

The HTSTR assembly is not orientation-sensitive. It is only important that the receiver be mounted coincident with the focal axis of the primary concentrator and that its window be at the focal point facing the mirror.

2.4.2 Interfaces

There are three system interfaces to be made with the HTSTR: (a) mechanical mounting interface via the vessel flange or mounting lugs which could be added, at slight additional cost, to accommodate other mounting systems; (b) working fluid ducting via flanges on the receiver rear dome; and (c) cooling air supply to the window flange fitting for distribution to the external window face.

2.4.3 Response Transients

Model runs have been performed for insolation of 251,934 Btu/hr at $\dot{m}$ = 840 lb/hr and at 50% of this insolation at $\dot{m}$ = 311.25 lb/hr (chosen to yeild about the same output temperature). As illustrated in Figures 27 and 28, the honeycomb response is the order of 2 minutes at full flow, while the storage response is at ~0.5 hr at full flow. At reduced insolation (with commensurately reduced flow), the time constants are approximately doubled. Figure 29 shows the response to solar outage.

A distinctive feature of the illustrated transients is the relatively weak "long term transient" that is not seen until slightly after 10 minutes have elapsed after turn-on. This is presumed to be the result of insulation warmup, not being very strongly coupled to the airstream.

2.4.4 Loss of Coolant Transient

In both Figures 27 and 28, the run terminates with a reduction in flow rate to 20% of starting value. This small residual flow is meant to simulate the natural convection levels that would be expected if the forced cooling were to fail.

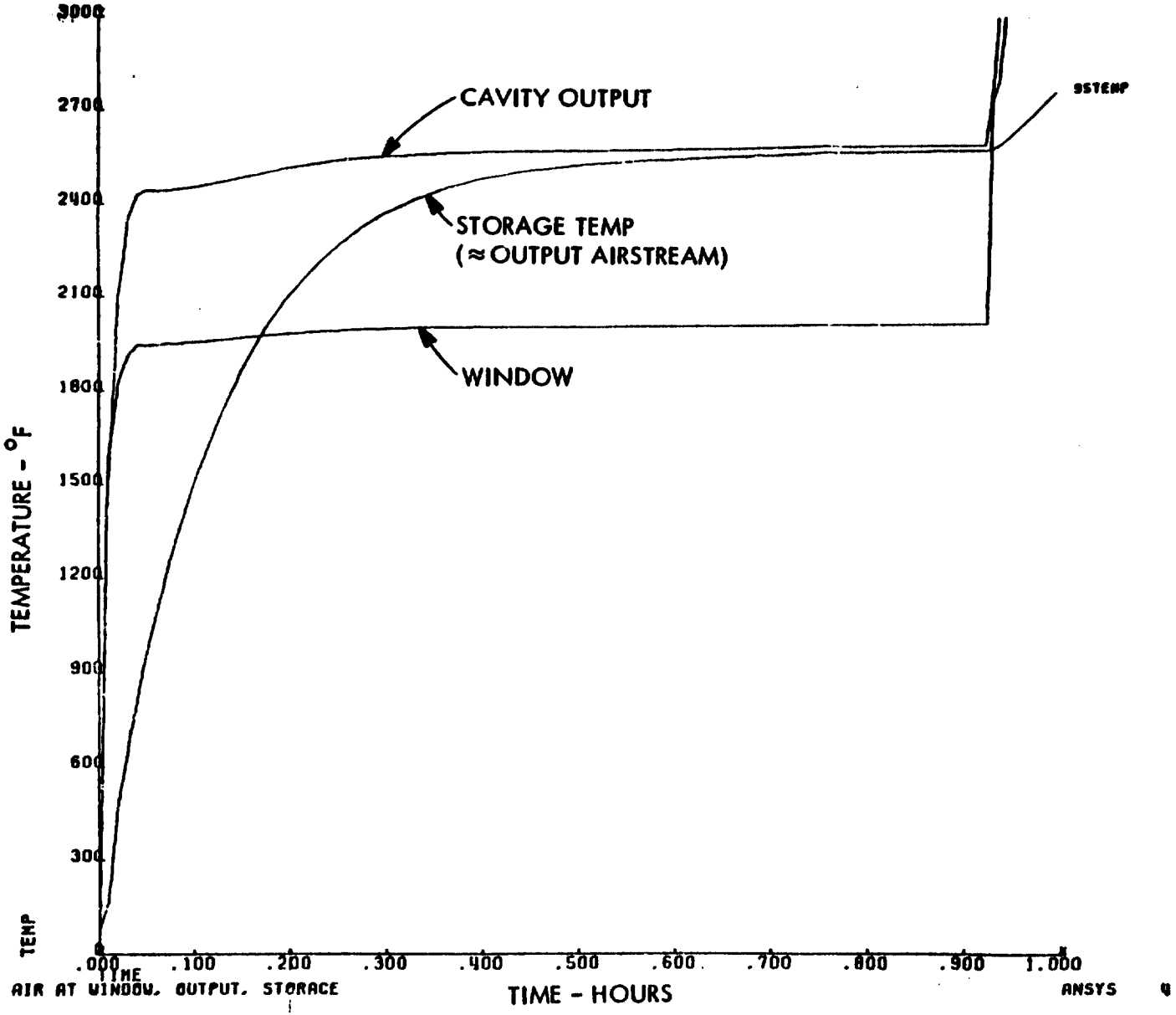

Figure 27. Temperature versus Time, 100% Insolation

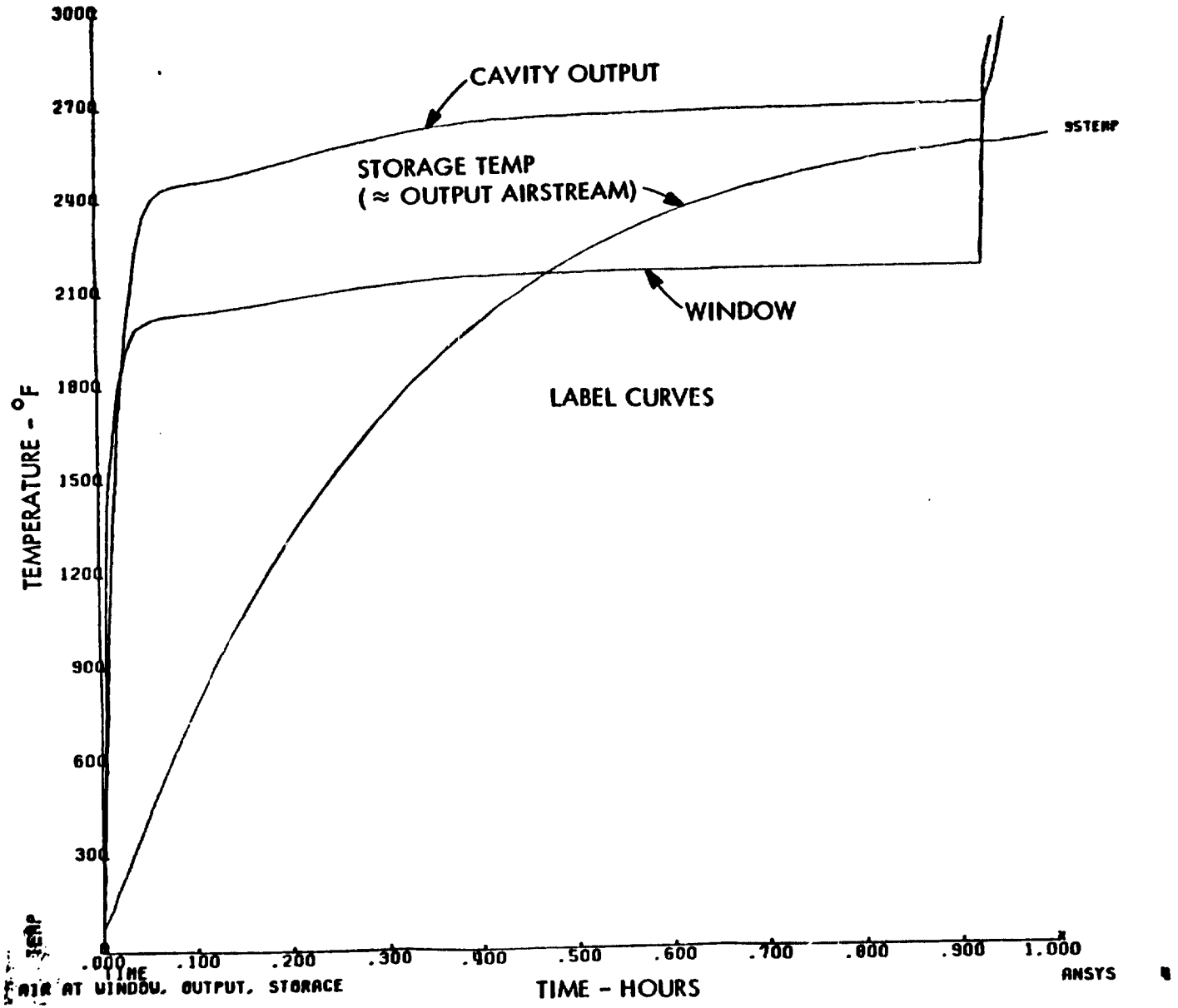

Figure 28. Temperature versus Time, 50% Insolation

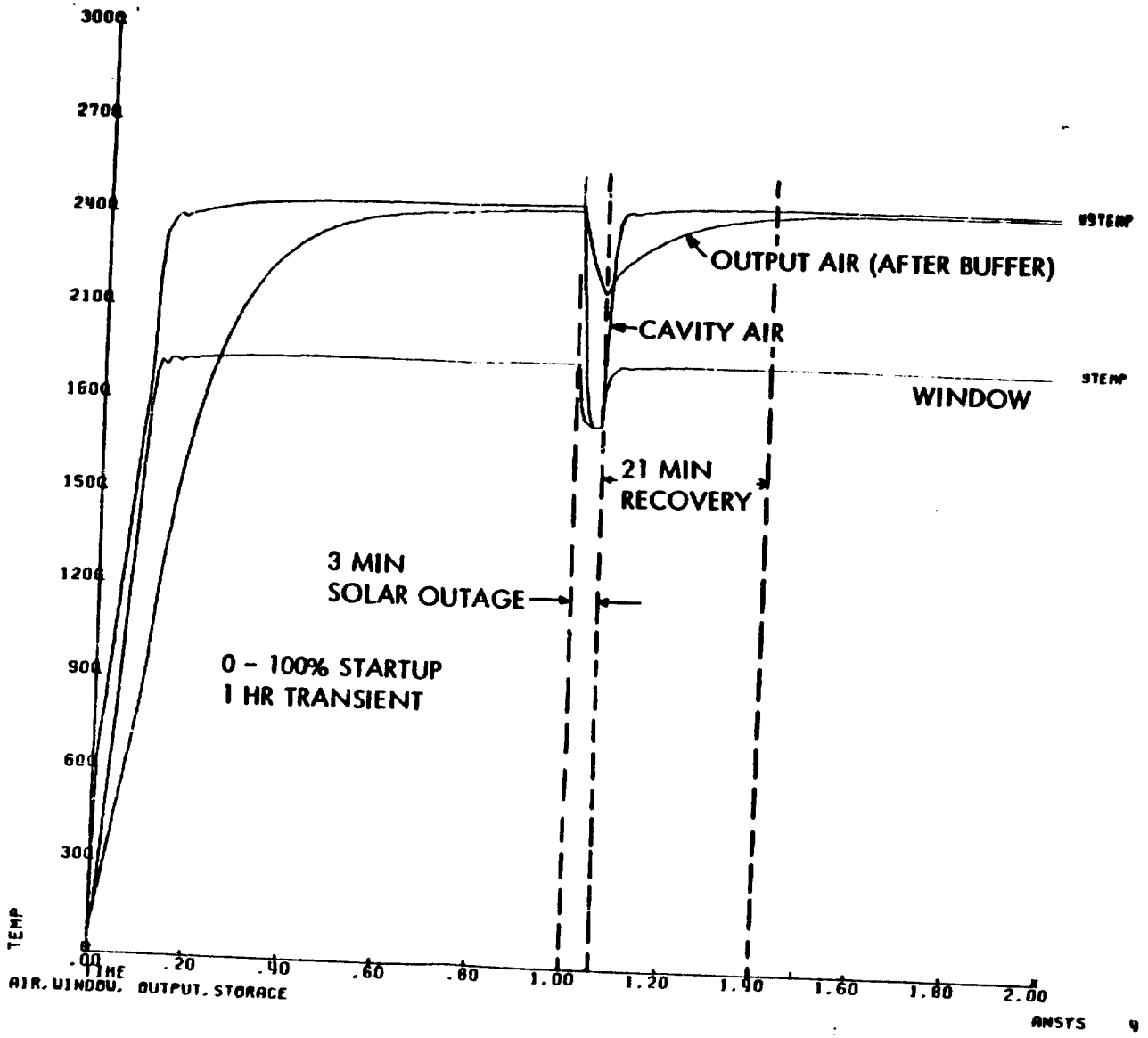

Figure 29. Response to Solar Outage

The honeycomb temperature is seen to climb rapidly by at least 500°F in a minute or two in both cases. The window, due to its weak coupling, increases in temperature at 1/2 to 1/3 this rate. The storage output, however, climbs at an order of magnitude or more reduced rate. This reduction indicates the degree of protection that could be provided for a turbine engine or other equipment using this receiver.

2.5 PROTOTYPE FABRICATION

2.5.1 Manufacturing Processes

2.5.1.1 General

Fabrication of prototype units of the HTSTR will not require the use of capital expenditure for either production equipment or facilities. Sanders' present production facilities have been used to manufacture infrared countermeasures (IRCM) systems (AN/ALQ-147) for aircraft self-defense. These IRCM systems utilize the same kinds of materials and have similar hot gas flow requirements as the HTSTR. The required low volume setups for refractory discs (receiver and storage) already exist and they are obtainable from the vendors used in prior development. In addition, the metal-forming to be used for the housing is common to the water and boiler tank industry.

A quartz window of the style used during Sanders' 10 KWt Receiver contract will be used in the HTSTR. Assembly fixtures and tools will be concerned with single unit work (a rate of one HTSTR per week). No exotic methods will be needed for Phase II prototype development.

2.5.1.2 Implementation of Fabrication Plan

The schedule of Figure 30 gives the timing of design release, parts procurement (purchase and/or in-house fabricate), and assembly/test of the prototypes. The prototype systems are designed to be functionally equivalent to the high volume production units. Physical differences between the prototype and production units represent a realistic trade-off to cost-effectively provide a working system demonstration unit

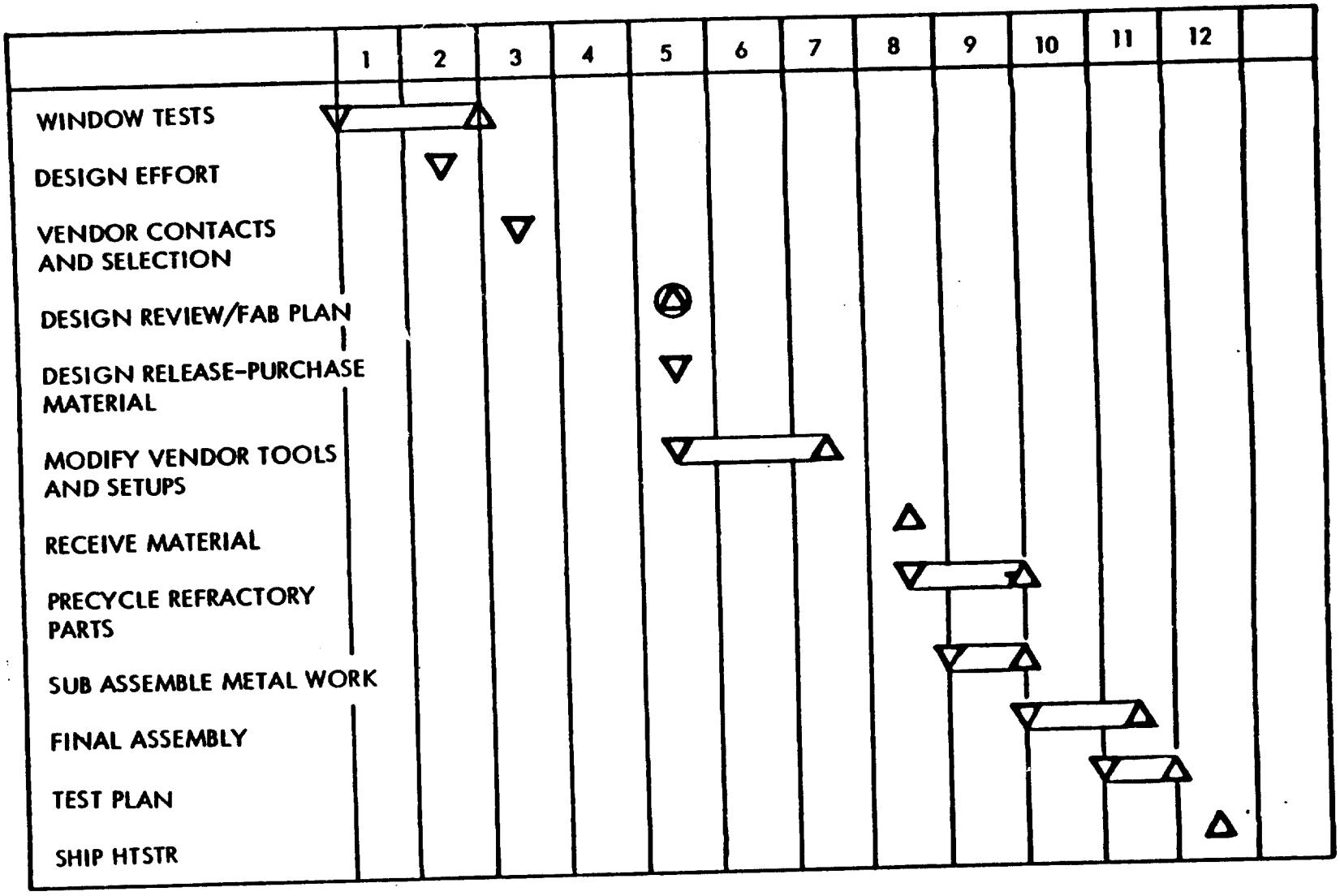

Figure 30. Prototype HTSTR Schedule

with extra instrumentation to collect engineering test data, and extra design flexibility to facilitate any required modifications, which may be necessary as a result of preliminary test findings.

The first unit components will be closely inspected for design compliance. During the assembly and instrumentation of the first unit, manufacturing processes and component compatibility will be validated. Any necessary processes and/or component dimension changes will be incorporated in the fabrication process sheets, and dimension changes will be recorded by the appropriate drawing revisions.

The prototype units will be fabricated in accordance with the system drawing level breakdown. The process corresponds in principle with the Production Flow Sequence of the HTSTR. Major differences are in the receiver and storage matrices; Sanders will purchase completed ceramic matrices for the prototype because in-house fabrication is not warranted for small lots.

Insulation in the prototype unit will be supplied in sawed segmental sections of cylinders approximately 12 inches long to minimize tooling cost.

A moving assembly line will not be used for the prototype lot. Tooling adjustments and secondary setup effort, by ceramics and insulation vendors has been planned. Sanders will prepare fixtures and dollies while awaiting parts. The necessary materials handling equipment will be identified and supplied from production support. Manpower allocation is shown in Figure 31.

2.5.2 Special Processes and Equipment

Extensive tooling will not be required for fabrication or assembly of the prototype receiver. There are, however, special forming techniques which have already been developed and are routinely used by Sanders' ceramic vendors.

The mullite storage mass will be extrusion formed and fired. The SiC receiver matrix is formed from green extrusion stock which is cut to shape (beveled and mitred) prior to firing. Insulation for the prototypes will be delivered, cut to size and in incremental thickness (discs), for fitting and joining at Sanders.

MANPOWER ALLOCATION - PROTOTYPE FABRICATION

FUNCTION	LABOR GRADE		MAN MONTHS	MONTHS ARO 1	2	3	4	5	6	7	8	9	10	11	12
WINDOW TESTS	MGR.	ENG.		▽		△									
VENDOR CONTACTS AND SELECTION	"	"	1 MM												
DESIGN REVIEW AND FAB PLAN	"	"			▽					△					
PROCESS CONTROL SHEETS	"	"													
HANDLING FIXTURES	"	"													
SHOP TEST SETUPS	"	"													
FAB FIXTURES	LAB TECH		.5 MM												
SUB ASSEMBLY	"		.75 MM												
ASSEMBLY	"														
PRECYCLE REFRACTORY PARTS	"		.5 MM								▽			△	
SHOT TESTS	"														
PACK AND SHIP	"		.2 MM												
			2.95 MM												

Figure 31. Manpower Allocations

2.5.3 Required Development

The design for the HTSTR unit uses common materials, automated fabrication techniques, and components which have all been used and tested by Sanders in previous receivers. The prototype HTSTR receiver design is a simplified, economical, and refined version of previously demonstrated hardware.

No new technology is required to design or fabricate any part in this receiver. The unit to be delivered is considered a development model, which means there is considerable production engineering and accelerated life testing needed before a final production model is available.

The Sanders HTSTR has no fundamental unanswered technical problems. The concept is proven and the technology is within the state of the art as demonstrated by Sanders' experience with both pressurized (10 kW) and unpressurized (250 kW) ceramic matrix receivers. Technical areas wherein further analyses and design finalization are required include window heat balance, storage mass support, and inlet air flow distribution control. Extensive modeling conducted during the design concept development indicates even with a very conservative analysis that the key item, the window, is viable. Obviously, the only way to resolve the doubts which linger is to prove by testing that the window will survive.

Sanders' experience with the 10 kW pressurized receiver tested at White Sands, NM, demonstrated concept validation and provided valuable data related to window cooling requirements. Flux concentration at the window of the proposed receiver is greater and window equilibrium temperatures below 1000^{o}C are anticipated. These temperatures do not significantly alter window characteristics.

The final design for storage mass support may involve simply holding the mass with a recess in the formed receiver insulation or holding it with discrete brackets. That determination will depend primarily on the impact of transportability and handling requirements on the design.

The cost estimates (Figure 32) for this receiver are valid for quantities of less than 1000. Beyond that the figures are high and do not reflect the high volume advantages that would be realized by thorough value engineering techniques and design modifications. The penalties of boiler plate design constraints would be displaced by a safe but cost effective reevaluation of design requirements.

The performance of such an extensive effort is outside the scope of this study, and inappropriate in view of the effort which was concentrated on window analysis. Frequent conversations with JPL made it eminently clear that the issue of prime concern during this contract study was the analytical resolution of key technical issues. To this end, the price estimates presented reflect quantity advantages in the manufacture of a product, but do not seriously address the design modifications which would be incorporated during an actual production program. Cost data, then, for quantities from 1 to 1000 are valid for the conceptual design presented. Meaningful cost estimates for quantities above 1000 would be made as part of the prototype development effort which should follow this study.

PART NUMBER	PART DESCRIPTION	SOURCE	PRICING BASE	LOT SIZE NO. 1			LOT SIZE NO. 2			LOT SIZE NO. 3			LOT SIZE NO. 1			LOT SIZE NO. 2		LOT SIZE NO. 3		NO. LINE
				QTY	UNIT PRICE	TOTAL PRICE	QTY	UNIT PRICE	TOTAL PRICE	QTY	UNIT PRICE	TOTAL PRICE	QTY	UNIT PRICE	TOTAL PRICE	QTY	TOTAL PRICE	QTY	TOTAL PRICE	
4021161P1	WINDOW	CE BEAM	X	1		165	10		106	100		101	1K		97	10K	92	100K	89	1.
4021162P1	CYLINDER, OUTER, INSULATOR	WARD-PROCESS		1		700			604			161			156		145		140	2.
4021163P1	CYLINDER, OUTER, INSULATOR	WARD-PROCESS		1		450			300			104			101		91		90	3.
4021164P1	TUBE, INNER, INSULATOR	WARD-PROCESS		1		150			129			35			34		32		30	4.
4021165P1	TUBE, INNER, INSULATOR	WARD-PROCESS		1		150			129			35			34		32		30	5.
4021179P1	APERTURE, INSULATOR	WARD-PROCESS		1		500			432			115			112		104		100	6.
4021167P1	BOWL, INSULATOR	WARD-PROCESS		1		500			432			115			112		104		100	7.
4021168P1	SPACER, INSULATOR	WARD-PROCESS		1		75			65			17			16		15		15	8.
4021169P1	SPACER, INSULATOR	WARD-PROCESS		1		75			65			4			4		3		3	9.
4021170P1	RETAINER, WINDOW	HIGHLAND TOOL		1		675			350			170			85		81		78	10.
4021172P1	SEGMENT, STORAGE	GEN REFRACT.		15	55	825		51	770		27	412			395		375		360	11.
4021176G1	VESSEL, PRESSURE, 50 KW	MASS ENG		1		3250			650	475		475			350		330		285	12.
4021173P1	GASKET, WINDOW	DV DIE		1		28			19			9			8		8		7	13.
4021178P1	PANEL, MATRIX	HORTON		12	150	1800	1	73	875		23	275		16	196		155		130	14.
4021175P1	CUSHION, WINDOW	DV DIE		1		15			11			4			9		3		3	15.
SS-200-1-2	CONNECTOR, SWAGE LOK			1		5			3			2			2		1		1	16.
E-C-1-007065	C-RING, HASTELLOY	ADV PROJ		1		73			69			40			32		29		27	17.
4021180P1	SHIELD	DV DIE		1		200			115			35			27		24		22	18.
4021181P1	SHIELD	DV DIE		1		75			28			22			17		14		13	19.
MAS566C41	BOLT, .375-24 x 1.20 LG			16		6			4			3			3		2		2	20.
	BOLT, .50-20 x 3.50 LG			30		60			48			30			24		20		19	21.
	ASSORTED HARDWARE, SET					75			60			35			28		23		21	22.
						9932			5352			2199			1837		1663		1565	23.

Figure 32. Material Estimate

SECTION 3
CONCLUSIONS AND RECOMMENDATIONS

3.1 CONCLUSIONS

- The Sanders High Temperature Solar Thermal Receiver (HTSTR) has a high probability of success as an economic and reliable device.

- The concept is within the state-of-the-art and represents an economic alternative to other gas flowing receivers used above 535°C (1000°F).

- The receiver window will, on the basis of extensive and conservative engineering analysis, survive the solar and infrared environment to which it is exposed.

- Operating efficiency is predicted to be equal to or greater than 75% at design power input and 2500°F output.

- Production cost estimates of ≈$25/kWt.

3.2 RECOMMENDATIONS

- Prototype development, fabrication and testing should be funded to provide a production baseline unit and to expedite the deployment of a viable solar powered fossil fuel offset heat source for fuels and chemicals and power generation applications.

- A separate Scientific Research Experiment (SRE) should be funded as a follow-on to this study program to further probe the window performance and to demonstrate its reliability.

- System trade-off studies should be initiated to determine the system cost impact of appending a terminal concentrator to the receiver to operate with primary mirrors that have surface slope errors greater than 2 milli-radians.